5-7-2024

Ammonia Recovery from Digester Centrate with Electrochemical Membrane Systems: Mechanism, Performance, and Application

Fubin Liu
Washington University – McKelvey School of Engineering

WASHINGTON UNIVERSITY IN ST. LOUIS

McKelvey School of Engineering
Department of Energy, Environmental & Chemical Engineering

Dissertation Examination Committee:
Zhen He, Chair
Peng Bai
Daniel E. Giammar
Xinhua Liang
Kevin D. Moeller

Ammonia Recovery from Digester Centrate with Electrochemical Membrane Systems: Mechanism, Performance, and Application

by

Fubin Liu

A dissertation presented to
the McKelvey School of Engineering
of Washington University in
partial fulfillment of the
requirements for the degree
of Doctor of Philosophy

May 2024
St. Louis, Missouri

Table of Contents

List of Figures

List of Tables

Acknowledgments

I would like to take this opportunity to express my sincere appreciation to everyone who helped me complete the dissertation and supported me with all aspects.

First, I would like to express my deepest gratitude to my advisor Dr. Zhen He. Apart from the amazing help to my research, he is excellent model during my PhD life who taught me how to be a good mentor and help students to achieve their goals. I will sincerely memorize the valuable guidance and suggestions for my dissertation and life. I respect and treasure his awesome guidance in my experiment and manuscripts. He is definitely the most important one I should show my gratitude to first.

I would also thank another advisor of mine during rotation, Dr. Peng Bai, who is also one of my committee members. His experience in electrochemistry and modeling made me interested in related research fields, which contributed to a great component in my dissertation. I would extend my gratitude to my other committee members: Dr. Daniel Giammar, Dr. Xinhua Liang, and Dr. Kevin Moeller. I sincerely appreciated their suggestions on my proposal and dissertation.

I would like to express my special thanks to Dr. Zixuan Wang, Dr. Bingyuan Ma, Mr. Michael Dyer, Dr. Yinjie Tang, Miss Alyssa Worland, Dr. Hanna Moustafa, Dr. Ivan Radin, Dr. Tucker Krone, and those who have assisted me to finish my thesis. Their valuable assistance including but not limited to: experiment equipment setup, data analysis, sample preparation, manuscript review, etc. Never will I finish my dissertation without their huge input.

I also have great pleasure to work with all the members in EBBL. I enjoy the research environment in our lab. I could always receive help when I have questions or something unexpected happens. They are the best group of people to collaborate with.

I would also take this opportunity to that the Department of EECE and McKelvey School of Engineering. I feel great honored to be one part of it. I would like to thank Monique Spears, Megan Morrissey, Megan Flake, Tammy Haney, Sanmathi Chavalmane Subbenaik and lots of staff in our department. I got great help from them when I work in our department to finish my dissertation.

Particularly, I must say thank you to my parents. They are the two strongest support from my heart who encourage me to keep pursuing my dreams. I know how much we mean to each other and nothing can change it.

Last, I would thank myself who made the decision five years ago to come to the United States to start my PhD program. This period of life is so special and memorable. I enjoyed the life here. Although I am planning to go back to China after graduation, I wish I could have chance to visit my alma mater in the future as an alumnus in the future.

Fubin Liu

Washington University in St. Louis

May 2024

ABSTRACT OF THE DISSERTATION

Ammonia Recovery from Digester Centrate with Electrochemical Membrane Systems: Mechanism, Performance, and Application

by

Fubin Liu

Doctor of Philosophy in Energy, Environmental, and Chemical Engineering

Washington University in St. Louis, 2024

Professor Zhen He, Chair

Nitrogen plays an indispensable role in living organisms and thus is a key element for agricultural production. Ammonia (NH_3), as an important part in nitrogen cycle, can be synthesized by nitrogen fixing bacteria and the Haber-Bosch process, the latter of which requires an extensive energy input. Wastewaters can contain a large amount of nitrogen compounds because of kitchen and toilet wastes being discharged to sewage. The concentration of ammonia nitrogen (NH_4^+-N) can be hundreds mg per liter in some wastewaters like anaerobic digester (AD) centrate. However, both Haber-Bosch process and conventional wastewater ammonia treatment process are energy intensive, which making direct ammonia recovery from wastewater streams become increasingly beneficial in order to achieve sustainable nitrogen management. Electrochemical and membrane technology are emerging technologies that can achieve ammonia recovery with high recovery efficiency, while many of the those are still energy- and chemical-intensive. These motivate us to develop novel integrated membrane and electrochemical systems for ammonia recovery from wastewater. Meanwhile, the mechanisms and performance of the new systems should be

investigated systematically through experiment and modeling, and the application of the recovery products also needs to be evaluated.

To start with, a microbial electrochemical system (MES) was used to recover ammonia from a mixture of AD centrate and food wastewater at an optimal volume ratio of 3:1. The catholyte of the MES, which contained the recovered ammonia, was used to prepare fertilizers to support the growth of a model plant *Arabidopsis thaliana*. It was observed that *A. thaliana* grown on the MES generated fertilizer amended with extra potassium, phosphorus, and trace elements showed similar appearance to the control group that was added with a commercial fertilizer. RNA-Seq analyses were used to examine *A. thaliana* genetic responses to the MES generated fertilizers or the commercial counterpart. The comparative study offered metabolic insights into *A. thaliana* physiologies subject to the recovered nitrogen fertilizers. The results of this study have demonstrated the potential application of using the recovered ammonia from AD centrate as a nitrogen source in fertilizer.

Next, a novel electrochemical membrane system (EMS) was developed to recover nitrogen from real AD centrate. The EMS synergistically coupled electrodialysis with membrane contactor to facilitate the selective recovery of target nutrient. Under a constant current of 10 mA cm^{-2}, the EMS recovered more 80% of NH_4^+-N. The results of this study have demonstrated the feasibility of the proposed EMS and encouraged further investigation to reduce its energy consumption and improve nutrient recovery. Afterwards, a four-chamber electrochemical membrane system was developed to reduce the energy consumption and nutrient recovery cost. The lowest specific energy consumption of 8.2 ± 0.2 kWh kg^{-1} N was achieved under 1.25 mA cm^{-2}. A preliminary cost analysis examined the relationship between acid price and dosage and estimated the operating

cost of \$0.58~0.83 $kg^{-1}N$; simultaneously recovered phosphorus would further increase the benefit of this system.

This work further studied the kinetics in different electrochemical systems to provide insights towards the operation and design of the system through mathematical modeling. Herein, we have performed Tafel analysis with Marcus-Hush-Chidsey (MHC) model for the first time to understand the anodic reaction kinetics in MES. After fitting the data over five months of cultivation, our results showed that MHC fitting curves can match better with a multi-electron transfer mechanism than with a one-electron transfer mechanism. To continue with, the kinetics of acid/base production, two important contributors to recover ammonia in the MES, was modeled with an empirical model by coupling MHC model and polynomial regression. When the EMS was fed with synthetic AD centrate, good fitting performance was achieved for both the anode and cathode half reactions. Moreover, the coupled model also showed decent prediction values when real AD centrate was fed into EMS if the bicarbonate concentration was included to modify the model.

Challenges and opportunities were identified for using electrochemical and membrane technologies for ammonia recovery. It is recommended that long-term operation of the EMS to be conducted in order to evaluate the performance of the system after a few months, this would help to get a more comprehensive economic analysis of the cost to recover nutrients from AD centrate in EMS. Also, developing versatile functions of EMS together with ammonia recovery will uplevel its value, such as volatile fatty acid recovery, carbon capture and storage, heavy metals removal, etc. It is still challenging to enlarge the EMS to pilot-scale, but with the experiment and modeling work conducted in this dissertation, the path to a more sustainable cycle of nitrogen resources is smoother.

Chapter 1 : Introduction

1.1 Background

1.1.1 The roles of nitrogen

Nitrogen (N) plays an essential role in living organisms as a key building block of DNA, and thus necessary for agricultural production. A balancing nitrogen cycle in natural system can be beneficial to the sustainable development of the human society. The major nitrogenous compounds involved in natural N cycle include nitrogen gas (N_2), organic N, ammonium (NH_4^+), nitrite (NO_2^-) and nitrate (NO_3^-) (Guo et al., 2019; MacFarlane et al., 2020). Ammonia nitrogen as an important composition in the nitrogen cycle, is commonly formed through biological nitrogen fixation from N_2, and is used in nitrification and assimilation processes to generate NO_3^- and organic N, which are also important for plants and microorganisms. However, it is worth emphasizing that the ammonia derived from the biological nitrogen fixation process itself is still not enough to support the world's demand for ammonia to grow crops. Therefore, alternative methods should be developed to support the demand of human beings for ammonia nitrogen as well (Daims et al., 2015; Levy-Booth et al., 2014; Wang et al., 2019).

The Haber-Bosch process is a great advance which was developed in 20th century and has become the major industrial procedure to produce ammonia today. This process directly combines 1 mol N_2 from the air with 3 mol hydrogen gas (H_2) under high temperature (400~450 °C) and high pressure (200 bar). Therefore, the Haber-Bosch process is energy-intensive, with a typical energy usage of 12.1 kWh kg^{-1} N, which contributes to around 1~2% of the annual global energy consumption (Erisman et al., 2008; Kitano et al., 2012; Pikaar et al., 2017). Moreover, carbon dioxide (CO_2) as a major greenhouse gas is generated together with H_2 from nature gas (CH_4) from

the process, and is often directly released to the air (Bose et al., 2022). Therefore, discovering renewable methods other than the Haber-Bosch process to sustainably produce ammonia for fertilizer production is a problem that must be urgently solved.

1.1.2 Ammonia removal from the wastewater

Wastewater is a huge tank for ammonia nitrogen. Currently, domestic wastewater comprises 20 million tons of ammonia annually, which is equivalent to ~19% of the annual ammonia production from the Haber-Bosch process. Additionally, it is estimated that the amount of ammonia that stores in domestic wastewater will further increase to 35 million tons annually by 2050 (Cruz et al., 2019). However, ammonia is usually considered as a pollutant in wastewater treatment plant (WWTP), because if excessive ammonia going back to the natural aquatic environment, eutrophication will appear, causing the death of aquatic life and destroying biodiversity (Kuntke et al., 2018b). Thus, WWTP usually considers ammonia N removal as an important goal in the wastewater treatment process.

Conventionally, ammonia is removed through nitrification-denitrification processes and finally converted into N_2. However, the conventional nitrification-denitrification process is energy intensive, typically requiring about 2.6~6.2 kWh kg^{-1} N (Schaubroeck et al., 2015). If the dosage of organics in the denitrification process is considered, energy equivalent to ~10 kWh kg^{-1} N is lost, which is almost 90% of energy consumption of the Habor-Bosch process (Cruz et al., 2019). Additionally, the formation of nitrous oxide (N_2O) during the N removal process is detrimental to the ozone layer, because N_2O is reported as a potent greenhouse gas (GHG) with a 300-fold stronger greenhouse effect comparing with CO_2. If nitrogen can be recovered directly from wastewater, the problems which come with conventional ammonia removal methods mentioned above would be partially alleviated.

1.1.3 Ammonia recovery from the wastewater

Ammonia recovery from wastewater can reduce the reduce the dependency on Habor-Bosch process to produce ammonia for agriculture, and avoid the problems of conventional ammonia removal process at the same time. Ammonia recovery from wastewater have been studied in the past decades (Subramani and Jacangelo, 2015; Yan et al., 2018; Yaqub and Lee, 2019). Domestic wastewater is most the dominant wastewater being investigated, but the typical NH_4^+-N concentration is only ~50 mg L^{-1} (Qin et al., 2023; Shin et al., 2022). Therefore, ammonia recovery from domestic wastewater is either directly achieved through absorption or biological uptake from the mainstream, or through concentrating with various technologies and then be recovered afterwards from the side-stream.

Apart form domestic wastewater, livestock wastewater, industrial wastewater, landfill leachate, and digester centrate have NH_4^+-N concentration of hundreds to thousands mg L^{-1}, which are more suitable to many recovery methods without concentrating and can be recovered directly (Kinidi et al., 2018; Lee et al., 2021b). However, the complicated components (such as toxic organics, heavy metals, competitive ions, etc.) in different wastewater might affect the ammonia recovery performance of various technologies. Some of these topics are still not well studied and the feasibility and cost of new systems to address the challenge need through investigation.

1.1.4 Ammonia recovery technologies

Generally, there are three approaches for recovering NH_4^+-N from a wastewater, physical, chemical, and biological processes. Physical processes take advantage of the positive charge of NH_4^+, which can transfer and be adsorbed due to the electric force. For example, capacitive deionization can accumulate the wastewater NH_4^+-N up to 927 mg L^{-1} (Zhang et al., 2019) or a special aluminosilicate adsorbent can selectively recover 90% of NH_4^+-N from wastewater (Manto

et al., 2018). However, it is difficult to separate NH_4^+ from other competing ions (e.g. Na^+, Ca^{2+}, Ni^{2+}, and Cu^{2+}) unless special adsorbents are used. Chemical processes usually involve pH adjustment to recover nitrogen either as precipitates (e.g., struvite) (Wang et al., 2015) or ammonia gas (dos Santos et al., 2020) at a cost of chemicals that are used to adjust pH and energy to remove water or provide aeration. Biological nitrogen recovery can be realized by microalgae that convert NH_4^+-N (or NO_3^-) to biomass with a high protein component, which can be used to produce biodiesel or other health supplements (Fernandes et al., 2015). This approach is limited by the slow growth of microalgae and potential inhibition by a high concentration of NH_4^+-N (Wang et al., 2018). Actually, the study of ammonia recovery is developed and improved by strategically combining various technologies.

Membrane technology is proposed as an effective method for ammonia recovery, because it can enrich the NH_4^+ within the reactor and separate NH_4^+ from specific matters, including organics, competing ions, and water. For example, forward osmosis (FO) and reverse osmosis (RO) membrane can sperate NH_4^+ from water and increase NH_4^+-N in liquid for subsequent recovery with osmotic pressure and external pressure (Vaneeckhaute et al., 2017; Wang and Liu, 2021). Gas permeable membrane (GPM) can selectively separate volatile matters from the liquid (such as NH_3 and CO_2), thus GPM is also applied in membrane distillation (MD) and membrane contactor (MC) to realize resource recovery (Al-Juboori et al., 2022; Pawar et al., 2022b). Cation exchange membrane (CEM) can separate cations, including NH_4^+, with anions and non-charged matters, which is widely used applied in (bio)electrochemical system and electrodialysis (ED) to achieve ammonia recovery (Kuntke et al., 2018b). With the ammonia being separated, membrane technology can also be coupled with chemical precipitation and ammonia stripping to acquire recovery products with higher quality.

Recovering ammonia through chemical precipitation is usually accomplished by forming struvite (MgNH4PO4·6H2O), and equation of this process is shown in Eq. (1.1).

$$Mg^{2+} + NH_4^+ + PO_4^{3-} + 6H_2O \rightarrow MgNH_4PO_4 \cdot 6H_2O(s) \quad (1.1)$$

Struvite has a slow-releasing rate compared to the traditional chemical fertilizer and liquid fertilizer, which can avoid the nutrient loss from leaching and surface runoff. However, struvite precipitation can only recover NH_4^+-N and PO_4^{3-}-P at equal ratio, but the molar ratio of N:P is usually higher that in common wastewater, resulting a low ammonia recovery efficiency (Tansel et al., 2018; Wu and Vaneeckhaute, 2022). Additionally, extra Mg^{2+} dosage is usually required due to the limited Mg2+ concentrations in wastewater.

Ammonia stripping is a simple desorption process in which the NH3 gas present in wastewaters is stripped out by a flow of air (Ochs et al., 2023). The major reaction is the equilibrium of NH_4^+ and NH_3 under different pH, as shown in Eq. (1.2).

$$NH_4^+ \leftrightharpoons NH_3 + H^+ \quad (1.2)$$

According to the pK_a value of NH_4^+/NH_3 is 9.25 at room temperature, ammonia stripping should be conducted above this pH value. Like chemical precipitation process, the extra chemical dosage (usually alkaline) is required to increase the pH above the pKa value, and acids are also needed to absorb the NH_3 that has been stripped out. Additionally, increasing temperature can facilitate ammonia stripping efficiency, but will also increase the cost of recovering ammonia from wastewater. The performance of the coupling system should be evaluated precisely, and the energy consumption and cost of the ammonia recovery process is also worth investigation.

1.1.5 Electrochemical system for ammonia recovery

Microbial electrochemical systems (MES) are bioelectrochemical reactors in which oxidation of organic compounds by electroactive bacteria (EAB) in the anode chamber, generating electrons and protons that move to the cathode chamber to reduce electron acceptors (such as O_2 and H_2O) (Li et al., 2020). Microbial electrolysis cell is one representative MES by applying external power to facilitate the function of electro-active microbes and the formation of H_2 from non-fermenting compounds makes MEC a promising approach for wastewater treatment and resource recovery (Pawar et al., 2022a). Although some key issues have been investigated, such as optimizing reactor configuration, improving nutrient recovering efficiency, and technical economic analysis. We must know that resource recovery is not completed until the recovered resource is applied. Although it is well acknowledged that the recovered ammonia may be used as fertilizer in agriculture, this has not been well examined with experimental proof.

Cultivating microbes in the MES for nutrient recovering is time-consuming, and the complicated components in different kind of wastewater might not always be suitable to feed the EAB to generate electricity, even harmful if heavy metals and toxic organic compounds are existing in wastewater. Therefore, non-bioelectrochemical system (use electrochemical system for simplification) has attracted increasing attention to achieve resource recovery. ED is a typical electrochemical separation process in which cations and anions are driven orientally to across ion exchange membrane (IEM) under the electric field (Gurreri et al., 2020). Specifically, the cations move towards the cathode, and the anions move to the anode in the opposite direction. Nutrients (such as NH_4^+-N and PO_4^{3-}-P) or other valuable ions can be recovered by means of ED (Liu et al., 2021). Although an ED system can recover >90% of both PO_4^{3-}-P and NH_4^+-N, pretreatment of a solution is needed and the presence of competitive ions, especially cations that include heavy

metals, can deteriorate the quality of fertilizer (Pan et al., 2020; Talekar and Mutnuri, 2021; Wang et al., 2015; Ward et al., 2018). Thus, modified electrochemical system should be investigated to solve this problem.

1.1.6 Modeling the electrochemical systems

Despite the progress in experiments, theoretical studies for understanding the reaction mechanisms of electrochemical system are still at the early stage. Mathematical models can be used to identify the key parameters to optimize the performance of electrochemical system, as well as guide the design and operation of this system. Current is one of the most important characteristics in electrochemical system because it directly affects the performance of electrochemical system, such as power output, energy consumption, and the rate of redox reaction. The precise modeling and correlation between the current and redox reaction happened on the electrodes will contribute to solving large-scale problems economically by saving time and effort. In MES, current generation is closely related to the kinetics of the electron transfer among substrate, biofilm, and electrodes, characterization and analysis of the kinetics of redox reactions in MES is of great significance (Lee et al., 2009; Torres et al., 2010). Similarly, the generation of protons and hydroxide on the electrode is also affected by the controlled current from the external power supply, thus influencing the ammonia recovery performance.

There are various models to describe the kinetics of the reactions happening in electrochemical system. Butler-Volmer (BV) model is conventionally applied to depict the electron transfer process at the electrode interface (Matsena and Chirwa, 2022; Yang and Saidi, 2022). The simplified model at high overpotentials, i.e. Tafel equation, is widely adopted to obtain the charge-transfer coefficient and the exchange current density that are used for evaluating the performance of the materials. However, the fitting curve would not always accurately match the kinetics. Therefore,

when investigating anode reactions involving the complex charge transferring process, more sophisticated models are needed to help us understand the kinetics more accurately. Butler-Volmer-Monod (BVM) model, which is an extensively used model to character charge transfer process in MES, combines biochemical oxidation of a substrate and electron transfer to the electrode interface together with BV model and mass balance equations (Hamelers et al., 2011). Although the good fitting performance was validated, BVM model contains excessive adjustable parameters that can lead to overfitting. Marcus-Hush-Chidsey (MHC) model that considers the microscopic molecular interaction effect, can be used to more accurately model the electron transfer process at a complex electrode interface in a wide range of overpotential (Henstridge et al., 2011).

While electrochemical systems offer significant advantages over existing state of the art methods for recovering ammonia from wastewater, there still remain barriers to its effective implementation which range from the economic feasibility of the electrochemical system to a lack of a clear experimental demonstration that shows how the ammonia nitrogen recovered from the wastewater can lead to an effective fertilizer, and to an effective model for proper predictive evaluation of the key electrochemical reactions happened in the system.

1.2 Research objectives

The goal of this dissertation is to develop innovative electrochemical systems to recover ammonia nitrogen from digester centrate, investigate key factors affecting the ammonia recovery performance, understand the system and electrochemical reactions assisted through modeling and achieve a practical way to utilize the recovery products.

Objective 1: To optimize the performance of microbial electrochemical system (MES) to recover ammonia from anaerobic digester (AD) centrate, and apply the recovered ammonia to support the growth of a model plant.

Objective 2: To understand a novel electrochemical membrane system (EMS) by coupling electrochemical water electrolysis with membrane contactor to recover ammonia from digester centrate.

Objective 3: To model and understand the electron transfer kinetics in both MES and EMS.

1.3 Overview of dissertation

The work in this dissertation can be divided into five tasks (Fig. 1.1). Task 1 optimized the performance of MES under various wastewater ratio of digester centrate and food wastewater, and then the recovered ammonia was used to grow the model plant, which corresponds to the first objective. Task 2 developed a novel EMS to achieve ammonia recovery from real digester centrate. The performance of EMS was further improved in Task 3 with modification to the structure of EMS, resulting lower energy consumption and cost of ammonia recovery. Both Task 2 and Task 3 pursued the second objective. Task 4 applied MHC model to study the electron transfer kinetics in MES. Meanwhile, Task 5 used the same model to understand the kinetics of acid/base production in EMS. These two tasks addressed the third objective. The results from Task 1 can be evidence for the application of the recovered products in Task 2 and Task 3. Task 4 and Task 5 help to understand the reactions happening with the ammonia recovery processes and guide the design and operation of electrochemical systems in previous tasks.

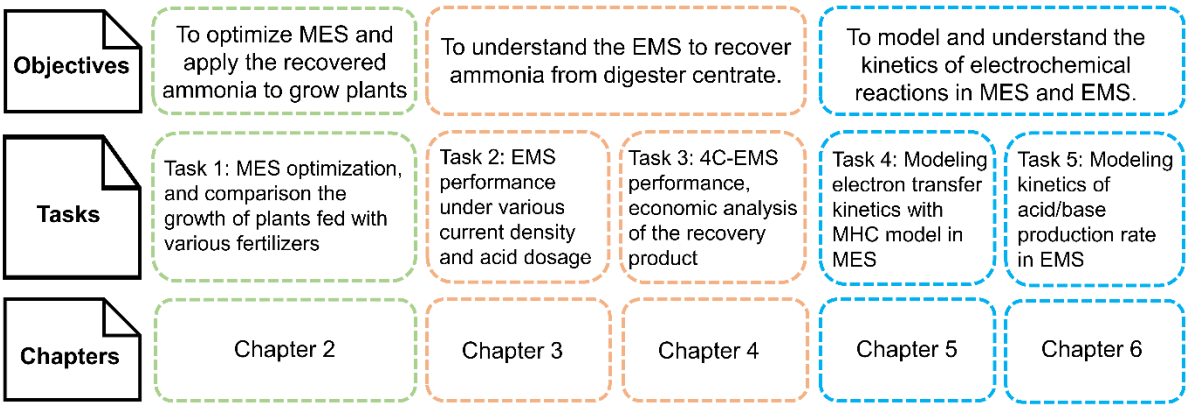

Figure 1.1 Overview of research objectives, tasks, chapters, and their connections.

Chapter 2: Ammonia recovery from anaerobic digester centrate with microbial electrochemical system (MES) and subsequent application to fertilize *Arabidopsis thaliana*.

This chapter has been published in *Water Research*, 2022, 220, 118667.

Abstract

Although ammonia recovery from wastewater can be environmentally friendly and energy efficient compared to the conventional Haber-Bosch process, there is a lack of research on the reuse of the recovered ammonia to exhibit a complete picture of resource recovery. In this study, a microbial electrochemical system (MES) was used to recover ammonia from a mixture of anaerobic digester (AD) centrate and food wastewater at a volume ratio of 3:1. More than 60% of ammonia nitrogen was recovered with energy consumption of 2.7 kWh kg^{-1} N. The catholyte of the MES, which contained the recovered ammonia, was used to prepare fertilizers to support the growth of a model plant *Arabidopsis thaliana*. It was observed that *A. thaliana* grown on the MES generated fertilizer amended with extra potassium, phosphorus, and trace elements showed comparable sizes and an even lower death rate (0%) than the control group (24%) that was added with a commercial fertilizer. RNA-Seq analyses were used to examine *A. thaliana* genetic responses to the MES generated fertilizers or the commercial counterpart. The comparative study offered metabolic insights into *A. thaliana* physiologies subject to the recovered nitrogen fertilizers. The results of this study have demonstrated the potential application of using the

recovered ammonia from AD centrate as a nitrogen source in fertilizer and identified the necessity of supplementing other nutrient elements.

2.1 Introduction

Nitrogen plays an indispensable role in living organisms and thus is a key element for agricultural production. Ammonia nitrogen can be synthesized by nitrogen fixing bacteria and the Haber-Bosch process, the latter of which requires an extensive energy input accounting for ~1% of the world's total energy usage and ~1.4% of the global carbon dioxide emissions annually (Kyriakou et al., 2020). Wastewaters can contain a large amount of nitrogen compounds because of kitchen and toilet wastes being discharged to sewage. The concentration of ammonia nitrogen can be tens of hundreds mg per liter in some wastewaters like anaerobic digester (AD) centrate or landfill leachate. Due to the toxic effects and a major component for causing eutrophication, ammonia nitrogen must be substantially reduced in a wastewater, typically via biological nitrification/denitrification. Other biological methods such as anaerobic ammonia oxidation (Bhattacharjee et al., 2017; Nawaz et al., 2021) and shortcut nitrification/denitrification (Lu et al., 2021b; Paredes et al., 2007) have been employed to effectively to remove ammonia nitrogen. Ammonia nitrogen can also be removed using a stripping method that consumes a substantial amount of energy and chemicals (Park and Kim, 2015). Sustainable nitrogen management during wastewater treatment expects to recover valuable nitrogen compounds, which will not only decrease energy/chemical consumption by removal, but also produce valuable nitrogen resources that reduce the need for ammonia synthesis by the energy-intensive Haber-Bosch process.

In general, there are three approaches for recovering NH_4^+-N from a wastewater, physical, chemical, and biological processes. Physical processes take advantage of the positive charge of NH_4^+, which can transfer and be adsorbed due to the electric force, for example capacitive

deionization can accumulate the wastewater NH_4^+-N up to 927 mg L^{-1} (Zhang et al., 2019) or a special aluminosilicate adsorbent can selectively recover 90% of NH_4^+-N from wastewater (Manto et al., 2018). However, it is difficult to separate NH_4^+ from other competing ions (e.g. Na^+ and Ca^{2+}) unless special adsorbents are used. Chemical processes usually involve pH adjustment to recover nitrogen either as precipitates (e.g., struvite) (Wang et al., 2015) or ammonia gas (dos Santos et al., 2020), at a cost of chemicals that are used to adjust pH and energy to remove water or provide aeration. Biological nitrogen recovery can be realized by microalgae that convert NH_4^+-N (or NO_3^-) to biomass with a high protein component, which can be used to produce biodiesel or other health supplements (Fernandes et al., 2015). This approach is limited by the slow growth of microalgae and potential inhibition by a high concentration of NH_4^+-N (Wang et al., 2018).

An emerging technology for nitrogen recovery is microbial electrochemical systems (MES), which couple biological, chemical, and physical processes driven by bioelectricity generation from biological oxidation of organic matter (Kelly and He, 2014). Nitrogen often exists in a wastewater as NH_4^+ and can migrate in an electric field. In an MES, this migration allows NH_4^+ to be separated from a wastewater and then concentrated in the recovering solution such as a catholyte (Kuntke et al., 2014) or a special solution in a microbial resource recovery cell (Chen et al., 2015). The MES technology has been studied to recover NH_4^+-N from a variety of wastewaters including domestic wastewaters, livestock wastewaters, landfill leachate, and source-separated urine (Ye et al., 2018). The NH_4^+-N recovery efficiency of an MES typically varies between 60% and 90% depending on the initial NH_4^+-N concentration in a wastewater (Arredondo et al., 2015), and can reach 100% under an optimized condition (Desloover et al., 2012). The MES can achieve an NH_4^+-N recovery rate of 0.02-11.57 kgN m^{-3} d^{-1} and consumed 0.8-8.5 kWh kg^{-1} N (Zou and He, 2018), less than 8-12 kWh kg^{-1} N by the Harbor-Bosch process (Giddey et al., 2017).

We must know that resource recovery is not completed until the recovered resource is applied. Although it is well acknowledged that the recovered nitrogen may be used as fertilizer in agriculture, this has not been well examined with experimental proof. To fill the knowledge gap in nitrogen recovery and reuse, this study aimed to extract ammonia from a real AD centrate using an MES and then apply the recovered ammonia to support the growth of a model plant. Real food wastewater was used to supplement carbon source. The specific objectives were to: (1) optimize the ratio of AD centrate and food wastewater to achieve enhanced nitrogen recovery performance of the MES; (2) investigate the efficacy of using the recovered ammonia as fertilizer for plants; and (3) understand the genetic effects of the recovered fertilizer on the tested plants at a transcriptional level.

2.2 Materials and methods

2.2.1 MES setup and operation

A bench-scale MES was built consisting of an anode chamber and a cathode chamber, each of which had an effective volume of 336 mL (6 cm × 16 cm × 3.5 cm) (Fig. A1.1). The anode electrode was made of two carbon brushes (length: 15 cm; diameter: 3 cm) that were electrically connected. The cathode electrode included carbon cloth coated with 5 mg cm^{-2} activated carbon and a piece of stainless-steel mesh (5.5 cm × 15.5 cm, L316, 10 mesh) as a current collector. The anode and cathode chambers were separated by a piece of cation exchange membrane (CEM, Membranes International Inc., Ringwood, NJ, USA) with an effective cross-section area of 96 cm^2. A power supply provided a constant voltage of 0.8 V across the anode electrode and cathode electrode, and an external resistor was connected in the circuit to monitor the current generation. The anode of the MES was inoculated with the effluent collected from the anode of a microbial fuel cell that had been operated to treat a municipal wastewater for over three months. During the start-up phase, a

synthetic anolyte was fed to the MES anode containing (per 1 L) 1 g NaAc, 0.153 g NH_4Cl, 0.031 g KH_2PO_4, 0.032 g $CaCl_2$, 0.066 g $MgSO_4$, 0.5 g $NaHCO_3$, and 1 mL trace elements (Largust T. Angenent, 2001). The initial catholyte was 50 mM phosphorus buffer saline. Both electrolytes were recirculated between the anode/cathode chambers and the external containers. To select electrochemically active bacteria (EAB), the external resistor was gradually reduced from 5400 to 1 Ω. After the start-up phase, the anolyte was changed to a mixture of AD centrate and food wastewater with different volume ratios. AD centrate was collected from the Missouri River Treatment Plant (St. Louis, MO, USA) and the food wastewater was sampled from the dining service of Washington University in St. Louis. Meanwhile, the catholyte was changed to tap water. To prevent ammonia from leaving the solution, a pH-control meter was used to keep the catholyte pH below 8 by adding 0.2 M sulfuric acid. After each operational cycle, the anolyte was replaced with a fresh influent solution and the catholyte was replaced with tap water. The removed catholyte was then used to prepare the fertilizer for further tests.

2.2.2 Experiment design

Nitrogen recovery in the MES was studied for the effect of the volume ratio between AD centrate and food wastewater, and three ratios were investigated at 1:1, 3:1, and 7:1. The key parameters including current generation, conductivity, pH, COD, and NH_4^+-N concentrations were examined. Once an optimal ratio was determined, the MES was operated to produce a catholyte that was used to prepare fertilizer (Table A1.1). For comparison and reference, house fertilizer (15-16-17 Peat-Lite, JR Peters Inc., PA, USA) was used (Group a) and analyzed for its pH, conductivity, and major cations and anions. The catholyte collected from the MES was diluted to achieve a similar total nitrogen concentration to the house fertilizer. Then, the diluted catholyte was divided into three groups to prepare the testing fertilizers. Group b was the diluted catholyte without any

additional chemicals. Group c contained KH_2PO_4 and K_2HPO_4 to make the similar concentrations of potassium and phosphorus to those in Group a. Group d, on the top of Group c, was supplemented with several trace elements at the concentrations comparable to that of Group a: H_3BO_3, $MnCl_2 \cdot 4H_2O$, $FeCl_2 \cdot 4H_2O$, $CuSO_4 \cdot 5H_2O$, $ZnCl_2$, and $Na_2MoO_4 \cdot 2H_2O$. The pH of all fertilizer groups was adjusted between 6.5 and 7.0 using H_2SO_4 or NaOH. The nitric acid was not used because it could bring extra nitrogen into the catholyte. We did not use the hydrochloric acid, as former research proved that high chloride concentrations would inhibit the growth of the model plant that was studied here.

Plant growth with the prepared fertilizer was conducted in the Jeanette Goldfarb Plant Growth Facility (JGPGF) of Washington University in St. Louis (St. Louis, MO, USA). *Arabidopsis thaliana* was chosen as a model plant due to its low demand for hydration and fast growth rate (five to eight weeks). Five parallel pots (named by position using numbers 1 through 5), each of which contained five plants (named by position using numbers 1 through 5 as well), were employed under each condition (Group a through d). For example, an individual plant with a name "a13" meant that it was in Group a, pot #1, and the third plant in the pot #1. All plants grew in the same reach-in chamber in the JGPGF that controlled the temperature at 21 ℃ and moisture at 50%. Light with 175 μmol intensity was provided 8 h/d to prevent flowering under a short-daylight condition; that would allow us to directly compare the size of *A. thaliana* without considering the nutrition for flowers. After seeding, all plants were kept in the chamber without any nutrition for 2 weeks. Starting from the third week, each pot was watered with 20 mL house fertilizer or the prepared fertilizers every other day for another 5 weeks. The first day of fertilizing was numbered as Day 0 and the last day was Day 36.

2.2.3 Analyses and measurements

The voltage of the MES was monitored using a multimeter (2700, Keithley Instruments Inc., Cleveland, OH, USA). The concentrations of ammonia nitrogen and chemical oxygen demand (COD) in both the anolyte and the catholyte were analyzed using a spectrophotometer (DR 890, Hach Company, Loveland, CO, USA). The solution pH was measured with a bench pH meter (Oakton Instruments, Vernon Hills, IL, USA). The solution conductivity was measured using a bench conductivity meter (Mettler Toledo, Columbus, OH, USA). The concentrations of cations and anions were measured using ion chromatography (Thermo Fisher Scientific, Waltham, MA, USA). The concentrations of trace elements were measured using inductively coupled plasma mass spectrometry (NexION 2000, PerkinElmer, Downers Grove, IL, USA). The electron-ion transfer efficiency (TE) for NH_4^+ migration was calculated according to Eq. (2.1):

$$TE = \frac{\mathrm{F}VC_{\mathrm{f}}}{\mathrm{M}\int_0^t Idt} \times 100\% \tag{2.1}$$

where I is the current (mA), t is the total cycle time (s), C_{f} is the final concentration of NH_4^+-N (mg L^{-1}) in the catholyte, V is the volume (L) of the catholyte, M is the molar mass of nitrogen (14 g mol^{-1}), and F is the Farady constant (96485 C mol^{-1}).

The individual plant was analyzed for its length (determined by the longest distance between the tips of two leaves) and width (the distance between the tips of two leaves in the direction perpendicular to the length) every 6 days during the 5-week fertilizing period. Then, the leaves in Groups a, b, and d were collected for RNA extraction and library construction. Those three groups represented commercial fertilizer (a), original catholyte (b), and fully supplemented catholyte (d). Those leave samples were cleaned with RNA free water, dried with Kimtech wipers, and frozen immediately in liquid nitrogen. Novogene (https://en.novogene.com/) provided RNA-Seq and data analysis. Methods of RNA extraction and library construction are described in the Appendix A1.

All the plants (above the surface of the soil) were collected to measure their wet weights with an analytical balance. If the wet weight of a plant was lower than 0.05 g, usually with flaccid and dried leaves (Noodén and Penney, 2001), we considered it as “dead” in the present study. Then, all plants were placed in coin envelopes and dried in drying oven at 60 ℃ overnight, and the dry weights were also measured. We conducted one-way ANOVA of Groups a, b, and d in terms of the sizes and weights of all the “live” plants using Origin software (α=0.05 and Tukey method is used for multiple comparison adjustment).

2.3 Results and discussion

2.3.1 Ammonia recovery in the MES

Ammonia recovery in the MES was investigated with the varied ratio between AD centrate and food wastewater to determine an optimal combination of ammonia input (AD centrate) and organic supply (food wastewater). It was observed that current generation exhibited a typical batch profile, reaching the highest after a fresh anolyte was supplied and then decreased when the organics were consumed (Fig. 2.1A). The highest peak current of 25 mA was obtained with the ratio 3:1. Although the peak current with 7:1 was higher than that with 1:1, the current generation with 7:1 decreased more sharply, resulting the lowest total coulomb of 836 ± 23 C. The highest coulomb production of 1241 ± 27 C was obtained with the ratio of 3:1, followed by 1035 ± 35 C with 1:1. The highest electricity generation with the ratio 3:1 was a result of the combined effects of both COD concentration and the influent conductivity. The initial COD concentration in the anolyte was 1620 ± 28, 1156 ± 20, and 940 ± 25 mg L^{-1} with the ratio 1:1, 3:1, and 7:1 (Fig. 2.1B), which was affected by the amount of food wastewater. The final COD concentration with three ratios was 992 ± 23, 771 ± 16, and 754 ± 20 mg L^{-1}, resulting in removal efficiency of 38.8 ± 1.4, 33.3 ± 1.4, and 19.8 ± 2.2%, respectively. The residue COD was mostly from AD centrate that could

not be easily utilized by EAB. Although the ratio 7:1 had the lowest COD input, its initial conductivity of 5.91 ± 0.06 mS cm^{-1} was the highest, followed by 5.52 ± 0.04 mS cm^{-1} (3:1) and 3.80 ± 0.08 mS cm^{-1} (1:1) (Fig. 2.1C), suggesting that more AD centrate would increase the solution conductivity and thus decrease the internal resistance of the MES. In the present MES, a low volumetric ratio 1:1 brought in more organics (from food wastewater) but had a lower conductivity (less AD centrate), leading to a relatively lower peak current (due to a high internal resistance) that could last for a longer period of time due to sufficient organic supply. A high ratio 7:1 generated a high peak current instantly, benefited from its high conductivity (and thus a lower internal resistance) but the current generation could not last longer due to less organic input. This combined effects from both organic input and solution conductivity led to the best performance of electricity generation with the ratio of 3:1.

The NH_4^+-N concentrations in the anolyte and the catholyte followed the similar trend as the conductivity (Fig. 2.1C-2.1F). With three ratios, 70.3 ± 1.1, 68.6 ± 1.5, 47.8 ± 1.2% of NH_4^+-N was removed from the anolyte, which had an initial NH_4^+-N concentration of 393 ± 12, 626 ± 12, and 690 ± 8 mg L^{-1}, respectively. The final NH_4^+-N concentration in the catholyte was 407 ± 12 mg L^{-1} when the volume ratio was 3:1, higher than 310 ± 8 and 280 ± 2 mg L^{-1} with 1:1 and 7:1. The transport efficiency of ammonium ions was similar under different conditions, 51.6, 56.5, and 57.7%, respectively, indicating that more than 50% of electric charge could be used to move ammonium ions. The rest of electric charge was likely used to migrate other cations. The energy used to recover ammonia nitrogen were estimated 3.0, 2.7, and 2.6 kWh kg^{-1} N under three conditions, comparable with other studies (Kuntke et al., 2018a; Qin et al., 2018).

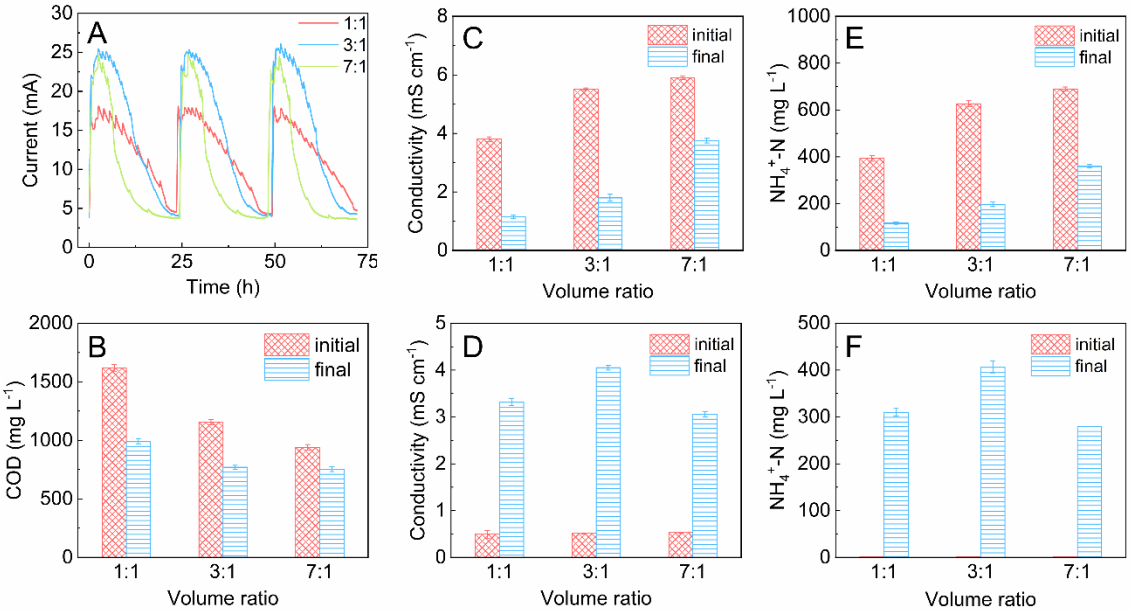

Figure 2.1 The performance of the MES under three volume ratios of anaerobic digester centrate and food wastewater, 1:1, 3:1, and 7:1. (A) Current production; (B) COD concentrations; (C) conductivities in initial and final anolyte; (D) conductivities in initial and final catholyte; (E) ammonia nitrogen concentrations in initial and final anolyte; and (F) ammonia nitrogen concentrations in initial and final catholyte.

Because of the highest NH_4^+-N concentration in the catholyte and a relatively lower energy consumption, the volume ratio of 3:1 was employed in a longer-term operation of the MES for producing the catholyte that was then used to prepare fertilizer. In a period of three weeks, the MES was able to perform consistently for current generation (Fig. 2.2A). The average NH_4^+-N concentration recovered in the catholyte of the MES was 294 ± 17 mg L^{-1} (Fig. 2.2B). The reason for a lower NH_4^+-N concentration was because we collected a new AD centrate, which had a lower NH_4^+-N concentration than the previous one (actual wastewater/centrate can have varied concentrations of contaminants). As a result, the initial NH_4^+-N concentration after mixing with food wastewater was 465 ± 7 mg L^{-1}, lower than 626 ± 12 mg L^{-1} in Fig. 2.1E. Because the recovered catholyte would need to be diluted, a varied initial NH_4^+-N concentration did not affect the NH_4^+-N concentration in the testing fertilizers. The conductivity of both anolyte and catholyte

were stable in this period (Fig. A1.2A and 2B). Likewise, the anolyte pH was also stable (Fig. A1.2C) but the final pH of the catholyte varied from 6 to 8 (Fig. A1.2D), influenced by the addition of acids.

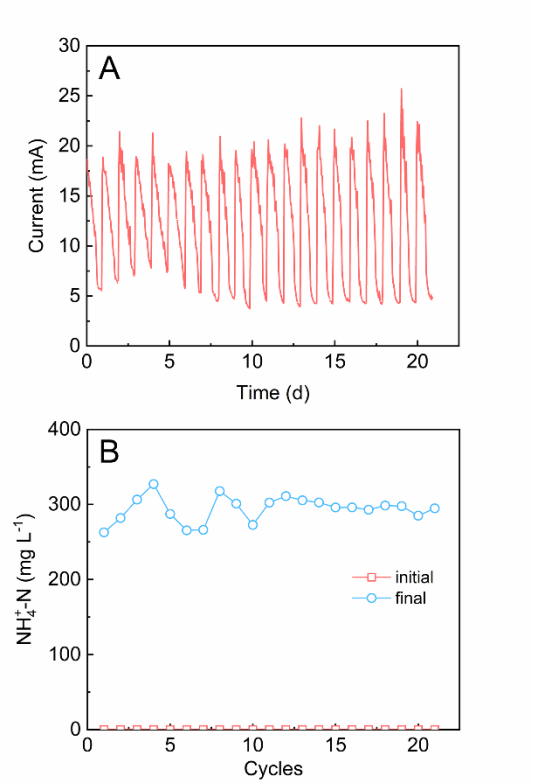

Figure 2.2 (A) Current generation and (B) ammonia nitrogen concentrations in catholyte of the MES during the three-week test fertilizer production period with volume ratio of 3:1 between anaerobic digester centrate and food wastewater.

2.3.2 Characterization of the prepared fertilizer

The key components of the house fertilizer are shown in Table A1.2 & A1.3, used as a reference to prepare three different testing fertilizers to investigate the effects of major nutrient elements (e.g., nitrogen, phosphorus, and potassium) and trace elements. It should be noted that nitrogen existed in both ammonium and nitrate in the house fertilizer (Group a), while only ammonia nitrogen was present in the other groups. However, the total nitrogen concentrations were similar among all groups. Our preliminary experiment found that there was no significant difference in

the growth of *A. thaliana* between the fertilizer containing ammonia nitrogen only and a mixture of ammonia and nitrate nitrogen (Fig. A1.3), likely due to the conversion of some ammonia to nitrate via nitrification by ammonia oxidizing bacteria and nitrite oxidizing bacteria that were present in the soil.

The catholyte of the MES contained 44.0 ± 1.8 mg L^{-1} of potassium and a few other elements, but had no phosphorus (Fig. A1.4), because CEM allows only cations such as NH_4^+ to migrate from the anolyte to the catholyte and would reject PO_4^{3-} ions. Six trace elements were analyzed in the catholyte according to the receipt of the house fertilizer, listed in Table A1.2. Three trace elements had very low concentrations, molybdenum (1.1 ± 0.2 μg L^{-1}), boron (< 30 μg L^{-1}), and copper (< 30 μg L^{-1}). The other three trace elements had relatively higher concentrations, though still lower than the target concentrations listed in Table A1.3.

Based on the element concentrations in the catholyte and house fertilizer, two more testing fertilizers were prepared. The cation and anion compositions of all four fertilizers are shown in Fig. 2.3A and 2.3B. One can see that the sulfate concentration in the testing fertilizers (Group b, c, and d) was much higher than that in the house fertilizer, because sulfuric acid was used to maintain the catholyte pH under 8 to prevent the escape of recovered ammonium from the catholyte and to further adjust the fertilize pH to 6.5-7.0.

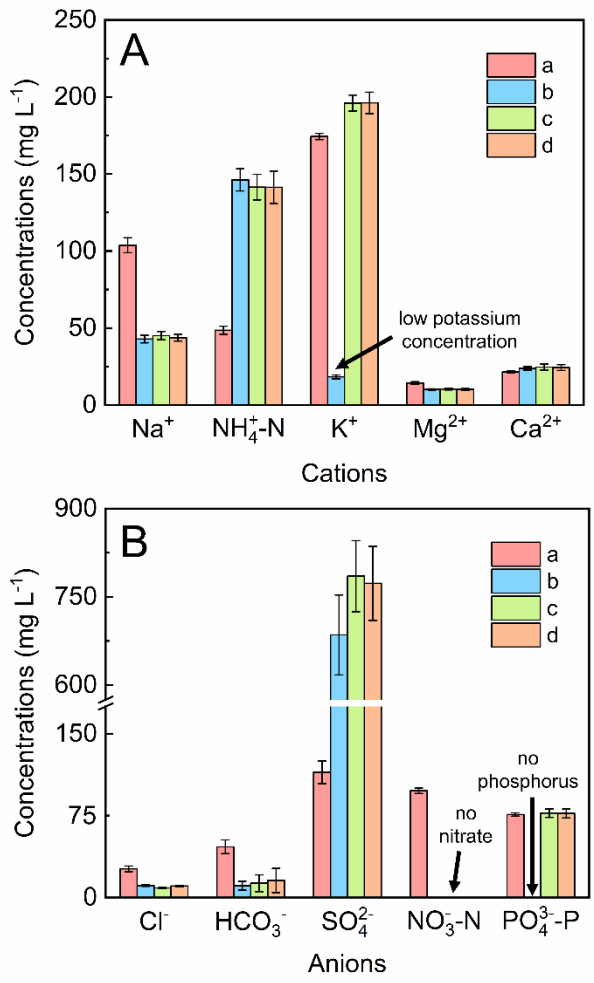

Figure 2.3 The concentrations of (A) cations and (B) anions in the house fertilizer and three testing fertilizers.

2.3.3 Application of fertilizer to support plant growth

Four groups of fertilizers were applied to the plants every other day as described in the Method section. Visual observation (Fig. 2.4) found that Group a and Group d grew better than the other two groups and had fewer dead plants (6 out of 25 for Group a and 0 out of 25 for Group d), compared 20 dead plants out of 25 in Groups b and 10 out of 25 in Group c during the five-week fertilizing period. The occurrence of dead plants in Group a was not expected and might be related to the intense competition among the plants for nutrient and light: the plants that were growing

more slowly could be more disadvantageous in the later phase when the faster-growing plants shaded light with their larger leaves. The poor growth of *A. thaliana* in Group b was mainly due to the lack of phosphorus and potassium, which are related to the health of roots and stems of plants. The growth of Group c plants might have been limited by the low concentrations of important trace elements.

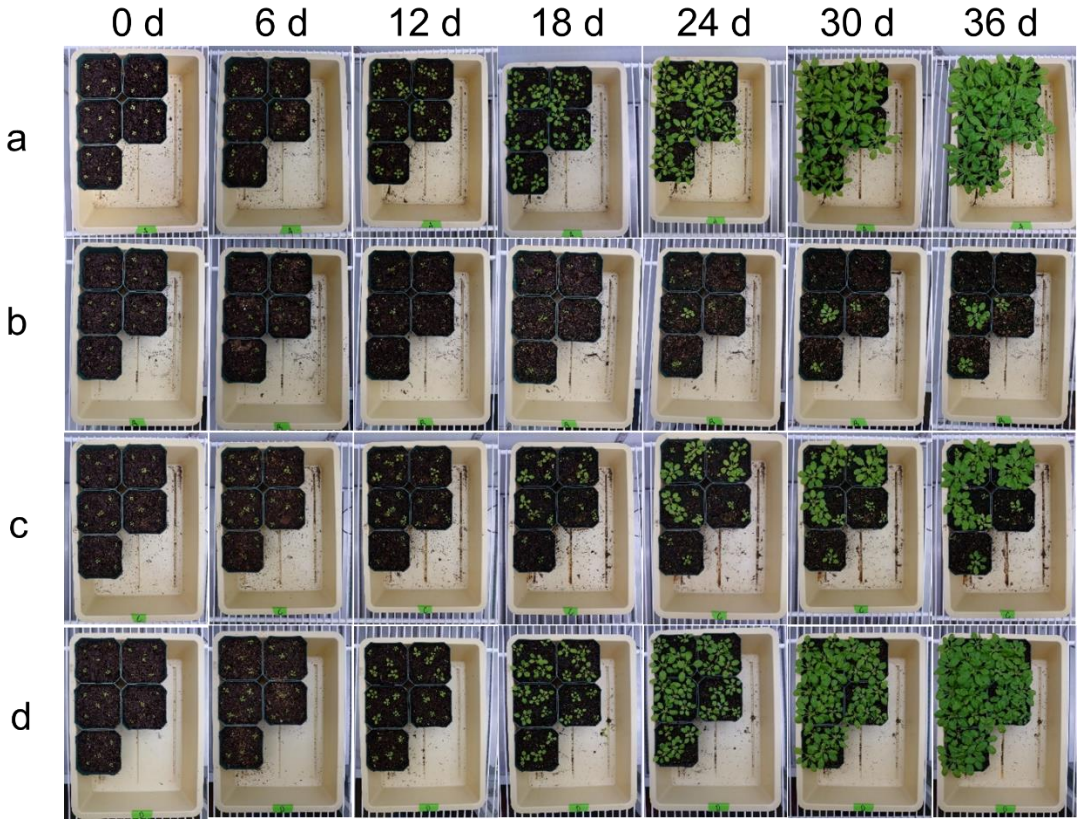

Figure 2.4 The growth of *Arabidopsis thaliana* in four groups every six days during the five-week fertilizing period.

The growth of plants was monitored via measuring their length and width every six days (Fig. 2.5) and compared by ANOVA (Table 2.1). Because most plants in Group b died during the fertilizing period, they were excluded from the measurement. Both the length and the width were similar among these three groups at 0 day (after kept at reach-in chamber for two weeks without fertilization) ($p>0.05$). However, the difference began to appear after different fertilizers was

applied. For example, the leaf length showed a significant difference between Group a and other groups ($p<0.05$). After 18 days, nearly all groups showed significant differences in terms of leaf length and width. The ANOVA results of wet weights and dry weights suggest that there was no significant difference between group c and d ($p>0.05$), while they both differed significantly from group a ($p<0.05$). We inferred that the trace elements did not have much effect on the total mass of *A. thaliana* as potassium and phosphorus, but they had some impact on the size of the plants.

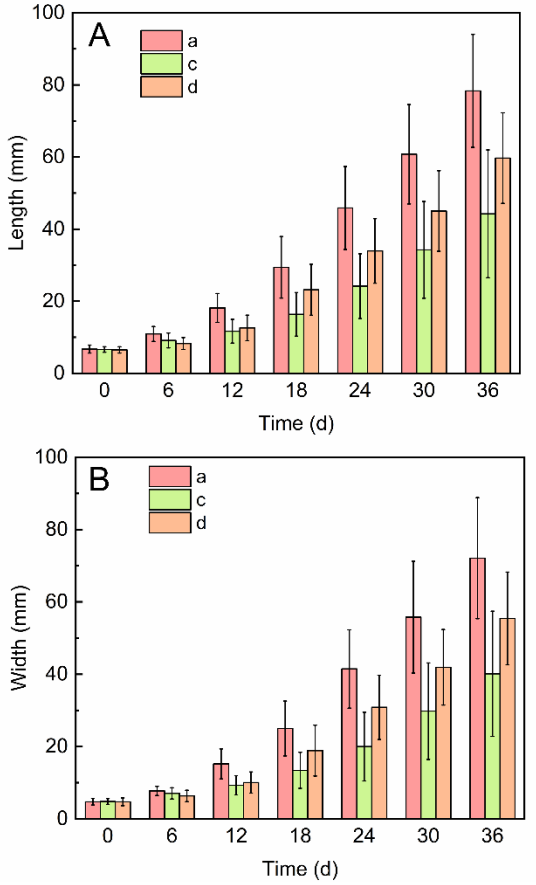

Figure 2.5 Change of the size of *A. thaliana* in terms of the (A) average length and (B) width over the fertilizing period.

Table 2.1 ANOVA results of length, width, and weight of plants. 0 means no significant difference ($p>0.05$), and 1 means significant difference ($p<0.05$) between selected groups. WW: wet weight, DW: dry weight.

Groups		a-c	a-d	c-d
Length	0 d	0	0	0
	6 d	1	1	0
	12 d	1	1	0
	18 d	1	0	1
	24 d	1	1	1
	30 d	1	1	1
	36 d	1	1	1
Width	0 d	0	0	0
	6 d	0	0	0
	12 d	1	1	0
	18 d	1	1	1
	24 d	1	1	1
	30 d	1	1	1
	36 d	1	1	1
Weight	WW	1	1	0
	DW	1	1	0

2.3.4 Effect of fertilizers on expressed genes

Gene expression of the leaves of *A. thaliana* in Group a, b, and d were analyzed to investigate the effect of applied fertilizers. As shown in Table S5, high rates of clean reads (≥94.44%) and Q_{30} (≥90.86%) are obtained. The distances and correlations in terms of the expressed genes in different groups are demonstrated by principal component analysis (PCA) and Pearson correlation analysis in Fig. A1.5 and A1.6. Higher similarity between Groups a and d than Groups a and b was found by comparing the distances between different samples on the PCA plot. Additionally, Fig. A1.5 shows that the correlation coefficients (R^2) between the paired samples from Group a and d were 0.823-0.853, larger than those between Group a and b (0.801-0.827). The number of differentially expressed genes are listed in the co-expression Venn diagram (Fig. A1.7A). All groups shared 14883 genes, indicating over 94% of the detected genes in three groups showed no significant

difference ($p>0.05$). Group a and d shared 931 similar genes that are expressed significantly differently in Group b, larger than the 282 uniquely existing in Group a and b. This can explain the stressed physiological characteristics (size and weight) when Group b is compared with other groups. According to the cluster analysis results based on the FPKM results from RNA sequencing, Group d has larger similarity to Group a compared with Group b (Fig. A1.7B). Although the above results acquired from differential expressed genes (DEGs) indicate that the extra nutrients added to the catholyte played an important role to support the growth of *A. thaliana*, the nitrogen ammonia recovered from digester centrate was a potential nitrogen source because less than 6% genes were expressed differently in Group a that was fed with house fertilizer.

Furthermore, we examined individual genes to reveal plant physiological responses based on Kyoto Encyclopedia of Genes and Genomes database. The top 20 genes that were mostly up or down regulated between each group are listed in Table A1.6 (log2 fold changes are in the ranges from 7 to 11). There are several interesting findings. First, when comparing differentially expressed genes between Groups a and d against Group b, genes related to phosphate starvation were shown to be upregulated in group b, indicating that phosphate supplementation in the commercial fertilizer and the recovered nitrogen fertilizer from Group d is essential for healthy plant growth. Second, UDP-glycosyltransferase (UGT) 76F2, was upregulated in Groups a and d when compared to Group b. UGT is responsible for many critical biological functions, like detoxification, cuticle formation, and olfaction (Zhou et al., 2019). This gene is not upregulated when only NH_4^+ is present, indicating impaired cell function in the absence of additional nutrients. Third, genes related to late embryogenesis abundant (LEA) proteins (related to plants environmental stress response, such as water-stress tolerance) were downregulated in Groups a and d when compared to Group b (Goyal et al., 2005; Hundertmark and Hincha, 2008). Moreover,

an LEA protein gene was significantly downregulated in Group d when compared to Group a (log2 fold change of -7.490). These observations indicates that Group d fertilizer may allow plants to better mitigate environmental stresses. Fourth, two genes related to auxin response were found to be downregulated in Group d compared to Group a. Auxin is a phytohormone that is often included in commercial fertilizers (Rocha et al., 2020), which influences plant growth and development. Finally, these individual genes with mostly drastic changes in expressions were not related to central metabolism. Therefore, we further examined the genes in central carbon pathways (Table A1.7). The highest similarity was seen again between Groups a and d (log2 fold changes were well below one unit). Expression of genes related to central carbon metabolism (glycolysis, TCA cycle, and pentose phosphate pathway) are most similar between Groups a and d, further suggesting the recovered fertilizer with nutrient supplements had similar effect on plant central pathways to the commercial fertilizer.

Additional analysis has been performed to examine photosynthesis, energy and nitrogen metabolisms with Gene Ontology (GO). When Group b was compared with Group a with GO enrichment, 4500, 4293 and 4141 DEGs were found in biological process, cellular component, and molecular functions, respectively. Among all the 3652 GO terms, 224 terms showed significant enrichment, and the first 20 terms were listed in Fig. 2.6A. Biological process and cellular component related to photosynthesis showed the largest difference. For example, thylakoid is the site for the light-dependent photosynthesis process and four thylakoid terms enriched significantly, with more than 200 DEGs in each term. Additionally, photosynthesis and photosystem terms also showed significant enrichment, indicating the photosynthetic processes were affected if phosphorus, potassium, and other trace elements were missing. When Group d was compared with Group a with GO enrichment, only 2083, 1994, and 1874 DEGs were identified in the three

categories. 214 out of 3323 GO terms were found to change significantly. However, when the corresponding terms were selected, terms of photosystem (GO:0009521), plastoglobule (GO:0010287), photosynthetic electron transport chain (GO:0009767), and photosystem II (GO:0009523) were not significantly different ($p>0.05$) from those in Group a (Fig. 2.6B), indicating that *A. thaliana* in Group d had more similar photosynthetic performance to Group a than those in Group b. When KEGG enrichment analysis was performed between Group b and Group a, 1228 DEGs were found in 115 pathways, and 13 pathways, including photosynthesis (ath00195), oxidative phosphorylation (ath00190), nitrogen metabolism (ath00910), etc., were significantly different between Group b and Group a (Fig. 2.7A). On the other hand, when Group d was compared with Group a, only 596 DEGs were found in 108 different pathways in *A. thaliana*. In addition, the number of significantly different pathways decreased to 7, although the other two pathways, 2-oxocarboxylic acid metabolism (ath01210) and valine, leucine and isoleucine biosynthesis (ath00290), were not listed in Fig. 2.7B. Considering the small number of pathways (7 out of hundreds of pathways in *A. thaliana* listed in KEGG database) were affected significantly between Group d and Group a, we infer that our test fertilizers with nitrogen recovered directly from actual digester centrate are appropriate to support the growth of *A. thaliana*.

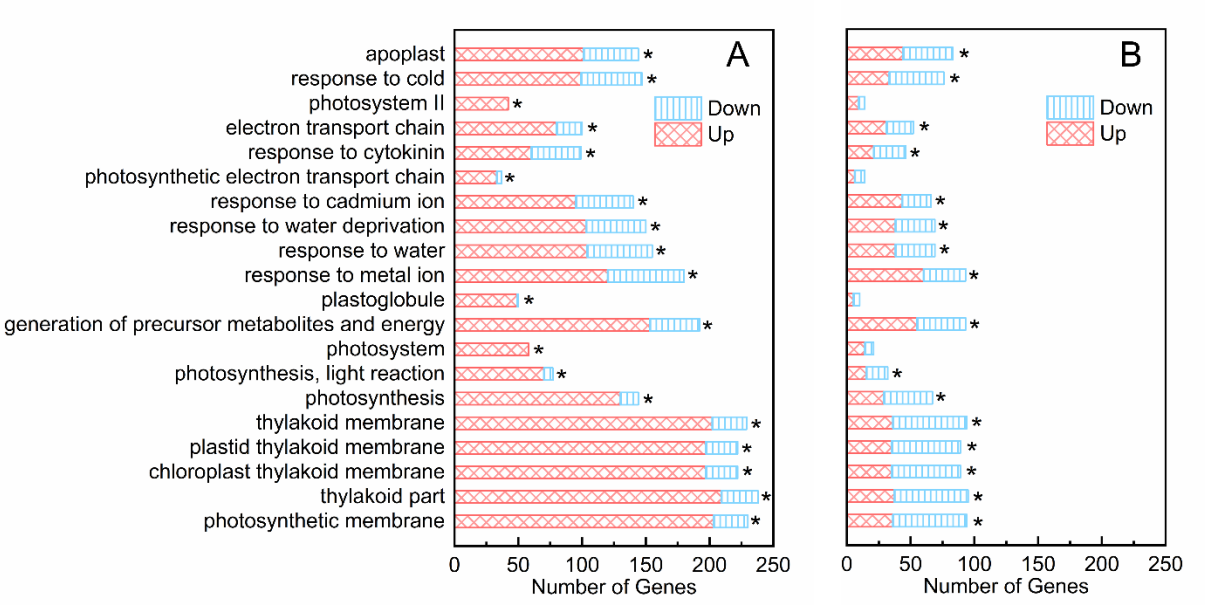

Figure 2.6 Number of genes that are downregulated and upregulated when Gene Ontology (GO) enrichment analysis is performed between (A) Group b and a, (B) Group d and a. Only the first 20 terms that are significantly enriched are shown in (A), and the same term are also shown in (B). The * represent the term is significantlydifferent ($p < 0.05$).

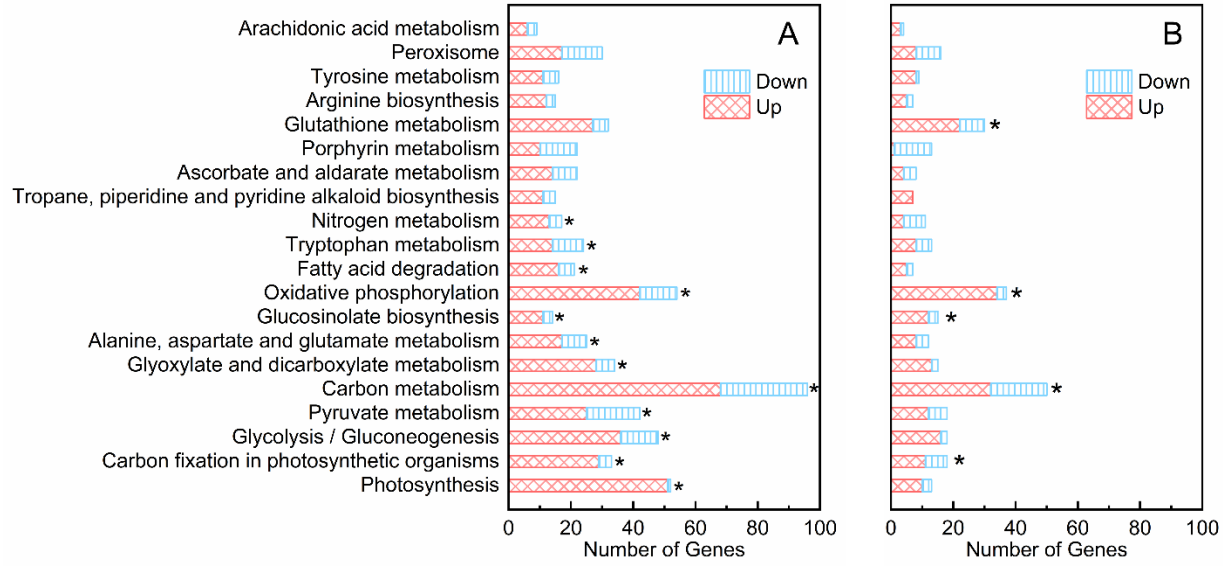

Figure 2.7 Number of genes that are downregulated and upregulated when Kyoto Encyclopedia of Genes and Genomes (KEGG) enrichment analysis is performed between (A) Group b and a, (B) Group d and a. Only the first 20 terms are shown in (A). Since the terms of significantly enriched pathway are less than 20, other terms are also included. The same terms are also shown in (B). The * represent the term is significantly different ($p < 0.05$).

2.4 Conclusions

This study has demonstrated a complete process of nitrogen recovery from real digester centrate, and reuse as a part of fertilizer for plant growth. The results can be inspiring to achieve economic and sustainable nutrient recovery from wastewater with the following main conclusions:

1. When the digester centrate was mixed with food wastewater at a volume ratio of 3:1, the MES achieved the best performance with an average current of 4.8 mA and over 60% nitrogen recovery efficiency. The transport efficiency of ammonium ions was 57%, and the energy consumption was estimated to be 2.7 kWh kg^{-1} N.
2. After three prepared testing fertilizers being applied to *A. thaliana*, Group d showed the best growth results with the largest final size and weight, close to Group a watered with house fertilizer as a control. Group d had the least dead plant after five weeks, compared with 6, 20, and 10 out of 25 for Group a, b, and c, respectively.
3. Plant RNA-sequencing analysis showed that *A. thaliana* grown on fully supplemented fertilizer had the highest similarity of differentially expressed genes compared to the commercial fertilizer, with the fewest genes related to central cellular metabolic processes.
4. The potential application of the fertilizer recovered from wastewater warrants further investigation of a detailed analysis of the health impact caused by heavy metals (e.g. Cr. and Cd), examination of other representative plants, and exploration of low-cost sources of supplementary nutrient elements to amend the prepared fertilizer.

Chapter 3: Effective nutrient recovery from digester centrate assisted by in situ production of acid/base in a novel electrochemical membrane system

This chapter has been published in *Chemosphere*, 2022, 307 (3), 135851.

Abstract

Nutrient recovery from wastewater is important to the circular economy and requires technological advancements. Herein, a novel electrochemical membrane system (EMS) was developed to recover both phosphorus and nitrogen from real digester centrate. The EMS synergistically coupled electrodialysis with membrane contactor to facilitate the selective recovery of individual nutrient. Under a constant current of 10 mA cm^{-2}, the EMS recovered more than 95% of PO_4^{3-}-P and 80% of NH_4^+-N, at energy consumption of 670 ± 48 kWh kg^{-1} P and 52 ± 2 kWh kg^{-1} N. It should be noted that the same energy was used to recover two nutrients. When the acid produced from the anodic reaction was directly reused for N absorption, the final concentrations of PO_4^{3-}-P and NH_4^+-N reached 144 ± 3 and 1232 ± 130 mg L^{-1}, respectively. Adding extra acid did not affect phosphorus recovery but significantly enhance nitrogen recovery to 1797 ± 83 mg L^{-1}. The results of this study have demonstrated the feasibility of the proposed EMS and encouraged further investigation to reduce its energy consumption and improve nutrient recovery.

3.1 Introduction

Phosphorus (P) and nitrogen (N) are the key components of fertilizer, and their production is typically energy and resource intensive. Alternative sources of P and N, particularly through resource recovery from wastewater, is of strong interest to circular economy and societal

sustainability (Govindan et al., 2021; Li et al., 2021; Liu et al., 2022b; Qing et al., 2021). To obtain high-purity nutrients from wastewater, selective recovery is preferred and can be done by taking advantage of specific properties of P and N compounds, for example ionic charge (e.g., PO_4^{3-}, NH_4^+, NO_3^-) and volatility (e.g., gaseous NH_3) (Brennan et al., 2021; Shao et al., 2022; Xu et al., 2019; Zhang et al., 2013). This drives the development of integrated membrane and electrochemical systems for nutrient recovery, such as electrodialysis (ED) that utilizes an electric field to drive cations and anions to transport orientally through cation exchange membrane (CEM) and anion exchange membrane (AEM) , respectively (Al-Amshawee et al., 2020; Gurreri et al., 2020). Although an ED system can recover > 90% of both PO_4^3-P and NH_4^+-N, pretreatment of a solution is needed and the presence of competitive ions, especially cations that include heavy metals, can deteriorate the quality of fertilizer (Pan et al., 2020; Talekar and Mutnuri, 2021; Wang et al., 2015; Ward et al., 2018). This issue motivated us to employ different recovery approaches for P and N: P is recovered via anion migration across AEM and N is recovered via ammonia gas movement through gas permeable membrane that prevents migration of metal ions. Each of those approaches has been demonstrated individually in separate systems, but there has not been a report to accomplish both in the same electrochemical system.

Herein, we report a novel electrochemical membrane system (EMS) to recover nutrients from anaerobic digester (AD) centrate (Fig. 3.1). In this EMS, water electrolysis and ammonia stripping were synergistically coupled by transforming NH_4^+ in AD centrate to NH_3 with the elevated pH in the cathode. Although similar processes were demonstrated previously (Hou et al., 2018; Kim et al., 2021; Liu et al., 2017; Tarpeh et al., 2018), the key novelty of the proposed EMS is the simultaneous phosphate migration across AEM and the use of acids generated in the anode for ammonia absorption, neither of which was reported to be linked to ammonia recovery previously.

The objectives of this study were to demonstrate the feasibility of the EMS to recover both P and N from AD centrate, explore a few key factors that affect the system performance, and provide preliminary results as a foundation towards further investigation.

3.2 Materials and methods

3.2.1 EMS setup

The EMS, as shown in Fig. 3.1, had three chambers with the identical dimension of 6.5 cm × 12.5 cm × 0.95 cm /each chamber: anode, cathode, and absorption chambers, separated by AEM (Membranes International Inc., Ringwood, NJ, USA) and hydrophobic gas permeable membrane (Amersham Hybond, Germany). A Ti/Ir-Ru plate (2 cm × 5 cm) was used as the anode electrode, and carbon cloth (CC, 2 cm × 10 cm) coated with 5 mg cm^{-2} Pt/C (10% Pt) acted as the cathode electrode. A power supply (maximum 18 V/5 A, CircuitSpecialists, USA) provided a constant current across the anode and the cathode electrodes.

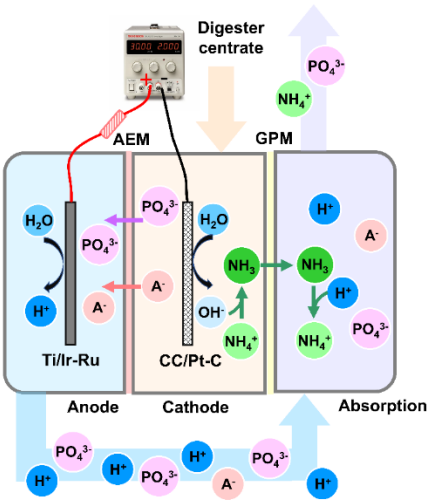

Figure 3.1 Schematics of the electrochemical membrane system. A^- represent anions except for phosphate. Ti/Ir-Ru refers to titanium plate electrode coated with iridium and ruthenium. CC/Pt-C refers to carbon cloth electrode coated with platinum and carbon.

3.2.2 Experiment design

The EMS was first operated under a constant current density varied from 0, 2.5, 5, 10, 15 to 20 mA cm^{-2}, with three chambers fed with deionized water (anode, 90 mL), AD centrate (cathode, 150 mL, detailed information of the AD centrate was shown in Table S1), and 0.1 M sulfuric acid (absorption, 10 mmol H_2SO_4 diluted in 90 mL deionized water. All solutions were recirculated using a peristatic pump at 2.5 mL min^{-1} for 8 h, or 6 h when the voltage of power supply reached the maximum 18 V under a high current density. Fresh solutions were used when a new testing cycle began. After the optimal current density was selected, we used about 50 mL of the anolyte effluent (determined from the mass difference of total anolyte at the start and end of each cycle) that was generated in the previous cycle to replace part of the absorption solution in the next cycle (~60 mL, determined from the mass difference of the absorption solution at the start and end of each cycle, as well as the amount of anolyte transferred from last cycle). 12-hour cycle was selected to allow easy operation, and the volume of AD centrate was increased to 200 mL accordingly. Considering the acid produced by the electrolysis process might not be enough to absorb the ammonia transferred from the cathode, extra sulfuric acid was provided. 0, 1, 1.5, and 2 mL of 25% H_2SO_4 (Recca Chemial, USA) to represent 0, 5, 7.5, and 10 mmol H_2SO_4, respectively. All the experiments were conducted in triplicates.

3.2.3 Analyses and measurements

The voltage across 1-Ω external resistance was monitored by a multimeter (2700, Keithley Instruments Inc., Cleveland, OH, USA). The solution pH was measured using a bench pH meter (Oakton Instruments, Vernon Hills, IL, USA). The conductivity was measured with a bench conductivity meter (Mettler Toledo, Columbus, OH, USA). The concentrations of cations and anions were measured using ion chromatography (Thermo Fisher Scientific, Waltham, MA, USA).

The calculations of the removal efficiency, recovery efficiency, specific energy consumption (SEC kWh kg^{-1}), and electron-ion transfer efficiency (TE) are shown below.

The removal efficiency and recovery efficiency of P and N was calculated according to Eq. (3.1) and Eq. (3.2):

$$Removal\ efficiency = \frac{(C_f V_f - C_0 V_0)}{C_0 V_0} \times 100\% \quad (3.1)$$

$$Recovery\ efficiency = \frac{(C_f V_f - C_i V_i)}{C_0 V_0} \times 100\% \quad (3.2)$$

Where C (mg L^{-1}) is the concentration of P and N, and V is the volume (mL) of electrolyte and acid absorption solution. Subscript f and i represent the finial and initial characteristics of anolyte, catholyte or acid absorption solution. While subscript 0 only refers to the initial characteristics of the digester centrate (catholyte).

The electron-ion transfer efficiency (TE) for PO_4^{3-} migration was calculated according to Eq. (3.3):

$$TE = \frac{\mathrm{F}(C_f V_f - C_i V_i)}{\mathrm{M} \int_0^t I dt} \times 100\% \quad (3.3)$$

where *I* is the current (mA), t is the total cycle time (s), C is the concentration of PO_4^{3-}-P (mg L^{-1}) in the anolyte, *V* is the volume (L) of the catholyte, subscript i and f represent initial and final concentrations/volumes, M is the molar mass of phosphorus (31 g mol^{-1}), and F is the Farady constant (96485 C mol^{-1}).

Specific energy consumption (SEC, kWh kg^{-1}) in this study was calculated according to Eq. (3.4):

$$SEC = \frac{U I_{avg} t}{3.6(C_f V_f - C_i V_i)} \quad (3.4)$$

where *U* (V) is the output voltage of power supply, *I* (A) the average current, t (s) the time of each cycle, *C* (mg L^{-1}) the concentration, *V* the volume (L) of the electrolyte, subscript i and f represent

initial and final concentrations/volumes (energy consumption pump was ignored since it was much less than the electric energy consumption).

The amount of acid produced from the anode was estimated based on the final pH of the anode according to Eq. (3.5)

$$N_{\text{acid}} = 10^{-pH}V \tag{3.5}$$

Where N_{acid} is the effective amount of acid generated from electrolysis (mol), *pH* the final pH of anolyte measured at the end of cycle, *V* the volume of anolyte transferred from anode to the acid absorption chamber (L).

3.3 Results and discussions

3.3.1 Feasibility of the EMS

A potential advantage of the proposed EMS is to use electrical current to control/affect both P and N recovery, although via different mechanisms: phosphate migration is directly driven by electron flow, and ammonia recovery requires the conversion of ammonium to ammonia in an alkaline solution and then ammonia absorption by an acidic solution that may be provided by the anolyte. Thus, electrical current plays a central role in the EMS operation. Under the open-circuit condition (zero current), little phosphate was removed from the catholyte (Fig. 3.2A), with the PO_4^{3-}-P concentration kept around 60 mg L^{-1}. Meanwhile, no phosphate was recovered in the anolyte (Fig. 3.2B). When electric current was applied, the EMS achieved over 95% removal of phosphate in 8 h when the current density was larger than 10 mA cm^{-2}. The PO_4^{3-}-P concentration in the anolyte increased from 36 ± 3 to 108 ± 2 mg L^{-1} with the increasing current density from 2.5 to 20 mA cm^{-2}. Interestingly, nearly 20% of NH_4^+-N was removed in the absence of electric current (Fig. 3.2C), likely because that migration of ammonia could still occur. The removal efficiency of NH_4^+-N increased from 33 ± 3 % to 79 ± 2 % in 8 h when the current density increased from 2.5 to 10 mA

cm^{-2} and accordingly, the recovered NH_4^+-N concentration increased from 479 ± 7 to 1035 ± 36 mg L^{-1} (Fig. 3.2D). This is related to the catholyte pH as a result of cathodic reaction driven by electric current. As shown in Fig. S1B, the catholyte pH was higher than 9.25 most of the time when the current density was larger than 10 mA cm^{-2}. Given that the pKa value of ammonia is 9.25, NH_4^+-N would be in its gaseous phase (NH_3-N) if the pH is higher than this value, and thus make it easier to transport through the gas permeable membrane. Meanwhile, the anolyte pH decreased to around 2 after an operating cycle, suggesting that the acid was continuously produced in the anode (Fig. A2.1A). The pH of the absorption solution after ammonia absorption was always lower than 2.5 (Fig. A2.1C), implying that 10 mmol H_2SO_4 in the absorption solution was over-supplied and could be decreased.

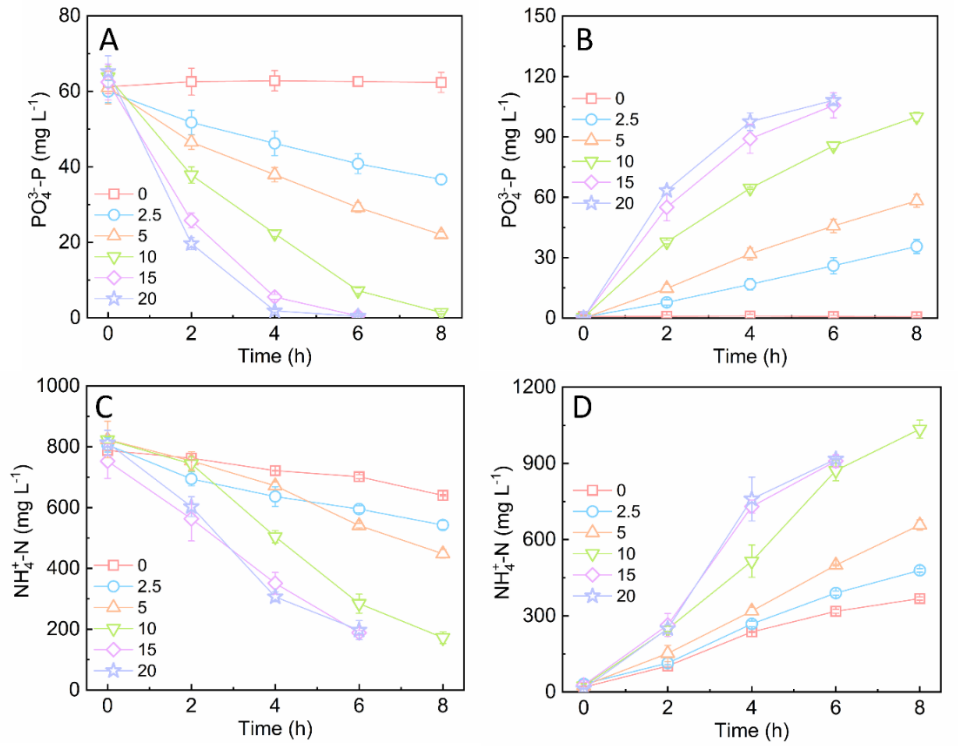

Figure 3.2 Nutrient recovery in the EMS under a current density varied from 0 to 20 mA cm^{-2}: (A) the PO_4^{3-}-P concentration in the catholyte; (B) the PO_4^{3-}-P concentration in the anolyte; (C) the NH_4^+-N concentration in the catholyte; and (D) the NH_4^+-N concentration in the absorption solution.

3.3.2 Reuse of the produced acid for ammonia absorption

We hypothesized that a byproduct of the anodic reaction – acid could be used to absorb ammonia. To examine whether the produced acid was sufficient to recover ammonia, the anolyte effluent was used as the absorption solution. As shown in Fig. 3.3A, after the 12-h cycle, the average PO_4^{3-}-P and NH_4^+-N concentrations in the acid absorption solution (anolyte effluent) reached 144 ± 3 and 1232 ± 130 mg L^{-1}, respectively. However, the final pH of the absorption solution was 8.90 ± 0.20, which was not good for further ammonia absorption, indicating the need for extra acid to recover more ammonia.

The extra acid of 5, 7.5, or 10 mmol H_2SO_4 was added to the acid absorption solution to enhance nutrient recovery in the EMS under 10 mA cm^{-2}. In general, the extra acid did not affect the PO_4^{3-}-P concentration (Fig. 3.3A), because the acid addition to the absorption chamber did not impact migration of phosphate anions from the cathode to the anode under a constant current density. However, the NH_4^+-N concentrations in the absorption solution reached 1332 ± 69, 1725 ± 72, and 1797 ± 83 mg L^{-1} with three amounts of extra acids, higher than 1232 ± 130 mg L^{-1} without acid addition. The NH_4^+-N recovery efficiency increased from 45 ± 6 to 74 ± 2% with more acid added (Fig. 3.3B). The final pH of the absorption solution was 8.90 ± 0.20 and 7.28 ± 0.54 with 0 and 5 mmol H_2SO_4, indicating the difficulty to absorb more N and more chance for NH_3 to escape. The pH decreased to 2.45 ± 0.07 and 2.17 ± 0.08, respectively, when the amount of acid increased to 7.5 and 10 mmol. There is a significant increase of the recovered NH_4^+-N from 5 to 7.5 mmol H_2SO_4 ($p<0.05$), while no significant difference was found between 7.5 and 10 mmol H_2SO_4 ($p>0.05$). The anolyte pH was 1.62, 1.68, 1.43 and 1.56 under four conditions, equivalent to 1.20, 1.04, 1.86, and 1.38 mmol protons, which contributed to 100%, 12%, 12%, and 7% of the total acids used to absorb the recovered ammonia. Thus, to obtain a good ammonia recovery for example the condition of 7.5 mmol H_2SO_4, the in situ generated acid (reflected by the anolyte pH)

was about 10% of the total acids and the additional 90% would need to be added. A large amount of protons that the anode generated could be consumed by hydroxide and bicarbonate that transported together with phosphate from the cathode into the anode. Therefore, reducing the competition from hydroxide and bicarbonate will provide more acid and decrease the need for extra acid.

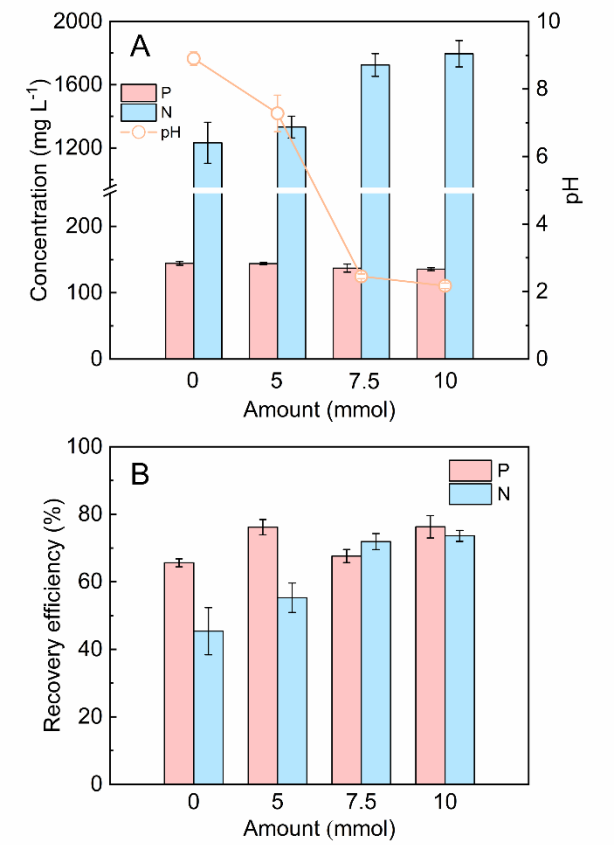

Figure 3.3 Effects of extra acids on the nutrient recovery: (A) the concentrations of PO_4^{3-}-P and NH_4^+-N, and pH in the absorption solution; (B) the recovery efficiency of P and N under various amount of 25% H_2SO_4 added into the absorption solution.

3.3.3 Energy consumption

When the EMS was operated under the varied constant current from 2.5 to 10 mA cm^{-2}, the SEC to recover phosphorus increased from 261 ± 48 to 670 ± 48 kWh kg^{-1} P. This energy consumption is comparable to that of ED systems that typically demand 114- 620 kWh kg^{-1} P (Ye et al., 2019). The same energy was used to recover nitrogen at 16 ± 1 to 52 ± 2 kWh kg^{-1} N (Table A2.2).

Although the estimated energy consumption is higher than conventional ammonia stripping and electrokinetic processes with a typical energy consumption of 5-20.4 kWh kg^{-1} N (Chen et al., 2021), it should be evaluated together with phosphorus recovery, because nutrients were synergistically recovered with cost of the same electric energy in the EMS. A detailed comparison of the performance in related electrochemical ammonia stripping system was listed in Table 3.1.

Table 3.1 Specific energy consumption (SEC) of phosphorus and nitrogen under various current density.

Current density mA cm^{-2}	SEC_p kWh kg^{-1} P	SEC_N kWh kg^{-1} N
2.5	261 ± 26	15.6 ± 1.2
5	368 ± 25	29.7 ± 1.4
10	670 ± 48	52.2 ± 1.7
15	1153 ± 45	113.2 ± 4.0
20	1489 ± 51	143.8 ± 0.7

The energy consumption might be further reduced through some strategies. First, the TE of PO_4^{3-} was only about 1%, indicating that electron movement mostly drove the migration of other anions. Hydroxide ions generated in the cathode chamber are a major competitor to PO_4^{3-} ions in anion transport across AEM, and thus limiting hydroxide ion transport may allow more energy used for moving PO_4^{3-}. The transport of other anions (e.g. HCO_3^- and Cl^-) can also decrease the efficiency of transporting PO_4^{3-}. To address those issues, a pair of AEM and CEM can be used between the anode and cathode chambers. In this way, CEM is facing the cathode and will prevent hydroxide ions from moving. Both PO_4^{3-} and NH_4^+ can still be recovered in the same way if the AD centrate is initially placed between AEM and CEM. Second, the EMS can be operated in a continuous flow mode, so that the protons generated in the anode would be used in time to absorb NH_3. Third, the cathodic reaction can produce hydrogen gas, which can be converted to electricity. A previous study of microbial electrochemical system estimated that the produced hydrogen gas could provide

up to 29% of energy demand (Zou et al., 2017). Fourth, alternative energy sources such as solar energy will reduce the input from fossil fuels. Particularly, solar energy is becoming popular and being installed in more and more wastewater treatment facilities (Pandey et al., 2021).

3.4 Conclusions

This study has demonstrated the feasibility of a three-chamber EMS for successfully recovery of both nitrogen and phosphorus from actual digester centrate. The EMS was able to recover more than 95% of PO_4^{3-}-P and 80% of NH_4^+-N under a constant current density of 10 mA cm^{-2}. The *in situ* produced acid and base were utilized synergistically. Although this study was preliminary, the results would encourage further exploration of the EMS in terms of reduced energy consumption and enhanced transport of target ions.

Chapter 4: Simultaneous recovery of nitrogen and phosphorus from actual digester centrate in an electrochemical membrane system

This chapter has been published in *Resources, Conservation and Recycling*, 2024, 203 (3), 107463.

Abstract

Recovering nutrients from wastewater will not only address pollution issues, but also reduce the need for nutrient from energy/resource - intensive production. Herein, a four-chamber electrochemical membrane system (4C-EMS) was developed to recover both nitrogen and phosphorus from real digester centrate through synergistically coupling electrodialysis with membrane contactor. The 4C-EMS successfully recovered more than 95% of nitrogen and 85% recovery of phosphorus. The lowest specific energy consumption of 8.2 ± 0.2 kWh kg^{-1} N was achieved under 1.25 mA cm^{-2}. A byproduct of the electrolysis – acid could compensate for 10~32% of total acid needed for ammonia absorption. The 4C-EMS effectively reduced heavy metals in struvite by 98% compared to the struvite formed directly from the digester centrate. A preliminary cost analysis examined the relationship between acid price and dosage and estimated the operating cost of \$0.58~0.83 kg^{-1}N; simultaneously recovered phosphorus would further increase the benefit of this system.

4.1 Introduction

The challenge of feeding 8 billion people worldwide with sufficient food has exemplified the need for sustainable fertilizer production (Ingram, 2020; Lu et al., 2021a). Both nitrogen (N) and

phosphorus (P) are the major components of fertilizer, and their production can be energy and chemical intensive. For example, the synthesis of ammonia, a key N source for fertilizer, is conducted through the Habor-Bosch process by combining nitrogen and hydrogen gas under high temperature and pressure (Osorio-Tejada et al., 2022), which consumes 1-2% of the world's electricity. P is acquired through mining phosphorus rock, which lacks sustainability and is estimated to last a few hundred years based on the estimated P reserve and the current mining rate (Cakmak et al., 2022). Therefore, alternative methods or sources to satisfy the increasing demand for fertilizer are becoming critically important to a sustainable society. Meanwhile, the excessive use of fertilizer and the increased food consumption has resulted in a large amount of waste nutrients in wastewater that creates a challenge to meet the strict discharge standards. Traditional methods to remove nutrients from wastewater such as nitrification/denitrification and chemical precipitation require much energy input and chemical dosage (Bunce et al., 2018; Rout et al., 2021). Considering the potential value and availability of waste nutrients in wastewater, recovery of these nutrients will not only reduce their concentrations in the treated effluent, but also offer a promising strategy of resource recovery that contributes to the circular economy (Rodrigues et al., 2022).

Current methods for nutrient recovery from wastewater mainly include physical separation and chemical recovery processes. Physical separation takes advantage of either the charged nutrient ions (i.e. NH_4^+ and PO_4^{3-}), which can migrate and/or be adsorbed under an electrical field, or the selectivity of various membranes to concentrate the nutrients. For example, electrodialysis (ED) can separate NH_4^+ and PO_4^{3-} ions from wastewater via nutrient movement under an electric field and through selective ion exchange membranes. Although an ED system can recover > 90% of both PO_4^3-P and NH_4^+-N, the transport of competitive charged ions together with the target nutrient species will affect the quality of the recovery products (Mohammadi et al., 2021). Adsorption is

another approach for nutrient recovery and a variety of natural or synthetic adsorbents such as biochar, zeolites, and other clay materials have been studied for adsorbing NH_4^+ and PO_4^{3-}, with typical recovery efficiency of 80~95% from synthetic wastewater or urine (Han et al., 2021; Liu et al., 2022a). The challenges with adsorption include the cost of adsorbent regeneration and the selection of target nutrients (Cheng et al., 2019; Ren et al., 2021). Chemical recovery processes usually involve pH adjustment to recover nutrients either as precipitates (e.g., struvite and apatite) (Wang et al., 2015) or ammonia gas. Although the target nutrients can be selectively recovered in some cases, the processes require chemical dosage to adjust pH and high energy consumption to provide aeration. It is estimated that the cost to recover P from municipal wastewater through chemical precipitation is \$5~20 kg^{-1} P (Mayer et al., 2016). The cost of ammonia stripping can be as high as \$2~3.5 kg^{-1} N including both the chemical and aeration cost (Van Eekert, 2012). Membrane contactor also takes advantage of the conversion of ammonium to ammonia gas, similar to air stripping, but instead of intensive aeration, the hydrophobic gas permeable membrane (GPM) is applied to separate ammonia gas, which will be further absorbed by acids on the other side of the membrane (Darestani et al., 2017). Over 95% ammonia recovery efficiency was achieved when membrane contactor was applied to treat digestate with 700-3000 mg L^{-1} NH_4^+-N (Boehler et al., 2015). A pilot-scale membrane contactor tested ammonia recovery from various waste streams and estimated the cost to be \$1.5~2.5 kg^{-1} N.

To accomplish selective recovery of target nutrients, we have developed an electrochemical membrane system (EMS) (Liu et al., 2022a). The EMS uses anion exchange membrane to separate PO_4^{3-} from anaerobic digestion centrate driven by an applied electrical current and takes advantage of high pH generated by the same electricity to transform NH_4^+ to NH_3 that is then separated by GPM. Although the abovementioned individual processes have been reported in various studies

(Tarpeh et al., 2018; Zhang et al., 2013), the EMS is able to integrate those processes to achieve the common goal of nutrient recovery. The EMS could recover more than 95% of PO_4^{3-}-P and 80% of NH_4^+-N under a constant current density of 10 mA cm^{-2}. However, the previous EMS encountered a major issue of high energy consumption of 670 ± 48 kWh kg^{-1} P and 52 ± 2 kWh kg^{-1} N, likely related to that the unstable pH, which was caused by the transport of hydroxide ions under the electric field, significantly decreased the amount of effective OH^-/H^+ for nutrient recovery.

To address this issue, the EMS was modified with an additional layer of cation exchange membrane in the present study. We hypothesized that this simple structure modification would prevent the acid-base neutralization, thereby allowing more acid/base to be used for nutrient separation and reducing energy consumption. The specific objectives of this study were to: 1) examine the feasibility and advantages of the present system to recover both P and N from actual digester centrate; and 2) evaluate the key factors affecting the nutrient recovery performance; and 3) perform a preliminary cost analysis to understand limitation of this system for further improvement.

4.2 Materials and methods

4.2.1 4C-EMS setup

The four-chamber EMS (4C-EMS) consisted of the anode, the wastewater, the cathode, and the absorption chambers (Fig. 4.1), with the same dimension of 6.5 cm × 12.5 cm × 0.95 cm (width × height × thickness) per chamber and separated by anion exchange membrane (AEM, Membranes International Inc., Ringwood, NJ, USA), cation exchange membrane (CEM, Membranes International Inc.), and hydrophobic GPM (Amersham Hybond, Germany), respectively. A commercial Ti/Ir-Ru plate (2 cm × 5 cm) was used as the anode electrode, and carbon cloth (CC,

2 cm × 10 cm) coated with 5 mg cm^{-2} Pt/C worked as the cathode electrode. A power supply provided a constant current (0 – 100 mA) across the anode and the cathode electrodes. Under an electric field, anions including PO_4^{3-} in wastewater will transport to the anode chamber and cations such as NH_4^+ and Na^+ will transport in an opposite direction to the cathode chamber where the generated OH^- can transform NH_4^+ to NH_3, which could then pass through GPM. Protons generated in the anode are transferred to the absorption solution, compensated with the additional acid to absorb ammonia. In this way, both ammonium and phosphate from wastewater can be separated and recovered. Digester centrate was collected from the Missouri River Wastewater Treatment Plant (St. Louis, MO) containing an ammonium concentration around 800 mg L^{-1} and a phosphate concentration of 60 -70 mg L^{-1} (detailed characteristics of digester centrate are listed in Table A3.1). The 4C-EMS was operated in batch mode: 150 mL fresh digester centrate was fed into the wastewater chamber, the initial anolyte and catholyte was deionized water (150 mL each), the adsorption chamber contained 150 mL 0.1 M H_2SO_4 or 150 mL anolyte from the previous operation cycle. All solutions were circulated at a slow flow rate of 2 mL min^{-1}.

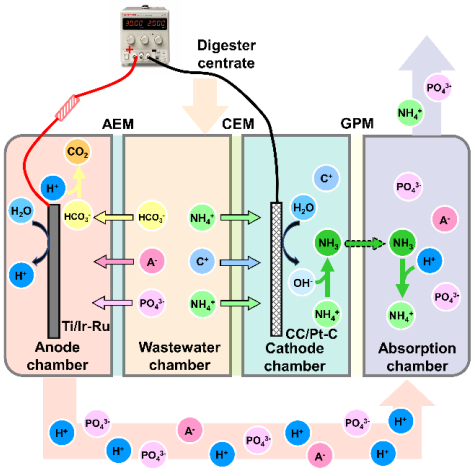

Figure 4.1 The schematics of the 4-chamber electrochemical membrane system. A^- represents anions except for phosphate. Ti/Ir-Ru refers to titanium plate electrode coated with iridium and ruthenium. CC/Pt-C refers to carbon cloth electrode coated with platinum and carbon.

4.2.2 Experiment design

The feasibility of the 4C-EMS was examined under varied current densities, 0, 0.68, 1.25, 2.5, 5.0, 7.5, and 10 mA cm^{-2}. The total charge being transferred during one operational cycle was kept the same when current density increased from 1.25 to 10 mA cm^{-2}, by changing the cycle time from 24 to 3 h. The cycle time was set at 24 h for the current density of 0 or 0.68 mA cm^{-2}. When cycle time was shorter than 24 h under the current density of 2.5 to 10 mA cm^{-2}, the circulation of peristaltic pump was not stopped until 24 h, to allow ammonia migration from the cathode chamber to the absorption chamber; that is, part of ammonia recovery was conducted without the applied electricity. Triplicate experiments were conducted under the current density of 1.25 to 10 mA cm^{-2}. To investigate the feasibility of the anode-produced acid as the adsorption solution, the anolyte of the previous cycle was used as the absorption solution of the next cycle. To compensate for the acid need, various extra acid dosage (equivalent mol H^+) was applied from 0, to 2.5, 5.0, and 7.5 mmol when the current density was controlled at 1.25 cm^{-2}.

To examine the stable nutrient recovery performance and cation distribution, the 4C-EMS was operated continuously for multiple cycles under the selected conditions (current density and extra acid dosage). The anolyte of the previous cycle was used as the absorption solution for the next cycle. To investigate the heavy metal, digester centrate was amended with 10 mg L^{-1} Cu and 10 mg L^{-1} Ni. Major cations (NH_4^+, Na^+, K^+, and Mg^{2+}) and heavy metals (Cu^{2+} and Ni^{2+}) were tested at the beginning and the end in the wastewater and acid absorption solution to evaluate the effectiveness of membrane separation.

For comparison in terms of energy consumption, a lab-scale membrane contactor was constructed, consisting of the wastewater (feed) chamber and the absorption chambers, with the same dimension of 6.5 cm × 12.5 cm × 0.95 cm per chamber and separated by hydrophobic GPM (Amersham Hybond, Germany). The membrane contactor was operated in a batch mode: the pH

of 150 mL fresh digester centrate was adjusted with 10 mM NaOH before being it was fed into the wastewater chamber, and the adsorption chamber contained 3.75 mmol H_2SO_4. The NH_4^+-N/PO_4^{3-}-P concentrations and pH in the wastewater and absorption chambers were measured during the operation.

4.2.3 Analyses and measurements

The current was monitored through measuring the voltage across 1-Ω external resistance by a multimeter (2700, Keithley Instruments Inc., Cleveland, OH, USA), and being determined according to Ohm's law. The solution pH was measured using a bench pH meter (Oakton Instruments, Vernon Hills, IL, USA). The conductivity was measured with a bench conductivity meter (Mettler Toledo, Columbus, OH, USA). The concentrations of cations and anions were measured using ion chromatography (Thermo Fisher Scientific, Waltham, MA, USA). The concentrations of Cu and Ni were tested using inductively coupled plasma mass spectrometry (NexION 2000, PerkinElmer, Downers Grove, IL, USA).

The removal efficiency and recovery efficiency of P and N was calculated according to Eq. (4.1) and Eq. (4.2):

$$Removal\ efficiency = \frac{(C_f V_f - C_0 V_0)}{C_0 V_0} \times 100\% \quad (4.1)$$

$$Recovery\ efficiency = \frac{(C_f V_f - C_i V_i)}{C_0 V_0} \times 100\% \quad (4.2)$$

Where C (mg L^{-1}) is the concentration of P and N, and V is the volume (mL) of electrolyte and acid absorption solution. Subscript f and i represent the finial and initial characteristics of anolyte, digester centrate, catholyte or acid absorption solution. While subscript 0 only refers to the initial characteristics of the digester centrate.

Specific energy consumption (SEC, kWh kg^{-1}) in this study was calculated according to Eq. (4.3):

$$SEC = \frac{UI_{\mathrm{avg}}t}{3.6(C_{\mathrm{f}}V_{\mathrm{f}} - C_{\mathrm{i}}V_{\mathrm{i}})} \quad (4.3)$$

where U (V) is the output voltage of power supply, I (A) the average current, t (s) the time of each cycle, C (mg L^{-1}) the concentration, V the volume (L) of the electrolyte, subscript i and f represent initial and final concentrations/volumes (energy consumption from pump circultation was ignored since it was much less than the electric energy consumption).

The amount of acid produced from the anodic water electrolysis was estimated based on the final pH of the anode according to Eq. (4.4)

$$N_{\mathrm{acid}} = 10^{-pH}V \quad (4.4)$$

Where N_{acid} is the effective amount of acid generated from electrolysis (mol), pH the final pH of anolyte measured at the ending moment of applying electricity, V the volume of anolyte solutions (L).

A preliminary cost analysis of nutrient recovery of 4C-EMS was calculated according to the electricity consumption of power supply, energy consumption of operating pumps and market prices of chemicals. The electricity consumption of power supply was determined from the SEC mentioned above. The energy consumption of operating pumps was calculated according to the method of a previous study (Wang et al., 2021). The prices of chemicals used for cost analysis was listed in Table A3.2.

4.3 Results and discussions

4.3.1 Feasibility of the proposed system

The 4C-EMS was started under a current density of 10 mA cm^{-2}. Within one hour, the anolyte pH decreased from 6.78 ± 0.85 to 2.53 ± 0.02 and the catholyte pH increased from ~7 to 11.37 ± 0.01,

indicating the successful generation of acid and base in each chamber. Meanwhile, the concentrations of NH_4^+-N and PO_4^{3-}-P in the wastewater chamber decreased from 825.7 ± 9.1 to 7.4 ± 2.9 mg L^{-1} and from 68.0 ± 0.3 to 10.5 ± 3.4 mg L^{-1}, respectively. The absorption chamber contained 768.6 ± 24.4 mg L^{-1} NH_4^+-N and the anode chamber had 81.9 ± 2.4 mg L^{-1} PO_4^{3-}-P. Therefore, the 4C-EMS effectively extracted nitrogen and phosphorus from digestion centrate for subsequent recovery.

To further examine the 4C-EMS performance, the applied current density was varied from 0 to 10 mA cm^{-2}. In the absence of an applied current or a very low current density of 0.63 mA cm^{-2}, the catholyte pH barely changed (Fig. A3.1). The proposed system showed good nitrogen removal/recovery performance at the current densities higher than 0.63 mA cm^{-2}: at the end of each cycle, more than 95% of ammonium was removed from the digester centrate (Fig. 4.2A). When current density increased from 1.25 to 10 mA cm^{-2}, the system achieved the similar NH_4^+-N concentrations after 24-h operation: 760.4 ± 28.1, 796.6 ± 9.2, 760.7 ± 3.2, 813.3 ± 2.4, 768.6 ± 24.5 mg L^{-1}, with recovery efficiency of 90.0~98.9% (Fig. 4.2B). This indicated that ammonia stripping could continue even without applying electricity as long as a basic catholyte was maintained. Reducing the period of electricity application would significantly decrease the energy consumption for ammonia recovery. The removal of phosphate was driven by electricity and the PO_4^{3-}-P concentration in the wastewater chamber decreased more quickly with the increased current density (Fig. 4.2C). Lacking electrical current kept the PO_4^{3-}-P concentration in the wastewater chamber over 60 mg L^{-1} and little phosphate was detected in the anode chamber (Fig. 4.2D). The P removal rate increased from 0.39 to 2.88 mgP h^{-1} when the current density increased from 1.25 to 10 mA cm^{-2}. The system maintained the P removal efficiency higher than 85% under all conditions (except no current was applied), because the total electrical charge applied to the

system was kept similar. However, that led to the different length of operation time, for example the higher current density, the shorter the operation time. This difference in operation time might have affected the P accumulation in the anode chamber, which was higher under a higher current density (Fig.4.2D). We inferred that adsorption to the anode electrode might occur due to a longer cycle time (increased from 3 h to 24 h) under a lower current density.

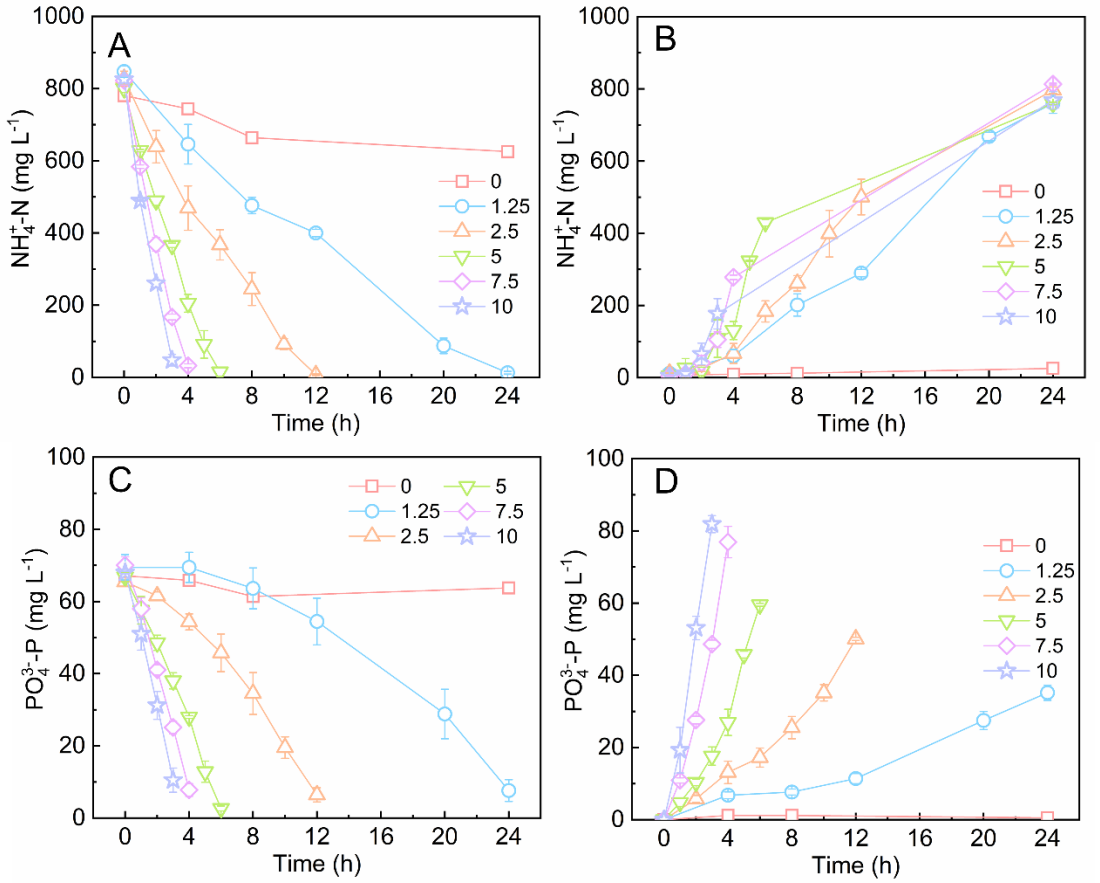

Figure 4.2 Recovery of both N and P in the 4C-EMS under different current densities: the NH_4^+-N concentration in the wastewater chamber (A) and the absorption chamber (B); the PO_4^{3-}-P concentration in the wastewater chamber (C) and the anode chamber (D).

The specific energy consumption to recover nitrogen and phosphorus was estimated under the tested current densities (Fig. 4.3A). The lowest energy consumption of 8.2 ± 0.2 kWh kg^{-1} N was achieved at the current density of 1.25 mA cm^{-2}. When the current density increased, more energy was consumed to recover NH_4^+-N, for example, 29.5 ± 0.6 kWh kg^{-1} N was needed under 10 mA

cm^{-2}, nearly four times of that under 1.25 mA cm^{-2}. As shown in Fig. 4.3B, both the energy consumption and recovery efficiency obtained in the present study were compared with those of other ammonia recovery processes, such as microbial electrolysis cells, capacitive deionization, membrane contactor, etc. (Arredondo et al., 2017; Desloover et al., 2015; Guo et al., 2023; Kuntke et al., 2017; Luther et al., 2015; Rodrigues et al., 2022; Zamora et al., 2017; Zhang et al., 2018b; Zhang and Angelidaki, 2015). One can see that the present study has relative low energy consumption among these studies, meanwhile achieving high ammonia recovery efficiency, indicating the potential advantages of the 4C-EMS for nitrogen recovery. The energy consumption for P recovery was estimated 178.0~278.8 kWh kg^{-1}P, comparable with the ED process to recover P from wastewater/sludge, which varies between 50 and 200 kWh kg^{-1}P (Wang et al., 2023; Ye et al., 2019). However, it should be emphasized that the present system used the same energy to recover both N and P, and this should be taken in consideration when comparing to the system that recovers only one of those nutrients. The current density of 1.25 mA cm^{-2} was selected for the subsequent experiments because of the lowest energy consumption and comparably good performance of nutrient removal/recovery.

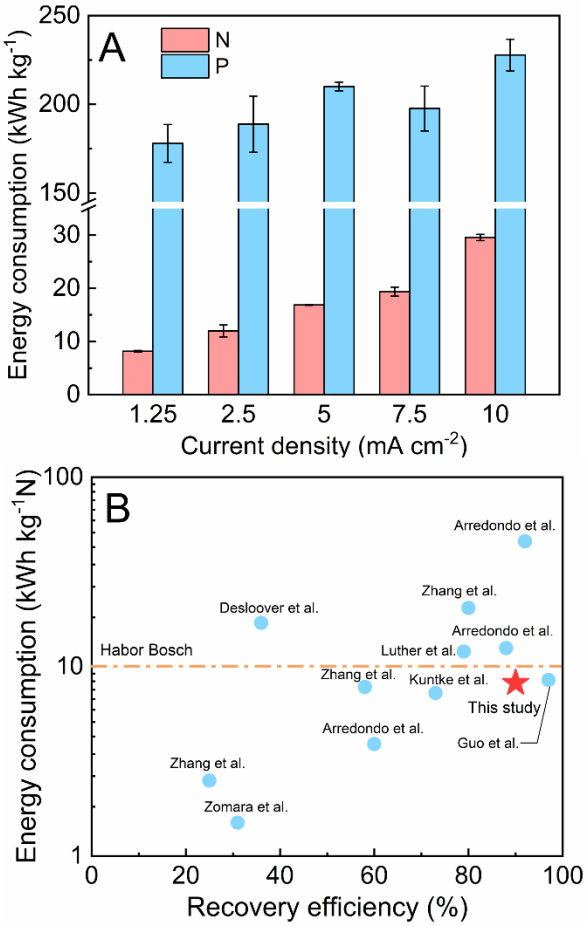

Figure 4.3 Energy consumption of the 4C-EMS: (A) specific energy consumption of recovering NH_4^+-N and PO_4^{3-}-P under different current density from 1.25 to 10 mA cm^{-2}; and (B) comparison of the specific energy consumption of recovering NH_4^+-N with literature.

4.3.2 Use of the produced acid for ammonia absorption

Ammonia recovery would typically need acid absorption. Because the anode of the proposed system generates acid as a part of the electrochemical reaction, the use of the anode-generated acid would further increase the benefit of the proposed system. It was observed that 38.2 ± 0.5 % of NH_4^+-N could be recovered using the anolyte as the absorption solution. The low recovery efficiency was likely related to the consumption of H^+ by HCO_3^- that is often present in digester centrate, thereby decreasing the availability of free H^+ to absorb NH_3. In theory, the generation of 1 mol of H^+ through water electrolysis will need 1 mol of electron to be transferred, coincidently

transporting 1 mol of cations (including NH_4^+ ions). Because of the presence of other cations, the amount of the generated H^+ is larger than NH_4^+ and thus theoretically should be enough to absorb ammonia if other H^+ scavengers like HCO_3^- are low. It is common that digester centrate contains a relatively large amount of alkalinity as a result of AD operation, which makes the anode-generated H^+ insufficient to absorb ammonia. Thus, extra acid would be needed.

When additional acid was added, an obvious increase of ammonia recovery efficiency was obtained (Fig. 4.4A). The ammonia recovery efficiency was almost doubled from 38.2 ± 0.5% to 76.2 ± 0.6% with 2.5 mmol of extra acid. It further increased to 98.2 ± 0.4% with 5 mmol of extra acid. However, no significant increase of recovery efficiency was found when acid dosage was higher at 7.5 mmol. The addition of extra acid did not obviously affect phosphorus recovery efficiency, which fluctuated around 80% (Fig. 4.4A). The amount of acid generated from water electrolysis was estimated according to the anolyte pH, for example 0.54 mmol H^+ at the pH of 2.44. It was estimated that the in-situ production of acid could compensate about 10~18% of the total acid used to absorb ammonia. A larger current density of 2.5 mA cm^{-2} could potentially provide 32% of the acid (at a lower anolyte pH of ~2.11), at the expense of higher electrical energy consumption. It is worth emphasizing that low acid concentrations (0.017 M H_2SO_4 with 5 mmol H^+ dissolved in 150 mL absorption solution) were used to absorb ammonia in this study, much less than other studies to recover ammonia with 0.1~1 M acid, reducing the chemical cost significantly (Ashrafizadeh and Khorasani, 2010; Hasanoglu et al., 2010). The specific energy consumption was closely related to nutrient recovery efficiency. As shown in Fig. 4.4B, the specific energy consumption was 21.4 ± 0.3 kWh kg^{-1} N without any extra acid, which decreased by 50% with extra acid being added because of more nutrient recovery. However, the specific energy consumption of the system between 5 and 7.5 mmol acid added was not significantly

different ($p>0.05$), at about 9 kWh kg^{-1} N, because of similar ammonia recovery efficiency. When specific energy consumption was normalized to P recovery, no obvious difference was obtained with the varied acid dosage.

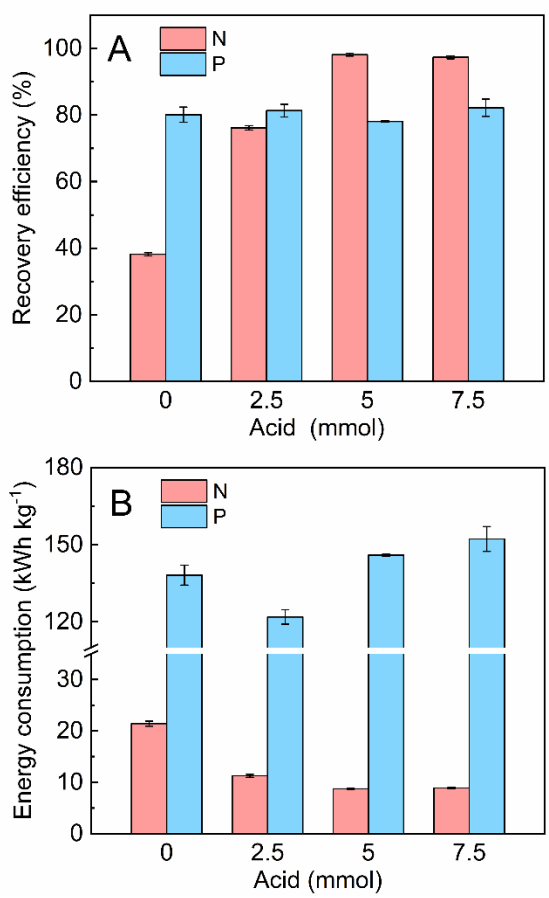

Figure 4.4 Nutrient recovery with varied acid dosages and under 1.25 mA cm^{-2}: (A) recovery efficiency (A); and (B) specific energy consumption of NH_4^+-N and PO_4^{3-}-P.

4.3.3 Cation distribution

Extended operation was conducted with multiple cycles under the selected conditions: 1.25 mA cm^{-2} current density and 5 mmol extra acid dosage and. The 4C-EMS exhibited a stable voltage profile (Fig. 4.5A): upon the feeding of fresh digester centrate, the voltage of the power supply to support the 4C-EMS was at 2.9 - 3.1 V, which started to increase with reaction time increasing. This increase was related to the increased internal resistance due to the transportation of ions from

the wastewater chamber to the anode/cathode chamber. The concentrations of major cations, including NH_4^+, Na^+, K^+, and Mg^{2+}, in both the digester centrate and absorption solution were shown in Fig. 4.5B. The initial NH_4^+-N concentration in the digester centrate was 791.7 ± 16.0 mg L^{-1}, over 98% of which was removed, resulting a remaining NH_4^+-N concentration in the wastewater chamber less than 15 mg L^{-1}. Meanwhile, an average NH_4^+-N concentration of 823.8 ± 50.3 mg L^{-1} was obtained in the absorption solution, demonstrating that most of the NH_4^+-N ions migrated from the digester centrate to the adsorption (recovery) solution. In addition, the 4C-EMS has effectively separated NH_4^+ from other cations. The concentrations of Na^+, K^+, and Mg^{2+} in the absorption solution were only 10.5 ± 2.2, 5.7 ± 1.6, and 9.7 ± 1.2 mg L^{-1}, respectively, which decreased by 93.1, 92.7, and 85.0% from their initial concentrations of 153.0 ± 4.9, 78.3 ± 7.8, and 64.5 ± 10.8 mg L^{-1} in the digester centrate. When the digester centrate was dosed with 10 mg L^{-1} Cu^{2+} and 10 mg L^{-1} Ni^{2+}, less than 0.1 mg L^{-1} of those heavy metals were detected in the absorption solution, representing the removal efficiency > 99%. We further investigated the effects of those heavy metals on struvite formation, a typical product from phosphorus recovery, by comparing between struvite precipitation from the digestion centrate directly and that from the 4C-EMS absorption solution. It was found that the struvite directly formed from the digestate centrate contained 48.5 mgCu kg^{-1} struvite and 62.1 mgNi kg^{-1} struvite. In the struvite formed from the adsorption solution, we detected 0.74 mgCu kg^{-1} struvite and 0.38 mgNi kg^{-1} struvite, 98% lower than the other struvite product. Those results have demonstrated that the 4C-EMS could prevent heavy metals from entering the final recovery products, thereby ensuring a comparably high quality of the recovered nutrients.

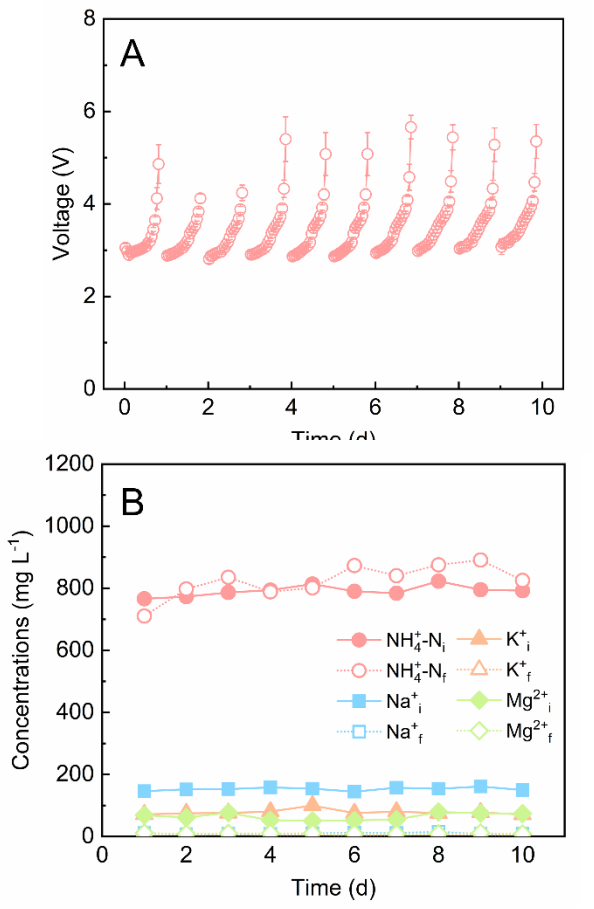

Figure 4.5 Cation distribution in the 4C-EMS: (A) voltage profile from the repeated operational cycles; and (B) major cation concentrations in wastewater and absorption solution. Solid legends refer to initial concentrations (subscript i) in wastewater, and hollow legends refer to final concentrations (subscript f) in absorption solution.

4.3.4 Preliminary economic analysis

The operational cost of the 4C-EMS was estimated based on the energy consumption and the market prices of electricity and chemicals, the unit prices of which used for calculation are listed in Table A3.2. The energy consumption was obtained from the experiments in Section 4.3.2 that examined various extra acid dosage under the current density of 1.25 mA cm^{-2}. In general, the operating cost includes chemicals (acid in the present study), applied electricity (power supply), and electrical energy for pumping. The energy consumption of pumping was calculated according to the method of a previous study (Wang et al., 2021) and was estimated to be less than 5% of the applied electricity; thus, it could be neglected for the purpose of cost estimation and the following

analysis will focus on applied electricity and acid cost. The price of sulfuric acid used for calculation varied between \$0.03 ~ \$0.50 kg^{-1}. In the absence of extra acid, the operating cost was dominated by the applied electricity and was estimated about \$1.29 kg^{-1}N (or \$1.06 kg^{-1} NH_3), shown as the horizontal solid line in Fig. 4.6A. When the acid price is lower than 0.23 kg^{-1}, the lowest cost was achieved when applying 5 mmol extra acid. Although adding extra acid increase the cost of chemicals, more N could be recovered in the acid absorption solution. With the same amount of electricity energy being consumed, the SEC of N decreased, and thus the electricity cost to recover 1 kg N decreased correspondingly. However, the extra acid dosage would no longer be cost effective compared with no extra acid when the acid price is higher than \$0.45 kg^{-1} (extra acid dosage of 2.5 mmol), \$0.39 kg^{-1} (5 mmol), or \$0.14 kg^{-1} (7.5 mmol).

The contributions of acid and electricity to the overall cost was further analyzed at a fixed acid price of \$0.15 kg^{-1} (Fig. 4.6B). Without extra acid, 100% of the operational cost was resulted from the electricity consumption; its contribution decreased to 77%, 64%, and 52% with the increased acid dosage from 2.5 to 7.5 mmol. The lowest cost was 0.83 kg^{-1} N (0.68 kg^{-1} NH_3) with 5 mmol acid dosage, indicating adding extra acid (e.g., a higher dosage of 7.5 mmol) would not always help to decrease the total cost. The estimated cost for N recovery can be comparable to or even lower than the market price of ammonia in the United States, for example \$0.61 kg^{-1} NH_3 in November 2023 (https://businessanalytiq.com/procurementanalytics/index/ammonia-price-index/). This low cost, plus the simultaneously recovered phosphorus, could potentially make the 4C-EMS an attractive approach for nutrient recovery from wastes.

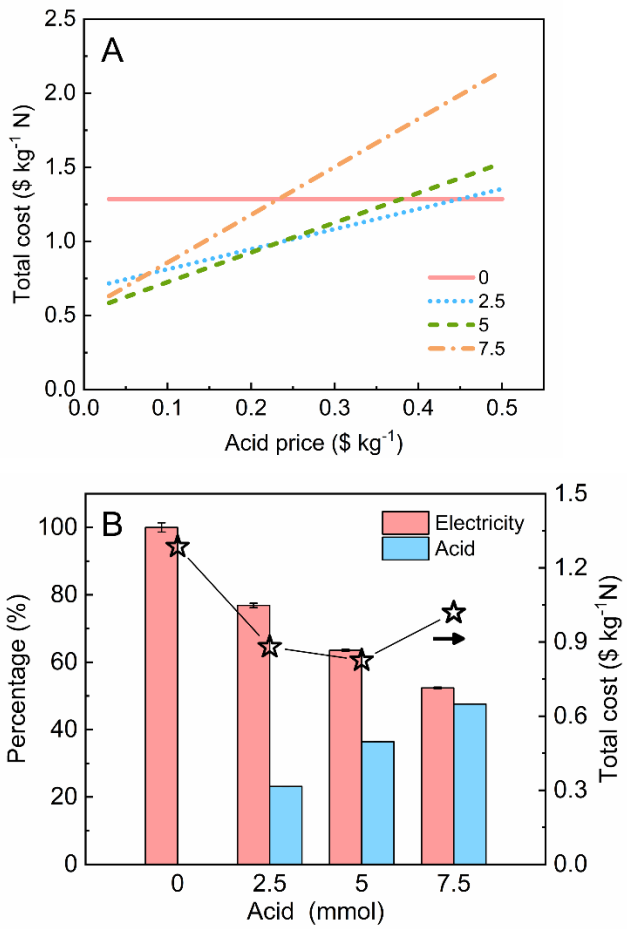

Figure 4.6 Preliminary cost analysis: (A) effects of acid price on the total cost of N recovery; and (B) contribution of applied electricity and acid cost (left y-axis) to the total cost (right y-axis) with various extra acid dosage (0, 2.5, 5, and 7.5 mmol) at a fixed acid price of \$0.15 kg^{-1}.

The cost analysis was extended to a comparison with nitrogen recovery in a membrane contactor that had the same chamber size and membrane area. The 4C-EMS was similar to a membrane contactor in terms of nitrogen recovery process, except that the base and part of acid used for ammonia absorption was generated *in situ* from electrolysis. The membrane contactor decreased the NH_4^+-N concentration in the digester centrate from 770.8 to 11.1 mg L^{-1} and achieved the NH_4^+-N concentration of 797.5 mg L^{-1} in the absorption solution after 24-hour operation (Fig. A3.3). Unlike the 4C-EMS, the membrane contactor could not recover phosphorus and thus the P concentration did not change. The estimated operation cost of the membrane contactor, based on

the chemical cost, was \$1.28~1.57 kg^{-1} N (\$1.06~1.29 kg^{-1} NH_3), much higher than that of the 4C-EMS. This result further demonstrated the potential benefit of the 4C-EMS for nutrient recovery.

4.3.5 Perspectives

The 4C-EMS was capable of simultaneous nitrogen and phosphorus recovery from the real digester centrate with high recovery efficiency. However, some limitations will need to be addressed to evolve this technology to be applicable. First, the high alkalinity (HCO_3^-) in the real digester centrate has consumed a large number of protons produced from the anodic electrolysis; that would increase the demand for extra acid to achieve ammonia recovery. Such an effect might be less serious when the 4C-EMS is used to treat wastewater with less alkalinity like domestic wastewater or digester centrate that is mixed with other wastewater. In addition, removing HCO_3^- from the digester centrate in pretreatment through precipitation with cations (such as Ca^{2+}, Mg^{2+}) would also help, but the trade-off between the cost of extra cations and extra acids needs to be investigated. Second, we propose that the H_2CO_3 formed in the anolyte from protons and bicarbonate may be used to absorb the ammonia through circulating the solution between the anode chamber and the absorption chamber. In this way, less CO_2 would be escaped from the system and be utilized as the "acid". However, the oxidation of ammonia catalyzed by the active chlorine species transformed from Cl^- in the anode may occur. Whether this will decrease the amount of recovered ammonia significantly warrants further investigation. Third, long-term experiment and operation of the 4C-EMS would help to evaluate the system stability and study the fouling of ion exchange membrane/GPM. To alleviate the membrane fouling, we may consider inverting the polarity of the power supply to generate protons in the initial cathode chamber, which will dissolve some inorganic precipitates formed under a basic pH in the previous operation cycle. Last but not least, the present study was conducted in bench-scale, which needs to be further scaled up. The design

of large-scale system may be assisted with kinetic model to correlate acid/base production rates and nutrient recovery performance with electric parameters (such as current, potential, etc.). A large-scale system will allow us to perform more detailed cost analysis including the cost of materials and profits from the recovery products.

4.4 Conclusions

This study has demonstrated an innovative technology through coupling electrolysis with membrane for nutrient recovery. Compared to the previous design, the addition of cation exchange membrane helped maintain the pH in different chambers that increased recovery efficiency and decreased energy consumption. The results showed that the produced acid could be used for absorption but to achieve a high recovery efficiency, extra acid would be required. A preliminary economic analysis revealed that the operating cost was controlled by acid dosage/price and electricity cost; that provides guidance to further reduction of energy consumption. Future development of the present system towards practical applications would need to address a few challenges identified in this study and through a long-term operation.

Chapter 5: Electron transfer kinetics at anode interface in microbial electrochemical systems

This chapter has been published in *Electrochimica Acta*, 2022, 432, 141188.

Abstract

Microbial electrochemical system (MES) is favored by its wide applications for wastewater treatment but demands a better understanding of its reaction kinetics for system development. Herein, we have performed Tafel analysis to understand the anodic reaction kinetics in MES. In addition to use the widely adopted Butler-Volmer-Monod model, we applied the Marcus-Hush-Chidsey (MHC) model with fewer adjustable parameters to understand the anodic kinetics. After fitting the data at three months of cultivation, where the current production reached the apex that indicated the maturation of the biofilm, our results showed that MHC curves match better with a multi-electron transfer mechanism than with an one-electron transfer mechanism. The experiment and fitting results agree better at three and five months, indicating that MHC model is only applicable to the anode with fully cultivated biofilms. Additionally, the reorganization energy determined from fitting with the MHC model is in the range from 5 to 10 under various transferred electron number with mature biofilm, consistent with the theoretical estimation. The good fitting performance of MHC model was also supported by the low root mean square errors of 7.4-22.9%. This work provides new insights to the reaction kinetics in MES and paves the way for the accurate systematic modeling works towards MES development.

5.1 Introduction

Microbial electrochemical system (MES) has received extensive attention in recent years due to its advantages to realize sustainable wastewater treatment with low energy consumption and sludge yield (Logan et al., 2006; Palanisamy et al., 2019). In MES, anode respiring bacteria (ARB) play a major role in decomposing organic contaminants in wastewater, transferring electrons to a solid anode and generating an electric current. Recent studies have significantly improved the performance of the MES by optimizing the reactor structure and operating conditions, which can effectively treat various wastewaters such as municipal wastewater, industrial wastewater, source-separated urine, etc. in both lab- and pilot-scale (He et al., 2017; He et al., 2019).

Despite the considerable progress in experiments, theoretical studies for understanding the reaction mechanisms of MES are still at the early stage (Santoro et al., 2017; Shi et al., 2016). Mathematical models can be used to identify the key parameters to optimize the performance of MES, as well as guide the design and operation of the system (Gadkari et al., 2018; Patel and Deb, 2018; Xia et al., 2018). Current generation is one of the most important characteristics in MES because it directly affects the MES performance, such as power output and substrate consumption. The precise modeling and prediction of the current output will contribute to solving large-scale problems economically by saving time and effort (Garg and Lam, 2017; Raychaudhuri and Behera, 2020). Since current generation is closely related to the kinetics of the electron transfer among substrate, biofilm, and electrodes, characterization and analysis of the kinetics of redox reactions in MES is of great significance. The electron transfer process that happens in the anode of an MES can be divided into two stages: intracellular and extracellular electron transfer (IET and EET). IET describes the process from substrate utilization, through intracellular electron transport chain to membrane-bound cytochromes, which will initiate EET subsequently. Three mechanisms have

been proposed for EET, namely direct electron transfer, electron shuttles, and solid conductive mechanisms (Torres et al., 2010). However, studies have suggested that the first two mechanisms could only achieve limited current density as a result of the inability of anaerobic respiratory bacteria to form large enough biofilm and the diffusion limitation of the mediators (Bond and Lovley, 2003; Lee et al., 2009). In order to describe the anodic kinetics in MES, Nernst-Monod model was put forward by assuming IET, which is highly associated with the dynamic substrate concentration, as the limiting step. However, a clear deviation of the fitting results from the experiment data was identified at the low overpotentials where the concentration gradient of the substrate can be negligible (Torres et al., 2008). Instead, in most of the operating conditions when enough substrate and circulation are provided, the EET becomes the rate-limiting step (Torres et al., 2010).

Butler-Volmer (BV) model is conventionally applied to depict the electron transfer process at the electrode interface of the EET process. The simplified model at high overpotentials, i.e. Tafel equation, is widely adopted to obtain the charge-transfer coefficient and the exchange current density that are used for evaluating the performance of the materials. However, the fitting curve would not always accurately match the kinetics (Liao et al., 2015; Lowy et al., 2006; Yuan et al., 2007). Therefore, when investigating anode reactions involving the complex charge transferring process, more sophisticated models are needed to help us understand the kinetics more accurately. Butler-Volmer-Monod (BVM) model, which is an extensively used model to character charge transfer process in MES, combines biochemical oxidation of a substrate and electron transfer to the electrode interface together with BV model and mass balance equations. Although the good fitting performance was validated, BVM model contains excessive adjustable parameters that can lead to overfitting (Hamelers et al., 2011; Radeef and Ismail, 2021). Is there an alternative kinetic

model applicable to describe the charge transfer at the anodic interface in MES? Based on the study from non-bioelectrochemical systems, the Marcus-Hush-Chidsey (MHC) model that considers the microscopic molecular interaction effect, can be used to more accurately model the electron transfer process at a complex electrode interface in a wide range of overpotential (Henstridge et al., 2012). But its application in MES is rarely discussed.

As a motivation, we made a comparison of the fitting capabilities between BV, BVM, and MHC models using the experimental data collected from literature (Hamelers et al., 2011), which reveals a similar fitting performance of MHC as BVM but with much lesser adjustable parameters. Then, for a detailed study of the application of MHC to the MES systems, a two-chamber MES was constructed to investigate the anodic kinetics of charge transfer reaction by performing Tafel analysis, which is a widely adopted method to extract the reaction kinetic parameters based on the current density and the reaction overpotential (Imran et al., 2019; Raghavulu et al., 2013). To ensure the reaction-limited conditions, the effect of substrate concentration was ruled out by providing sufficient substrate and circulation of the electrolytes and each data point was collected at a kinetic-controlled steady state. The fitting performance of MHC model was discussed based on data collected at different times during the 5-month cultivation period.

5.2 Materials and methods

5.2.1 Reactor construction and start-up

As shown in Fig. 5.1, a two-chamber MES was constructed with the same size of the anode and the cathode chamber (12.5 cm × 6.6 cm × 1.9 cm). An anion exchange membrane (AEM) was used to separate the two chambers. The anode electrode was a piece of carbon cloth (length: 12 cm, width: 6 cm), which is a common electrode material in MES field and can provide enough surface area for microbes to grow. Microbes utilized the organics and provided electrons to the anode. An

Ag/AgCl reference electrode was inserted in anode. The cathode was also a piece of carbon cloth with the same size but coated with 5 mg cm^{-2} Pt/C as catalyst. Both the anode and cathode were fixed with titanium wire and connected with an external resistor.

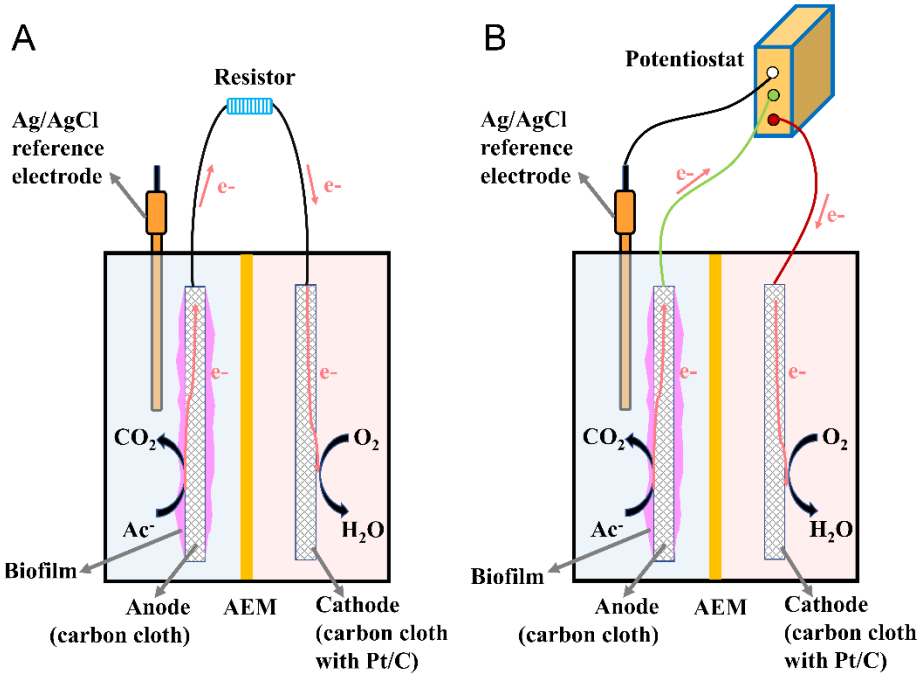

Figure 5.1 Schematic of microbial electrochemical system during (A) cultivation stage, and (B) electrochemical-tests (chronopotentiometry and electrochemical impedance spectroscopy) stage, where anode is working electrode and cathode is counter electrode. AEM: anion exchange membrane, Ac-: acetate.

Sodium acetate was used as the electron donor in the anode, and continuous aeration in the catholyte provided enough oxygen as the electron acceptor. The two half reactions happened in the MES are listed below:

$$\text{anode: } CH_3COO^- + 4H_2O \rightarrow 2HCO_3^- + 9H^+ + 8e^- \quad (5.1)$$

$$\text{cathode: } O_2 + 4H^+ + 4e^- \rightarrow 2H_2O \quad (5.2)$$

The MES was first inoculated with anaerobic digester sludge collected from Missouri River Treatment Plant (St. Louis, MO, USA). In addition to the 1 g L^{-1} sodium acetate as the substrate for microbes, 0.15 g L^{-1} NH_4Cl, 0.02 g L^{-1} $CaCl_2$, 0.015 g L^{-1} $MgSO_4$, 0.1 g L^{-1} $NaHCO_3$, 0.5 g L^{-1} NaCl and 1 mL/L trace elements were added to provide important growth elements. 20 mM phosphate buffer solution (PBS) was used to maintain stable pH in the anode. Similarly, 20 mM PBS was also used as the catholyte. During the start-up process, each chamber of the MES was circulated with 1 L electrolyte stored in a plastic bottle with a peristaltic pump. Half of the anolyte were renewed every day to provide adequate substrate for microbes to utilize. Catholyte was renewed completely every five to seven days. After three weeks, the MES can achieve good electricity generation with current density and power density of 0.52 A m^{-2} and 14.4 W m^{-3}, respectively.

5.2.2 Electrochemical testing

The overpotential data was obtained from chronopotentiometry test within the micro- to mili-ampere range that is consistent with the typical current output. Ten current points (twelve points for 3-month data due to larger current generation during cultivation) were chosen accordingly on the logarithmic plot. Considering two sides of the carbon cloth electrode, the projected electrode area was determined to be 144 cm^2 for the current density calculation. Four sets of data at 1 week, 1 month, 3 month and 5 months were collected after the startup of MES. Before each test, the system was rested for at least 2 hours at open circuit potential.

5.2.3 Analyses and measurements

Scanning electron microscopy (SEM) (Thermofisher Quattro S environmental SEM) was used to monitor the shape of carbon cloth and the biofilms grown on the carbon cloth at the end of the experiment. Carbon cloth was collected from the MES after five months, and transferred into 2.5%

glutaraldehyde solution to fix for 4 h at 40 °C. Then the samples were rinsed three times with deionized water and dehydrated in a series of ethanol solutions with increasing concentration (30%, 50%, 70%, 80%, 90 % and 99.9% ethanol) for 10 min each.

The output voltage of the MES during the start-up process was measured with a multimeter (2700, Keithley Instruments Inc., Cleveland, OH, USA). Both the chronopotentiometry and electrochemical impedance spectroscopy (EIS) tests were completed with a potentialstat (600+, Gamry, Warminster, PA, USA).

5.2.4 Models for fitting

BV, BVM, and MHC model were applied to perform Tafel analysis. Eq. 5.3 describes the BV model.

$$j = j_0\{exp[\alpha\tilde{\eta}] - exp[(\alpha - 1)\tilde{\eta}]\} \tag{5.3}$$

where j (A m^{-2}) is the current density, j_0 (A m^{-2}) the exchange current density, α the charge transfer coefficient, $\tilde{\eta} = n(E\text{-}E^0)/k_BT$ the normalized kinetic overpotential, n the stoichiometric number of the transferred electron, k_B Boltzmann constant, T (K) the temperature, E (V) the anode potential at selected current density, and E^0 (V) the anode potential at open circuit.

Eq. 5.4 describes the BVM model.

$$j = j_{max}\left\{\frac{1 - exp(-\tilde{\eta})}{K_1 \exp[(\alpha - 1)\tilde{\eta}] + K_2 \exp(-\tilde{\eta}) + K_3}\right\} \tag{5.4}$$

where j (A m^{-2}) is the current density, j_{max} (A m^{-2}) the maximum current density, K_1, K_2 and K_3 are three lumped parameters.

Eq. 5.5 describes the MHC model.

$$j = \mathrm{A} \int_{-\infty}^{+\infty} exp\left\{-\frac{\left(x - \tilde{\lambda} \pm \tilde{\eta}\right)^2}{4\tilde{\lambda}}\right\} \frac{dx}{1 + exp(x)} \tag{5.5}$$

where $\tilde{\lambda}$ is a dimensionless parameter, representing the reorganization energy scaled to k_BT (k_B is Boltzmann constant and T (K) is thermodynamic temperature). A is the pre-exponential factor with the unit A m^{-2}. And x is the integral variable accounting for a specific electron energy in the Fermi statistics. The stoichiometric number of the transferred electron was taken as 1 to fit the data collected from the literature, and the effect of n will be discussed in section 5.3.3.

5.3 Results and discussions

5.3.1 Comparison of different kinetic models in describing experimental data

The three kinetic models were applied to fit the experimental data taken from the literature introducing the BVM model (Hamelers et al., 2011) As shown in Fig. 5.2, while the conventional BV model describes well for the low overpotentials, the data clearly deviates from the BV prediction for overpotentials larger than $5k_BT \approx 154$ meV. The charge transfer coefficient α was 0.37. This implicates the general macroscopic outer-sphere electron transfer model is invalid in this heterogeneous charge-transfer system. Fig. 5.2 showed that BVM provides good fit to the data using the parameters of 2.8 A m^{-2}, 0.47, 7.2, 21.2, and 1.2 for j_{max}, α, K_1, K_2, and K_3, respectively. The difference between our fitting results and those listed in (Hamelers et al., 2011) is attributable to the different initial values. Note that for BVM, there exist multiple parameter sets to properly fit the data. MHC curves show a similar trend as BVM model while slightly overpredict the current densities at low overpotentials. As a microscopic physical model with only two adjustable kinetic parameters, the good agreement of MHC model with the experimental data motivated us to further investigate the applicability of this model in MES.

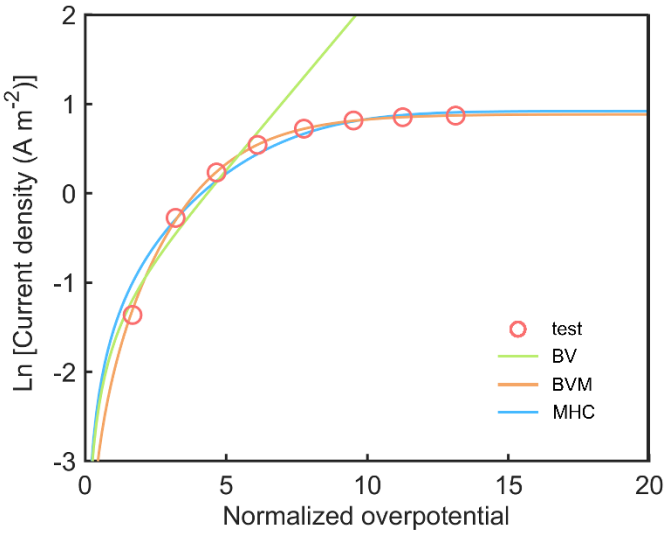

Figure 5.2 Comparison among Butler-Volmer, Butler-Volmer-Monod, and Marcus-Hush-Chidsey model based on experiment data extracted from Fig. 2B in (Hamelers et al., 2011).

5.3.2 Determination of the reaction overpotential

The overall overpotentials at each current density were obtained by subtracting the steady-state voltage value by the open circuit potential. Each data point was repeated by three times and Fig. 5.3A is one of the triplicate chronopotentiometry tests at one week. More detailed chronopotentiometry results are shown in Fig. A4.1. Interestingly, the average overpotentials at the same controlled currents decrease from 1 week to 3 months, and then increase from 3 months to 5 months (Fig. 5.3B). The initial decrease of the overpotential is attributable to the gradual maturing of the biofilm. However, the biofilm aged and lost good charge transfer capability from 3 months to 5 months. Above all, the overpotentials at 3 months are the lowest compared with other times, indicating the best performance of power generation in our study.

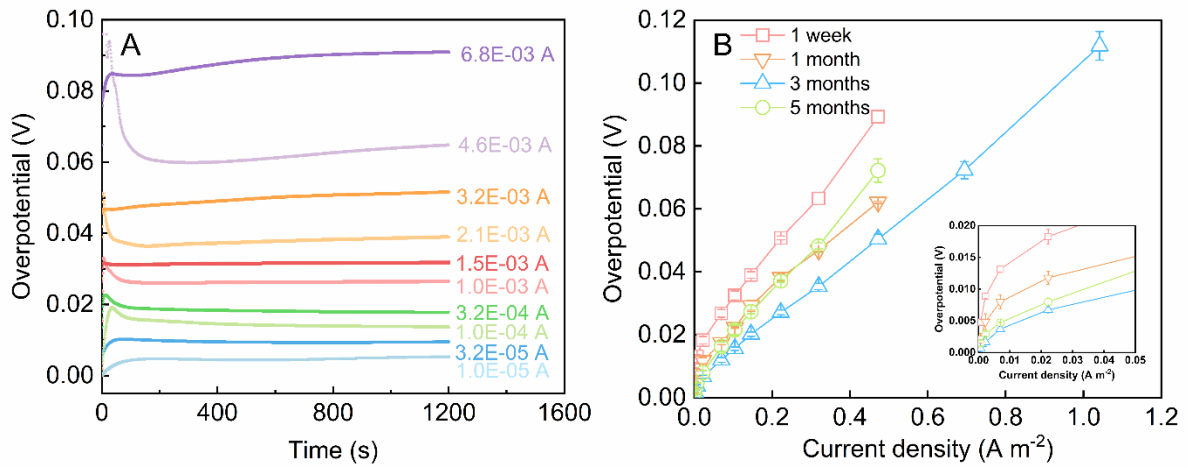

Figure 5.3 (A) Chronopotentiometry curve of MES at one week; (B) The change of overpotentials at selected current densities from 1 week to 5 months.

Since the system is reaction-controlled at these low current densities and the concentration variation at the surface of the electrode is negligible, the kinetic overpotential can be directly obtained after the bulk IR compensation, where the bulk ohmic resistances are determined by EIS with the frequency range of 10^{-3} to 10^{6} Hz (Fig. 4). The Nyquist plot clearly reveals a semicircle at low frequencies for all cases that is attributable to the charge transfer process through the interface. The smaller arcs at high frequency range might relate to the impedance of biofilms (Song et al., 2020). However, we could not prove it with convincing calculation yet. This may be verified in well-designed control experiments but is beyond the scope of this study, as the negligible differences do not affect the fitting results of charge transfer kinetics at anode. The fitting results are shown in Table A4.1 with the equivalent circuit showed in Fig. 5.4A. With their characteristic frequencies at their apexes (0.01259, 0.03983, 0.01259, 0.01413 Hz) and the fitted diameter of the semicircle as the resistance across the interface, their capacitances are calculated to be 0.58, 0.69, 1.04, and 1.02 F, respectively, according to Eq. (5.6)

$$C = \frac{1}{2\pi R f} \tag{5.6}$$

where C is the capacitance, R is the resistance and f is the frequency at the apex. The dielectric constant (ε) of the interface can then be calculated using Eq. (5.7).

$$C = \frac{\kappa \varepsilon_0 \varepsilon A}{d} \tag{5.7}$$

Assuming the interfacial capacitance comes from the double layer, the thickness of the double-plate capacitor (d) can be determined based on the diameter of the adsorbed acetate ions that is 0.150 nm (estimated with Avogadro software). The factor κ of 2 is applied considering the meshy and rugged surface of the carbon cloth (Fig. A4.2), yielding the total surface area A = 288 cm^2. With the vacuum permittivity ε_0, the dielectric constants ε are calculated to be 54, 65, 98, and 96, respectively, which are close to the dielectric constant of water (ε = 78) as the solution for the acetate. The ohmic resistances are then determined to be 1.73, 0.76, 1.05, and 1.36 Ω, respectively (Table A4.1) for the IR compensation.

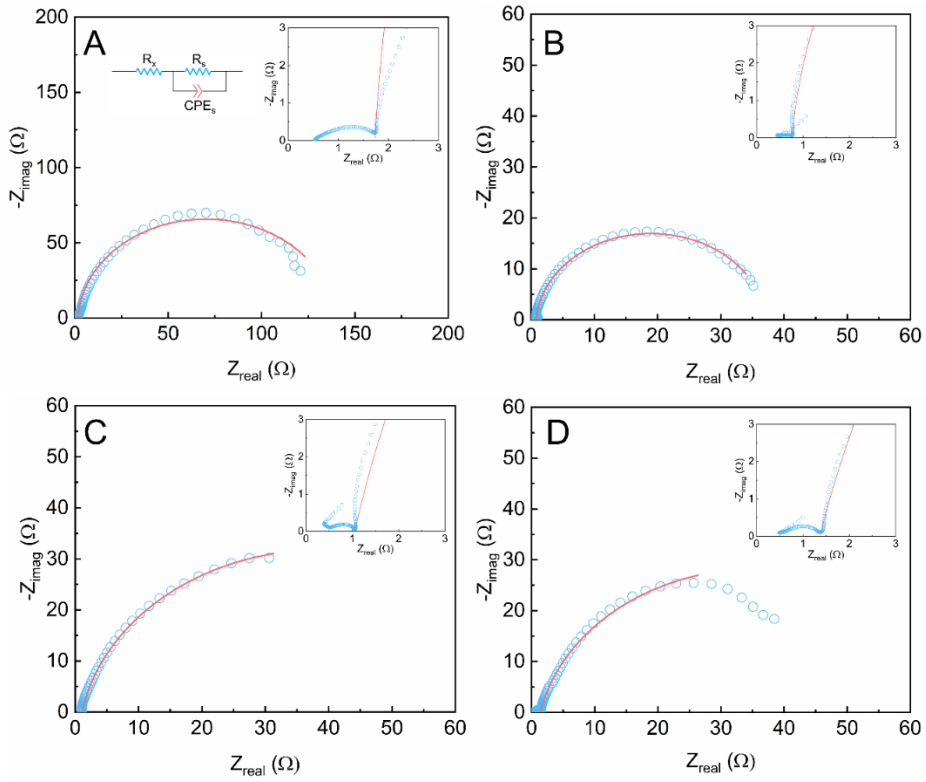

Figure 5.4 Electrochemical impedance spectroscopy (EIS) results of the microbial electrochemical system at (A) one week, (B) one month, (C) three months, and (D) five months. Blue circles are test data, and red lines are fitting curves. The inserted figures at the upper right corner are enlarged figures of EIS results. The equivalent circuit used for EIS fitting is at upper left of the first figure. R_x is the real resistance of the start point of the semicircle on Nyquist plot. R_s is the fitting diameter of the semicircle. CPE is constant phase element of the semicircle.

5.3.3 Electron transfer number of the limiting reaction step and Tafel analysis

MES showed the largest current density around 3 months. Therefore, kinetic analysis based on the 3-month data was conducted first. The overpotentials were first modified through IR compensation and then normalized with Eq. (5.8).

$$\tilde{\eta} = \frac{n\eta}{k_B T} \tag{5.8}$$

Where n is the stoichiometric number of the transferred electron, η (V) the overpotential after IR compensation, k_B Boltzmann constant, T (K) the temperature. $\tilde{\eta}$ the normalized overpotential.

While the complete oxidation of one mole of acetate at the anode involves 8 moles of electron, n is undetermined since the reaction is composed of several steps where the number of electron transfer of the limiting step is unclear (Butler et al., 2010; Coppi et al., 2007). Our experimental data were fit via MHC model and BVM model starting from n=1 to n=8 (Fig. 5.5) where the fitting parameters are listed in Table 5.1 and Table A4.2. Note that as the electron number n increases, the normalized overpotential at the same current density increases subsequently. When the electron number is 1, although the fitting curve of MHC model is close to the experiment result at high overpotential, the curve overpredicts the current density at low overpotential range. As the electron number increased to 2 and 4, MHC model showed better fitting performance than one-electron transfer, although there is still a little deviation at low overpotential range. When electron number is 8, the fitting curve of MHC model fit starts to deviate from the experimental data at high-overpotentials, but still have good fitting performance at low-overpotentials. As shown in Fig. 5.5, BVM showed great fitting results under all four cases. However, it was found that the fitting parameters changed significantly when different initial values were selected. Therefore, we would not discuss the fitting results of BVM model in detail in this study.

We also estimate the dimensionless reorganization energy (scaled to k_BT) by the Born energy of solvation:

$$\tilde{\lambda} \approx \lambda_0 = \frac{e^2}{8\pi \mathrm{k}_B T}\left(\frac{1}{a_0} - \frac{1}{2d}\right)\left(\frac{1}{\varepsilon_{op}} - \frac{1}{\varepsilon_s}\right) \tag{5.9}$$

Where ε_0 is the vacuum permittivity, k_B the Boltzmann constant, T the thermal dynamic temperature, a_0 the effective radius of the reactant, d the distance of the reactant to the electrode surface, ε_{op} the optical dielectric constant (ε_{op} = 1.78 determined from first-principle calculations) and ε_s the static dielectric constant (ε_s=78 in water). The electron is assumed to transferred from

the outer-membrane proteins (such as cytochromes), which typically have radius about 1~3 nm (Aivaliotis et al., 2003; Erickson, 2009). The d can be assumed to be much larger than a_0 if EET is through conductive matrix mechanism (Torres et al., 2010). So the $\tilde{\lambda}$ is theoretically estimated to be 5~15, and the parameters according to the MHC model have values belonging to this range.

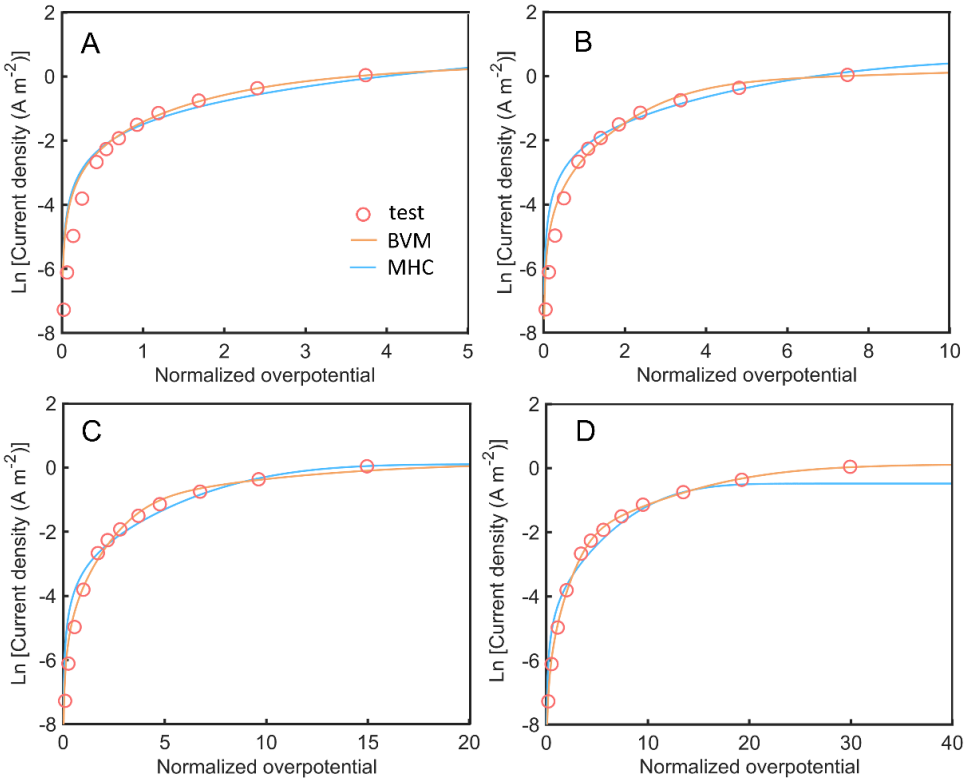

Figure 5.5 Comparison of the fitting curves based on Marcus-Hush-Chidsey model (blue line), Butler-Volmer-Monod model (orange line) and the test data (red circle) at 3 months when the stoichiometric number of the transferred electron equals to (A) 1, (B) 2, (C) 4, and (D) 8.

Table 5.1 Fitting results Marcus-Hush-Chidsey model with various transferred electron number based on data of 3 months.

Electron number n -	Pre-exponential factor A A m^{-2}	Reorganization energy $\tilde{\lambda}$ -
1	0.33	5
2	0.20	6
4	0.11	8
8	0.06	10

The remaining experiment data at different cultivation times was also examined with MHC model and BVM model considering various electron transfer number (n=1, 2, 4 and 8), as shown in Fig. A4.3-A4.5. Besides, all the fitting parameters got from MHC model are listed in Table A4.2-A4.3. Similar to the fitting results of 3-month data, when the electron transfer number was 1, the fitting curves deviated from the experiment data, especially when the overpotential is small. The better fitting results of 3 and 5 months than 1 week and 1 month were likely related to the maturity of biofilm growing on the anode electrode.

The fitting results of MHC model were further evaluated quantitively by calculating their root mean square errors (RMSE) (Luo et al., 2016) listed in Table 5.2. Generally, the MHC model has good fitting performance because most of the RMSE were lower than 20%. The RMSE were the lowest when MHC model was applied to fit the experiment data at 3 months, indicating the formation of mature biofilm would affect the applicability of MHC model to analyze the kinetics in the anode of MES. Interestingly, the RMSE decreased with the electron transfer number. Therefore, fitting with MHC model at relatively larger overpotential would be more accurate to conduct Tafel analysis.

Table 5.2 Root mean square errors (RMSE) of the fitting results for Marcus-Hush-Chidsey (MHC) model.

Electron number (n)	1 week %	1 month %	3 months %	5 months %
1	22.9	20.3	13.1	16.3
2	22.0	18.9	12.9	15.1
4	17.1	16.1	10.4	12.3
8	10.9	11.0	7.4	8.2

5.3.4 Discussions

According to the fitting results of all the experiment data with various electron transfer number, the $\tilde{\lambda}$ is in the range of $5k_BT \approx 129$ meV to $14k_BT \approx 360$ meV. To reach a good agreement with

the experimental data, $\tilde{\lambda}$ need to be increased when a higher number of transferred electrons is assumed. For example, $\tilde{\lambda}$ increased from 129 meV to 257 meV with the electron transfer number increasing from 1 to 8 to fit the 3-month experiment data. As for the fitted pre-exponential factor, which can be an indicator of the exchange current density, decreased from 0.33 to 0.06 A m^{-2}. Here, the anode surface area we applied to calculate the current density were simplified as double the projective area of the carbon cloth. However, when we monitored the morphology of the clean carbon cloth and the carbon cloth collected from the anode after five months, the surface of the anode was actually larger than flat and smooth surface (Fig. A4.2). Therefore, the real current densities would be smaller than those we applied to do model fitting, but hard to be accurately quantified. Nevertheless, all the currents were divided by the same area, the shape of the Tafel plots would not change indeed, and thus the fitting results of reorganization energy in MHC model will also not be affected.

The flexibility of fitting the same Tafel plot with different combinations of reorganization energy and electron transfer numbers reflects that the charge transfer kinetics in MES is intrinsically more complex than that in simple electrochemical systems like a monolayer electrode. However, it appears that MHC model can be applied to fit the Tafel plot if appropriate electron transfer number is selected. MHC model is advantageous over BV model, which is conventionally utilized to conduct Tafel analysis in MES, because the fitting curves of MHC model coincide more accurately with the experiment data. On the other hand, BV model is included in the BVM model to describe the charge transfer kinetics at electrode interface. Therefore, we propose that MHC model could substitute BV model as a fundamental equation of BVM model when considering the effect of reactant concentrations and analyzing the overall kinetics in MES. Moreover, to overcome the disadvantage of the MHC model that the complicated integration had to be included when using

MHC model, the simplified MHC model that have already been used in battery system could also be applied in the MES to save effort and time, as well as increase the precision of model fitting in the future.

5.4 Conclusions

The reaction kinetics of MES were rigorously studied in this work. Inspired by the good fitting performance of MHC model on the data collected from literature, a two-chamber MES was constructed and the anode overpotentials at selected current densities were monitored to understand the applicability of MHC to analyze Tafel plot in MES. When one-electron transfer mechanism is used, MHC could only fit the data at high overpotential range, but the model's performance can be improved if changed to multi-electron transfer mechanism. However, it is still mysterious the exact electron number is involved at the biofilm-electrode interface in MES. The true mechanism needs further investigation in the future. This study proposes to use MHC model for MES for the first time and proved the advantages of this advanced kinetic model for Tafel plot analysis.

Chapter 6: The kinetics of acid/base production in electrochemical membrane system

Abstract

Electrochemical membrane system (EMS) can recover nitrogen and phosphorus simultaneously with low cost from digester centrate by taking advantage of the in-situ acid/base produced from water electrolysis. However, the kinetics of acid/base production lacks detailed investigation. Herein, an empirical model by coupling Marcus-Hush-Chidsey (MHC) model and polynomial regression to describe the relationship between acid/base production rate with the overpotential, aiming to estimate the kinetics of reactions under various wastewater components and operating conditions. When EMS was fed with synthetic anaerobic digester (AD) centrate, good fitting performance was achieved with MHC model with errors less than 10%. Moreover, the R-square values were over 0.99 when polynomial regression was used to fit both the anode and cathode half reactions. The coupled model showed decent prediction values when real AD centrate was fed into EMS, and the fitting performance could be further improved if the bicarbonate concentration was included to modify the model, indicating the effectiveness of our model to estimate the kinetics of electrochemical processes, which was the production rate of acid/base used for nutrient recovery in this study.

6.1 Introduction

Nowadays, energy crisis is one of the most important challenges for mankind and needs to be addressed with sustainable strategies (Albert, 2021). The utilization of renewable energy such as wind, solar power, hydrogen, etc. is considered as effective solution for alleviating energy crisis and reducing the greenhouse gases released to the environment (Kannan and Vakeesan, 2016; Qazi et al., 2019). Although expanding the application of renewable energy is of urgent priority, several bottlenecks need to be concerned, including the management of energy storage and transportation, the improvement of energy efficiency, and abatement of energy cost. Hydrogen is one of the most promising clean and sustainable energy carriers, because it only emits only water as the product of and carries no carbon. Additionally, it has high energy density, making it superior to traditional fuels. Hydrogen can be generated from a variety of sources, such as fossil fuels, biomass, and water (Ursúa et al., 2012).

Water electrolysis to generate hydrogen has the advantages to play a critical role in future energy cycle due to the two energy carriers: electricity and hydrogen (Carmo et al., 2013; Veeramani et al., 2023). This is because the renewable energy sources, mainly solar, wind, and hydropower, could be coupled with the water electrolysis processes easily to produce sustainable hydrogen. Meanwhile, protons and hydroxide are also formed during water electrolysis process, and the utilization of such byproducts from water electrolysis adds up the economic advantages of water electrolysis. For example, previous study used the acid generated from anode through water electrolysis to absorb the ammonia gas transported across the gas permeable membrane from cathode, and achieved good nutrient recovery performance with low cost (Liu et al., 2024). The optimization of water electrolysis involves a few aspects: the electrode structure, the alternative power sources, the transport of reactants and products, and the type of electrolyzers (Hu et al.,

2022). However, the afore-mentioned studies usually focused on experimental aspects, the mathematical models of water electrolysis are also helpful to understand and optimize this process for broader applications.

The water electrolysis process is usually analyzed according to the current-voltage relationship, where empirical models can be applied to describe the electrode kinetics. In addition, Butler-Volmer model can also be used to describe the overpotentials of anode and cathode with the current, where the exchange current density and charge transfer coefficient are two parameters to model the electrode kinetics (Dickinson and Wain, 2020; Nudehi et al., 2018; Shen et al., 2011). Recently, the analysis of electrode kinetics based on Marcus theory is receiving increasing attentions (Anderson, 2017; Rajan and Carter, 2020). Moreover, some studies considered the effect of various physical parameters including temperature, mass transfer, flow pattern and electrochemical processes to set up multiphysics modeling in different types of water electrolyzers (Chen et al., 2020; Hammoudi et al., 2012; Lin et al., 2022). These studies helped to give guidance to optimize the water electrolysis systems and direct laboratory studies based on the modeling results. However, most studies about the kinetics of water electrolysis processes are usually analyzed together with hydrogen evolution, the generation of protons and hydroxide and their usage for nutrient recovery are often neglected when modeling the kinetics of water electrolysis.

In this study, an electrochemical membrane system (EMS) was operated under a variety of constant current densities to get the Tafel profile of both anodic and cathodic half reactions. We hypothesize that the electrode kinetics of the water electrolysis will follow the Marcus-Hush-Chidsey (MHC) theory, similar to other electrochemical systems, and the electrode kinetics can be used to simulate the production rate of acid and base. The specific objectives of this study were to: 1) acquire the Tafel plot to be modeled with MHC model with synthetic anaerobic digester (AD) centrate; 2)

connect the production rate of acid/base in the EMS with the electrode kinetics through statistical regression; 3) examine the feasibility of the model when real AD centrate was used.

6.2 Materials and methods

6.2.1 Reactor construction

As shown in Fig. 6.1, a four chamber MES was constructed with the same size of the anode chamber, wastewater chamber, cathode chamber, and the acid absorption chamber (12.5 cm × 6.6 cm × 1.9 cm), separated by anion exchange membrane (AEM, Membranes International Inc., Ringwood, NJ, USA), cation exchange membrane (CEM, Membranes International Inc.), and hydrophobic GPM (Amersham Hybond, Germany), respectively. A commercial Ti/Ir-Ru plate (2 cm × 5 cm) was used as the anode electrode, and carbon cloth (CC, 2 cm × 5 cm) coated with 5 mg cm^{-2} Pt/C worked as the cathode electrode. A power supply provided a constant current across the anode and the cathode electrodes. This system has similar structure as that in Chapter 4, with two additional Ag/AgCl reference electrodes inserted next to the anode and cathode, respectively, for measuring the electrode potential. Herein, the two half reactions happened in the EMS are listed below:

$$\text{anode: } 2H_2O \rightarrow 4H^+ + O_2 + 4e^- \quad (6.1)$$

$$\text{cathode: } 4H_2O + 4e^- \rightarrow 4OH^- + 2H_2 \quad (6.2)$$

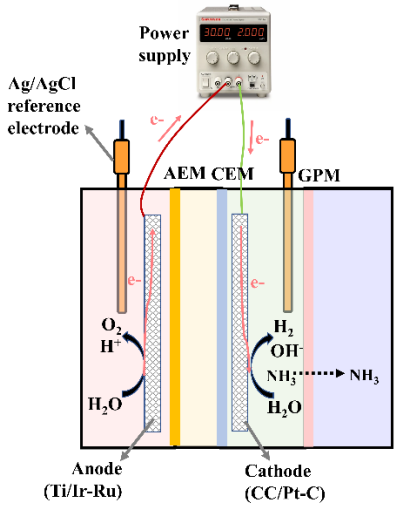

Figure 6.1 The schematics of the electrochemical membrane system. AEM refers to anion exchange membrane. CEM refers to cation exchange membrane. GPM referes to gas permeable membrane. Ti/Ir-Ru refers to titanium plate electrode coated with iridium and ruthenium. CC/Pt-C refers to carbon cloth electrode coated with platinum and carbon.

6.2.2 Operation

The EMS was operated under constant current density: 1.25, 2.5, 5, 7.5, and 10 mA cm^{-2}. The cycle time under each current density was 24, 12, 6, 4, and 3 h under each current density, 150 mL synthetic digester centrate with 3.77 g L^{-1} $(NH_4)_2SO_4$ (equal to 800 mg L^{-1} NH_4^+-N, in consistence with previous experiment) was used in the wastewater chamber to avoid the influence of complicated ion components in the real AD centrate. In this way, we could correlate the accumulation of acid/base in the electrolytes with the kinetics of electrochemical reactions more precisely. 150 mL deionized water was used as the initial anolyte and catholyte. While acid solution was replaced with 150 mL deionized water as well to decrease the transport of NH_3 across the gas permeable membrane, in order to restrict the escape of NH_3 and accumulate more OH^- in the catholyte. All solutions were circulated at a slow flow rate of 2 mL min^{-1}. After establishing models of acid/base production rate under various current density with synthetic AD centrate, real AD centrate was applied in the EMS to further investigate the model performance under selected current densities.

6.2.3 Analyses and measurement

The anode potential, cathode potential, and output voltage of power supply was recorded with a multimeter (2700, Keithley Instruments Inc., Cleveland, OH, USA). During each cycle, samples of anolyte, wastewater, and catholyte were collected multiple times to acquire more precise change of their characteristics including pH, conductivity and ion components. The solution pH (anolyte, catholyte, and synthetic AD centrate) was measured using a bench pH meter (Oakton Instruments, Vernon Hills, IL, USA). The conductivity was measured with a bench conductivity meter (Mettler Toledo, Columbus, OH, USA). The concentrations of cations and anions were measured using ion chromatography (Thermo Fisher Scientific, Waltham, MA, USA).

The rate of acid/base produced from the water electrolysis was estimated based on the pH of the anolyte and catholyte according to Eq. (6.3) and (6.4)

$$r_{\text{acid}} = \frac{10^{-pH}V}{t} \tag{6.3}$$

$$r_{\text{base}} = \frac{10^{pH-14}V}{t} \tag{6.4}$$

Where r_{acid} and r_{base} are the average production rate of acid/base generated from water electrolysis (mol s^{-1}), pH is the pH of anolyte and catholyte measured at selected moment of applying electricity, V is the volume of anolyte and catholyte solutions (L), t is the time of water electrolysis (s).

The overpotentials were calculated according to Eq. (6.5) and then normalized with Eq. (6.6).

$$\eta = E - E_0 - \frac{RT}{nF} ln \frac{[Red]}{[Ox]} \tag{6.5}$$

$$\tilde{\eta} = \frac{n\eta}{\mathrm{k}_B T} \tag{6.6}$$

Where n is the stoichiometric number of the transferred electron, η (V) the overpotential, E_0 the standard electrode potential of a half reaction (1.23 V for anode half reaction and 0 V for cathode half reaction), k_B is the Boltzmann constant, T (K) the temperature. $\tilde{\eta}$ is the normalized overpotential. Considering the pH of anolyte and catholyte were close to 2 and 11, respectively, most of the time, pH of 2 and 11 were applied to get the concentrations of protons and hydroxide in Eq. (6.5) to estimate the overpotential.

Eq. (6.7) describes the MHC model.

$$j = \mathrm{A} \int_{-\infty}^{+\infty} exp\left\{-\frac{\left(x - \tilde{\lambda} \pm \tilde{\eta}\right)^2}{4\tilde{\lambda}}\right\} \frac{dx}{1 + exp(x)} \tag{6.7}$$

where $\tilde{\lambda}$ is a dimensionless parameter, representing the reorganization energy scaled to k_BT. A is the pre-exponential factor with the unit mA cm^{-2}. And x is the integral variable accounting for a specific electron energy in the Fermi statistics. j (mA cm^{-2}) is the constant current density controlled by the power supply.

Linear regression and polynomial regression are used to correlate the acid/base production rate to the current density and then coupled in the empirical functions to determine the production rate according to the measured electrode potentials.

6.3 Results and discussions

6.3.1 Acid/base production

The EMS was operated under current densities from 1.25 to 10 mA cm^{-2}. The anolyte pH quickly decreased to 3 and below within one hour. For example, the anolyte pH decreased from ~7 to 2.18 in the first hour, which further decreased to 1.90 and 1.74 in two hours and three hours, respectively when current density was 10 mA cm^{-2} (Fig. 6.2A). At the end of electrolysis, the final pH of anolyte

was 1.92, 1.92, 1.91, 1.78, and 1.74 when the current density increased from 1.25 to 10 mA cm^{-2}. Meanwhile, the catholyte pH also showed a sharp increase in the first hour from ~7 to over 10.2, indicating the successful generation of base in the cathode chamber (Fig. 6.2B). When the cycles ended, the final pH of catholyte was 10.25,10.68, 10.90, 10.95, and 11.14 when the current density increased from 1.25 to 10 mA cm^{-2}. With the intense sampling of both anolyte and catholyte, the short-term change of pH was able to describe a detailed profile of the production of acid and base under various current densities and helped to determine the kinetics of electrochemical reactions.

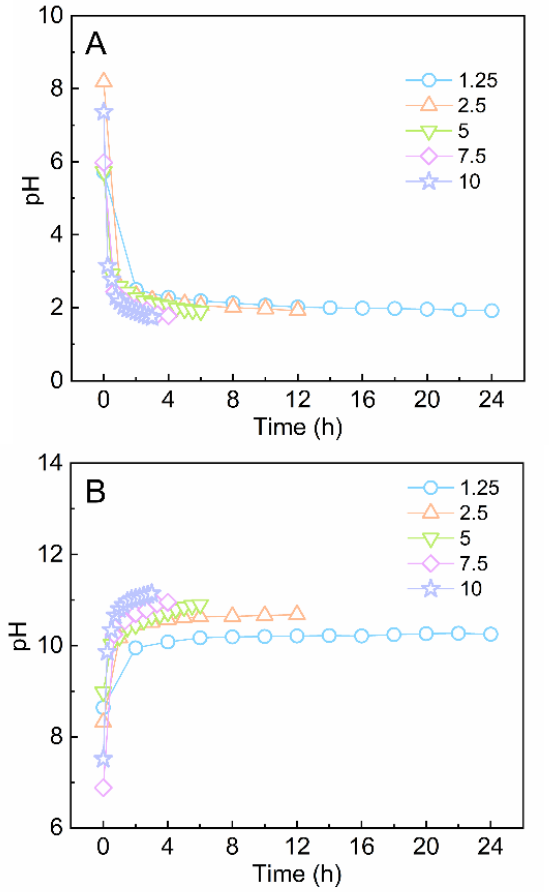

Figure 6.2 The change of pH throughout the cycle under current density from 1.25 to 10 mA cm^{-2} in the (A) anolyte, and (B) catholyte with synthetic digester centrate as initial wastewater.

The pH data in Fig. 6.2 was then used to be interpreted as the concentrations of protons and hydroxides and their corresponding production rates according to Eq. (6.3) and (6.4). The detailed results are summarized in Fig. 6.3. Generally, the concentrations of both protons and hydroxide kept a steady increase rate with a linear line showed in Fig. 6.3, especially when the current density was larger than 5 mA cm^{-2}. In Fig. 6.3A, the average acid production rate increased almost 11 times with the current density from 2.09×10^{-8} mol s^{-1} at 1.25 mA cm^{-2} to 2.53×10^{-7} mol s^{-1} at 10 mA cm^{-2}. Thus, the current density played a significant role to determine the protons generation in the anode chamber. Under the other conditions, the acid production rates were 4.17×10^{-8}, 8.54×10^{-8}, 1.73×10^{-7} mol s^{-1}, which were 8.3, 4.1, and 2.0 times of the rate at 1.25 mA cm^{-2}. Fig. 6.3B showed that the production rate of hydroxide in the cathode chamber followed a similar trend as acid production. When current density was 1.25 mA cm^{-2}, the hydroxide production rate was low with an average value of 3.01×10^{-10} mol s^{-1}. The hydroxide production rate increased to 1.65×10^{-9}, 5.45×10^{-9}, 9.28×10^{-9} mol s^{-1}, and 1.92×10^{-8} mol s^{-1}, which were 5-64 times of the rate at the lowest current density. The production rate of hydroxide was also far lower than the production rate of protons. We inferred that the association of NH_4^+ with hydroxide decreased the amount of free hydroxide ions in the cathode, which determined the pH of catholyte.

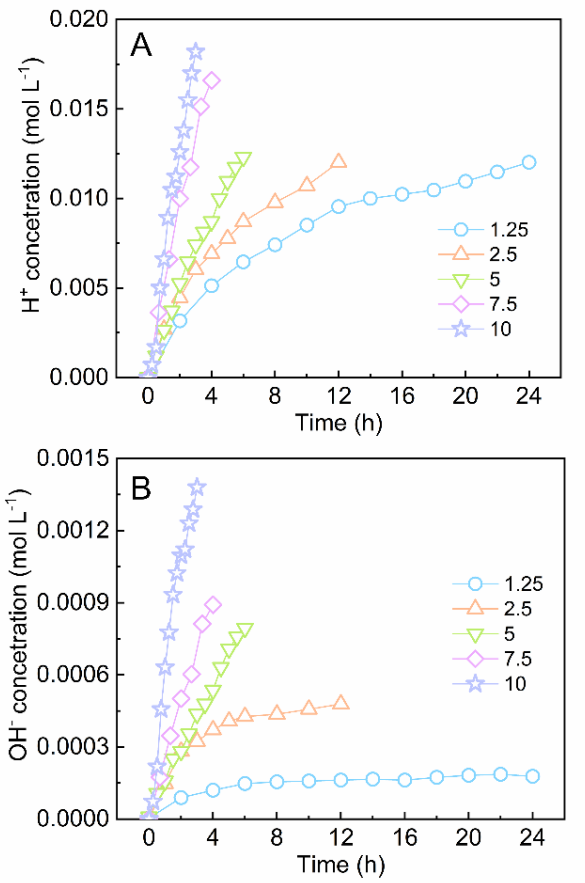

Figure 6.3 The change of H^+ and OH^- concentrations throughout the cycle under current density from 1.25 to 10 mA cm^{-2} in the (A) anolyte, and (B) catholyte with synthetic digester centrate as initial wastewater.

6.3.2 Modeling the reaction kinetics

Tafel analysis was conducted according to the electrode potentials measured at controlled current densities from 1.25 mA cm^{-2} to 10 mA cm^{-2}. Considering the pH of anolyte and catholyte were around 2 and 11, respectively, the potentials were modified with Eq. (6.5) and used to calculate the normalized overpotentials according to Eq. (6.6). MHC model was applied in Tafel analysis to model the kinetics of the electrochemical reaction to produce protons and hydroxides. The results of Tafel analysis were shown in Fig. 6.4. MHC model showed good fitting performance for both the anode (Fig. 6.4A) and the cathode (Fig. 6.4B) half reactions. As a result, the fitting parameters of anode half reaction were 13 and 1.26×10^{-5} mA cm^{-2} for the dimensionless reorganization

energy $\tilde{\lambda}$ and the pre-exponential factor A in Eq. (6.7). Meanwhile, the fitting parameters of cathode half reaction were 7 and 1.99×10^{-5} mA cm^{-2} for the dimensionless reorganization energy $\tilde{\lambda}$ and the pre-exponential factor A, respectively. The fitting results of applying MHC model were further evaluated quantitively by the root mean square errors (RMSE), which were 8.0% and 4.3% for the anode and cathode, indicating good fitting performance could be achieved with MHC model for Tafel analysis in EMS when synthetic AD centrate was used.

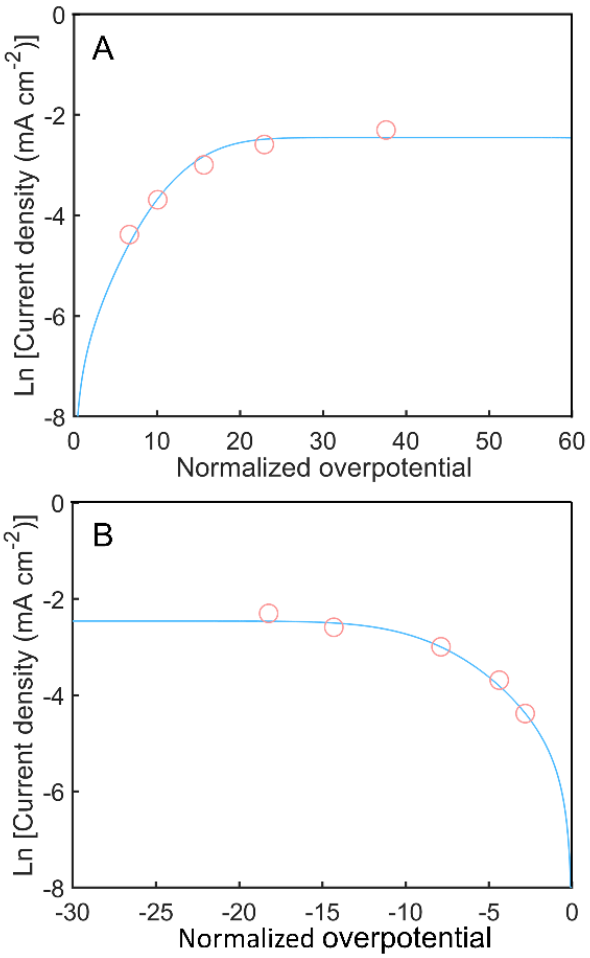

Figure 6.4 The fitting curves based on Marcus-Hush-Chidsey model (blue line) and the test data (red circle) of the (A) anode and (B) cathode.

How the production rates of protons and hydroxides can be related to the overpotentials? In fact, we already found that the production rates were affected by the current density according to the

results in Section 6.3.1, but a mathematical model should be applied to describe the relationship between production rate and current density. In this way, an empirical mathematical model to determine the production rate of acids and bases can be achieved. Both linear regression and polynomial regression were applied to set up the statistical relationship between production rates of acids/bases and current densities. The regression results are presented in Fig. 6.5 and Fig. 6.6.

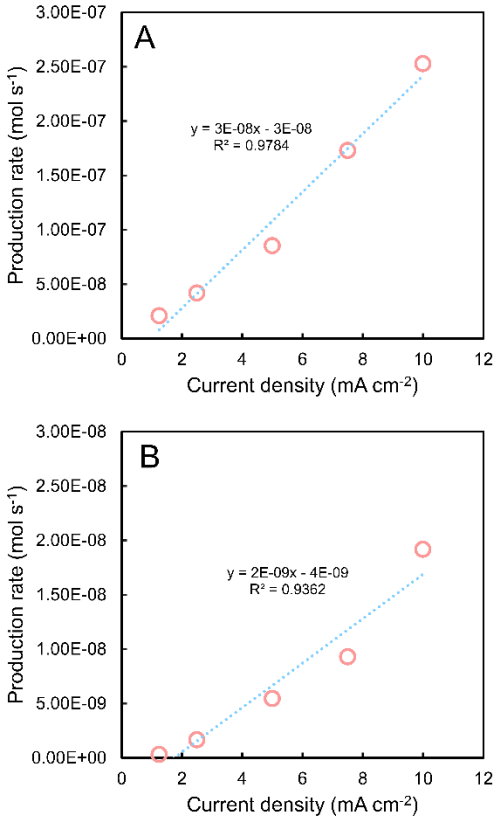

Figure 6.5 The linear regression results between current density and (A) production rate of acids, (B) production rate of bases. The blue dotted lines are the fitting curves and the red circles are the measured data.

Overall, the linear regression could depict the general trend in terms of the increase of production rate with the increase of current density. As shown in Fig. 6.5A, the R-squared value was 0.9784, indicating a strong relationship between the production rate of protons and the current density.

Linear regression also showed good fitting performance of the cathode reaction, with a R-squared value of 0.9362 (Fig. 6.5B). As a comparison, polynomial regression was further conducted with the same measured data, and the fitting results were shown in Fig. 6.6. Generally, the fitting performance was improved because the R-squared increased to 0.9965 and 0.9896, respectively, for the fitting of acid and base production rate with current density. The results of polynomial regression were chosen due to its better fitting performance than linear regression, and the combination of the fitting results of Tafel analysis and polynomial regression could establish an empirical function which used the measured overpotential to estimate the production rate of acid/base.

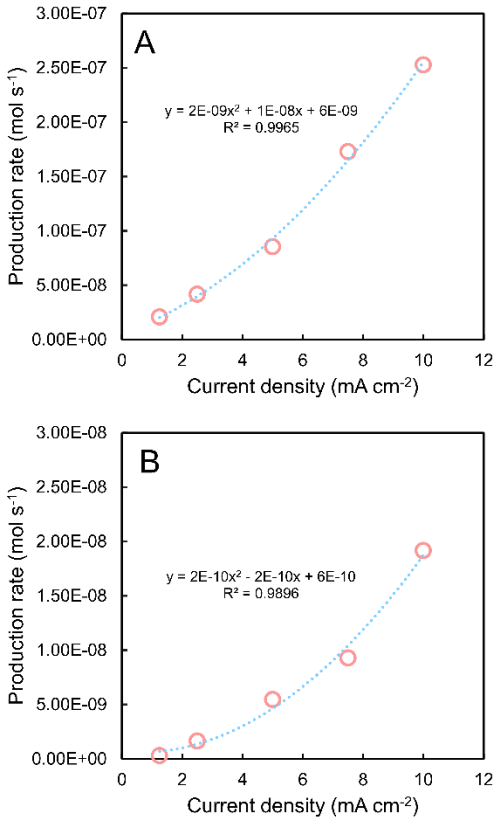

Figure 6.6 (A) The polynomial regression results between current density and the production rate of acids, (B) the polynomial regression results between current density and the production rate of bases. The blue dotted lines are the fitting curves and the red circles are the measured data.

6.3.3 Model validation

After establishing the mathematical model to using the measured overpotential to estimate the production rate of acid and base with synthetic AD centrate, which combined the MHC model and the polynomial regression of production rate and current density, the wastewater was changed to real AD centrate to validate the model performance. Similarly, the EMS was operated under the same constant current densities. The pH change throughout the cycles was monitored and then was converted to the production rate of acid and base according to Eqs. (6.3) and (6.4). More detailed information of the concentrations of acid and base was shown in Fig. 6.7. The normalized overpotentials of anode and cathode under various current densities were calculated according to Eqs. (6.5) and (6.6), and the results are listed in Table 6.1.

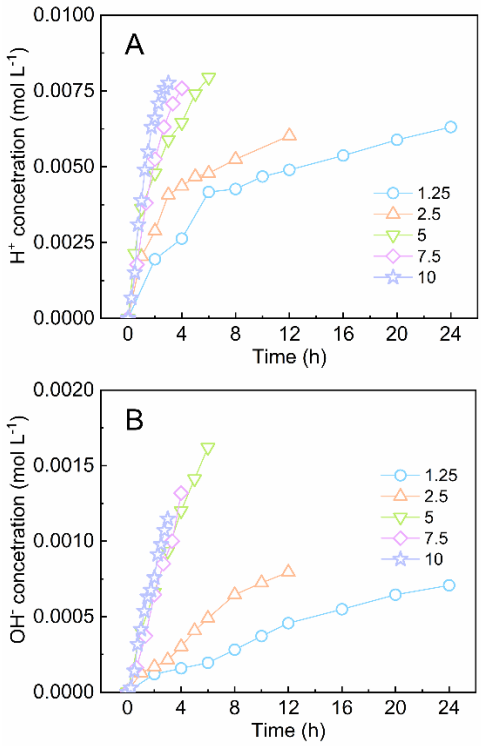

Figure 6.7 The change of H^+ and OH^- concentrations throughout the cycle under current density from 1.25 to 10 mA cm^{-2} in the (A) anolyte, and (B) catholyte with real digester centrate as initial wastewater.

Table 6.1 Normalized overpotentials under various current densities with real digester centrate as initial wastewater

Current density mA cm^{-2}	Anode normalized overpotential -	Cathode normalized overpotential -
1.25	8.65	-4.37
2.5	11.58	-6.55
5	17.74	-11.48
7.5	25.51	-19.17
10	42.52	-32.48

Then, the normalized overpotential was applied in the models established in section 6.3.2 to calculate the prediction values of acid and base production rate under various current density. The detailed results of the prediction values are presented in Table 6.2. Overall, the model worked well to predict the base production rate when the wastewater was changed to real digester centrate. The percent errors of predicted values from the measured values were 7.1, 4.0, 12.1, 2.2, and 15.6%, indicating the successful application of the mathematical model to estimate the kinetics of base production in the cathode chamber of EMS when real AD was used. However, the prediction of the acid production in the anode chamber was not accurate. As shown in Table 6.2, the models overpredicted all the acid production rates under all current densities, which were 2-3 times of the measured acid production rate. We inferred that the large errors to predict the acid production rate in the anode chamber were due to the consumption of acid by the bicarbonate transported from the real AD centrate, and decrease the acid concentrations accumulated in the anolyte which were calculated from pH measurement.

Table 6.2 Comparison of the measured acid/base production rate with the model predicted acid/base production rate.

Current density mA cm^{-2}	Measured acid production rate mol s^{-1}	Predicted acid production rate mol s^{-1}	Measured base production rate mol s^{-1}	Predicted base production rate mol s^{-1}
1.25	1.10×10^{-8}	3.07×10^{-8}	1.22×10^{-9}	1.14×10^{-9}
2.5	2.09×10^{-8}	6.35×10^{-8}	2.74×10^{-9}	2.85×10^{-9}
5	5.52×10^{-8}	1.73×10^{-7}	1.13×10^{-8}	9.89×10^{-9}
7.5	8.66×10^{-8}	2.36×10^{-7}	1.37×10^{-8}	1.34×10^{-8}
10	1.08×10^{-7}	2.40×10^{-7}	1.59×10^{-8}	1.34×10^{-8}

The bicarbonate concentration was around 870 mg L^{-1} in the real AD centrate, and it is assumed that all the bicarbonate could transported from the wastewater chamber to the anode chamber. It is also assumed that 1 mol bicarbonate would consume 1 mol protons at acidic environment, thus the amount of acid used by the bicarbonate could be estimated. Another assumption was that the acid consumed by the bicarbonate at a stable speed, so the average acid consumption rate should be added to the measured acid production rate to get the modified acid production rate. Based on the above assumptions, the modified acid production rates were 3.57×10^{-8}, 7.04×10^{-8}, 1.54×10^{-7}, 1.86×10^{-7}, and 2.07×10^{-7} mol s^{-1}, respectively. After modification, the percent errors decreased to 14.1, 10.0, 12.3, 23.4, and 16.3% when current density was 1.25, 2.5, 5, 7.5, and 10 mA cm^{-2}.

6.3.4 Perspectives

This study successfully established the empirical models which combined the MHC model and regression model to estimate the production rate of acid/base based on the collected overpotential data. The production rate of acid/base is important in EMS, because it helps to estimate the amount of acid/base accumulated over a period of time. EMS needs the acid generated from anode electrolysis to compensate part of the acid in the acid absorption chamber, an accurate estimation of the amount of acid produced in anode chamber will help to guide the selection of operating parameters (current density, electrolysis time, etc.) to decrease the cost of nutrient recovery. In

addition, it could be told from the model that how much extra dosage of acid is needed to recover a certain percentage of NH_4^+-N in the wastewater chamber.

However, some limitations will need to be addressed to improve the accuracy of the model. First, the model was established on the "average" values under the same conditions, including average overpotentials and average acid/base production rates. Decreasing the time interval would get more data points for establishing the model, which will further increase the accuracy of the model. Second, the model was first set up with the data from synthetic AD centrate. Although good prediction could be achieved for the base production from the cathode, and the fitting performance of acid production was improved by modifying the measured acid production rate with the bicarbonate concentrations, using synthetic wastewater with major ions similar to the real AD centrate would also be beneficial to either establish the model or validate the model as well. Third, validation of the model under different conditions need to be conducted. For example, the performance of this model when EMS is operating under current density larger than 10 mA cm^{-2} or smaller than 1.25 mA cm^{-2} needs to be evaluated, as well as changing the bicarbonate concentrations in the wastewater to examine whether the modification of acid production rate would still work well with the model.

6.4 Conclusions

The kinetics of acid/base production were studied in this work. EMS was operated with synthetic AD centrate first under 5 various constant current densities to get the Tafel profile for both anode and cathode half reactions. MHC model achieved good fitting performance with 8.0% and 4.3% RMSE for estimating the electron transfer kinetics of anode and cathode. Polynomial regression showed better fitting performance than the linear regression to describe the relationship of acid/base production rates with current density. The empirical kinetic model showed good

prediction values for the cathode half reactions when EMS was fed with real digester centrate. Moreover, better fitting performance for the anode half reactions could be acquired if the concentrations of bicarbonate in the real digester centrate was considered to modify the measured acid production rate.

Chapter 7: Conclusions and recommendations for future work

7.1 Conclusions

Facing the emerging demand of nutrients for agriculture with low cost, this present work developed innovative electrochemical strategies to achieve ammonia nitrogen recovery from real anaerobic digester (AD) centrate. In particular, the effect of the recovered ammonia nitrogen applied in agriculture, the feasibility of various electrochemical membrane system, and mathematical models which help to understand the electrochemical processes in our systems were studied.

Task 1 recovered ammonia nitrogen from real digester centrate through separating target ions under the electric field of an microbial electrochemical system (MES) and the optimal ratio of 3:1 for AD centrate and food wastewater achieved the best performance with the lowest energy consumption. It also proved the feasibility of applying the recovered ammonia as the nitrogen source in the fertilizer by feeding test fertilizers to the model plant, *Arabidopsis thaliana*, and got similarity of plants in the test group and the control group in terms of the appearance of the plants and gene expression. The results from these experiments are convincing evidence to support the application of recovered nutrients as fertilizers to grow plants, which was usually overlooked in study about nutrient recovery from wastewater.

The three-chamber electrochemical membrane system (EMS) in Task 2 took advantage of the *in situ* acid and base generated from water electrolysis and recovered both nitrogen and phosphorus from real digester centrate. Task 3 added an extra cation exchange membrane in the EMS to inhibit the neutralization of acid and base from transporting under electric field, achieving improved recovery efficiency and decreased energy consumption. The low cost of nitrogen recovery from

wastewater with high recovery efficiency in EMS made it competitive than many existing nutrient recovery technologies, smoothing the path for future development of EMS towards pilot-scale and long-term operation.

The remaining tasks of this work focus on understanding the electrochemical processes through modeling the kinetics of the electrochemical half reactions happening in various systems. Task 4 used Macus-Hush-Chidsey (MHC) model in MES for the first time, and proved the advantages of MHC model to conduct Tafel analysis based on the experiments results collected from different period of the MES. Task 5 also used MHC model to describe the kinetics of electrochemical reactions in EMS, and established an empirical model which successfully estimated the production rate of acid and base when EMS was fed with either synthetic or real AD centrate. These models will guide the operation of electrochemical systems to achieve better performance and lower cost, and open the door for conducting research in larger scale based on both the experiment and modeling results in laboratory scale.

7.2 Recommendations for future work

7.2.1 Long-term operation of electrochemical membrane system

The EMS achieved stable performance during the 10-d operation period under the selected optimal conditions. Although there was no membrane fouling being found based on the repetitive voltage profile and specific energy consumption, it is recommended that long-term operation of the EMS to be conducted in order to evaluate the performance of the system after a few months. Particularly, whether and when the fouling of ion exchange membrane and gas permeable membrane would occur needs to be figured out during the long-term operation, this would help to get a more comprehensive economic analysis of the cost to recover nutrients from AD centrate in EMS if the cost of materials and corresponding lifespan can be included. In case the fouling of membrane

occurs, it also recommended to invert the polarity of the power supply and generate protons in the initial cathode chamber, which will dissolve some inorganic precipitates on membranes or electrodes formed under a basic pH in the previous operation cycles.

7.2.2 Versatile utilization of acid/base in electrochemical system

This work used the *in situ* acid and base in two major aspects: 1) the hydroxide generated in the cathode increased the pH of catholyte and converted NH_4^+ to NH_3 to be separated with gas permeable membrane; 2) the protons generated in the anode was collected and transported to the acid adsorption chamber to compensate part of the acid needed for ammonia recovery and decreased the chemical cost. In fact, the acid and base generated in electrochemical system can have versatile applications. For example, it is interesting to study the gas permeable membrane to be inserted close to the anode chamber instead of the cathode chamber of the electrochemical membrane system, because with the acid generated in the anode chamber, bicarbonate and volatile fatty acids could also be transformed into gas form and be separated by the gas permeable membrane like ammonia gas as well. This would open the door for studying more applications of electrochemical system such as volatile fatty acid recovery, carbon capture and storage, etc. In addition, the protons and hydroxide generated in the electrochemical system could also be used as the chemicals needed to dissolve and precipitate various salts and compounds in wastewater, biosolids, or even polluted gas, which is a promising and sustainable way to achieve reactions involving acid and base in the future.

7.2.3 Machine learning model to simulate the kinetics in electrochemical membrane system

MHC model and polynomial regression methods were mainly used in this work to study the relationship between acid/base production rate, current density, and overpotentials. However, there are a variety of variables in EMS that might also affect the kinetics in EMS, which we have not

dug into yet. Machine learning can overcome such limitations and make efficient and accurate prediction of target variables based on a large data set. In this way, the effect of flow rate, membrane area, electrode catalysts, temperature, etc. could also be including in the modeling process in order to get a more comprehensive modeling of EMS under various conditions. Although it is still limited to use machine learning in our EMS yet due to the limited number of experiment data, study the kinetics in EMS with machine learning is promising to reduce the cost and effort the optimize the EMS for nutrient recovery when more data could be acquired in similar systems.

References

Aivaliotis, M., Samolis, P., Neofotistou, E., Remigy, H., Rizos, A.K. and Tsiotis, G. 2003. Molecular size determination of a membrane protein in surfactants by light scattering. Bba-Biomembranes 1615(1-2), 69-76.

Al-Amshawee, S., Yunus, M.Y.B., Azoddein, A.A.M., Hassell, D.G., Dakhil, I.H. and Abu Hasan, H. 2020. Electrodialysis desalination for water and wastewater: A review. Chem Eng J 380.

Al-Juboori, R.A., Kaljunen, J.U., Righetto, I. and Mikola, A. 2022. Membrane contactor onsite piloting for nutrient recovery from mesophilic digester reject water: The effect of process conditions and pre-treatment options. Sep Purif Technol 303.

Albert, M.J. 2021. The Climate Crisis, Renewable Energy, and the Changing Landscape of Global Energy Politics. Alternatives 46(3), 89-98.

Anders, S. and Huber, W. 2010. Differential expression analysis for sequence count data. Genome Biol 11(10).

Anderson, A.B. 2017. Concepts and computational methods for the electrochemical interface and applications: Past, present, and future. Curr Opin Electroche 1(1), 27-33.

Arredondo, M.R., Kuntke, P., Jeremiasse, A.W., Sleutels, T.H.J.A., Buisman, C.J.N. and ter Heijne, A. 2015. Bioelectrochemical systems for nitrogen removal and recovery from wastewater. Environ Sci-Wat Res 1(1), 22-33.

Arredondo, M.R., Kuntke, P., Ter Heijne, A., Hamelers, H.V.M. and Buisman, C.J.N. 2017. Load ratio determines the ammonia recovery and energy input of an electrochemical system. Water Res 111, 330-337.

Ashrafizadeh, S.N. and Khorasani, Z. 2010. Ammonia removal from aqueous solutions using hollow-fiber membrane contactors. Chem Eng J 162(1), 242-249.

Bhattacharjee, A.S., Wu, S., Lawson, C.E., Jetten, M.S.M., Kapoor, V., Domingo, J.W.S., McMahon, K.D., Noguera, D.R. and Goel, R. 2017. Whole-Community Metagenomics in Two Different Anammox Configurations: Process Performance and Community Structure. Environ Sci Technol 51(8), 4317-4327.

Boehler, M.A., Heisele, A., Seyfried, A., Grömping, M. and Siegrist, H. 2015. $(NH_4)_2SO_4$ recovery from liquid side streams. Environ Sci Pollut R 22(10), 7295-7305.

Bond, D.R. and Lovley, D.R. 2003. Electricity production by Geobacter sulfurreducens attached to electrodes. Appl Environ Microb 69(3), 1548-1555.

Bose, A., Lazouski, N., Gala, M.L., Manthiram, K. and Mallapragada, D.S. 2022. Spatial Variation in Cost of Electricity-Driven Continuous Ammonia Production in the United States. Acs Sustain Chem Eng 10(24), 7862-7872.

Brennan, B., Lawler, J. and Regan, F. 2021. Recovery of viable ammonia-nitrogen products from agricultural slaughterhouse wastewater by membrane contactors: a review. Environ Sci-Wat Res 7(2), 259-273.

Bunce, J.T., Ndam, E., Ofiteru, I.D., Moore, A. and Graham, D.W. 2018. A Review of Phosphorus Removal Technologies and Their Applicability to Small-Scale Domestic Wastewater Treatment Systems. Front Env Sci-Switz 6.

Butler, J.E., Young, N.D. and Lovley, D.R. 2010. Evolution of electron transfer out of the cell: comparative genomics of six genomes. Bmc Genomics 11.

Cakmak, E.K., Hartl, M., Kisser, J. and Cetecioglu, Z. 2022. Phosphorus mining from eutrophic marine environment towards a blue economy: The role of bio-based applications. Water Res 219.

Carmo, M., Fritz, D.L., Merge, J. and Stolten, D. 2013. A comprehensive review on PEM water electrolysis. Int J Hydrogen Energ 38(12), 4901-4934.

Chen, Q., Wang, Y., Yang, F. and Xu, H. 2020. Two-dimensional multi-physics modeling of porous transport layer in polymer electrolyte membrane electrolyzer for water splitting. Int J Hydrogen Energ 45(58), 32984-32994.

Chen, T.L., Chen, L.H., Lin, Y.P.J., Yu, C.P., Ma, H.W. and Chiang, P.C. 2021. Advanced ammonia nitrogen removal and recovery technology using electrokinetic and stripping process towards a sustainable nitrogen cycle: A review. J Clean Prod 309.

Chen, X., Sun, D.Y., Zhang, X.Y., Liang, P. and Huang, X. 2015. Novel Self-driven Microbial Nutrient Recovery Cell with Simultaneous Wastewater Purification. Sci Rep-Uk 5.

Cheng, H.M., Zhu, Q. and Xing, Z.P. 2019. Adsorption of ammonia nitrogen in low temperature domestic wastewater by modification bentonite. J Clean Prod 233, 720-730.

Christiaens, M.E.R., Udert, K.M., Arends, J.B.A., Huysman, S., Vanhaecke, L., McAdam, E. and Rabaey, K. 2019. Membrane stripping enables effective electrochemical ammonia recovery from urine while retaining microorganisms and micropollutants. Water Res 150, 349-357.

Coppi, M.V., O'Neil, R.A., Leang, C., Kaufmann, F., Methé, B.A., Nevin, K.P., Woodard, T.L., Liu, A. and Lovley, D.R. 2007. Involvement of SfrAB in acetate metabolism rather than intracellular, respiration-linked Fe(III) citrate reduction. Microbiol-Sgm 153, 3572-3585.

Cruz, H., Law, Y.Y., Gues, J.S., Rabaey, K., Batstone, D., Laycock, B., Verstraete, W. and Pikaar, I. 2019. Mainstream Ammonium Recovery to Advance Sustainable Urban Wastewater Management. Environ Sci Technol 53(19), 11066-11079.

Daims, H., Lebedeva, E.V., Pjevac, P., Han, P., Herbold, C., Albertsen, M., Jehmlich, N., Palatinszky, M., Vierheilig, J., Bulaev, A., Kirkegaard, R.H., von Bergen, M., Rattei, T., Bendinger, B., Nielsen, P.H. and Wagner, M. 2015. Complete nitrification by bacteria. Nature 528(7583), 504-+.

Darestani, M., Haigh, V., Couperthwaite, S.J., Millar, G.J. and Nghiem, L.D. 2017. Hollow fibre membrane contactors for ammonia recovery: Current status and future developments. J Environ Chem Eng 5(2), 1349-1359.

Desloover, J., De Vrieze, J., de Vijver, M.V., Mortelmans, J., Rozendal, R. and Rabaey, K. 2015. Electrochemical Nutrient Recovery Enables Ammonia Toxicity Control and Biogas Desulfurization in Anaerobic Digestion. Environ Sci Technol 49(2), 948-955.

Desloover, J., Woldeyohannis, A.A., Verstraete, W., Boon, N. and Rabaey, K. 2012. Electrochemical Resource Recovery from Digestate to Prevent Ammonia Toxicity during Anaerobic Digestion. Environ Sci Technol 46(21), 12209-12216.

Dickinson, E.J.F. and Wain, A.J. 2020. The Butler-Volmer equation in electrochemical theory: Origins, value, and practical application. J Electroanal Chem 872.

dos Santos, H.A.P., de Castilhos, A.B., Nadaleti, W.C. and Lourenço, V.A. 2020. Ammonia recovery from air stripping process applied to landfill leachate treatment. Environ Sci Pollut R 27(36), 45108-45120.

Erickson, H.P. 2009. Size and Shape of Protein Molecules at the Nanometer Level Determined by Sedimentation, Gel Filtration, and Electron Microscopy. Biol Proced Online 11(1), 32-51.

Erisman, J.W., Sutton, M.A., Galloway, J., Klimont, Z. and Winiwarter, W. 2008. How a century of ammonia synthesis changed the world. Nat Geosci 1(10), 636-639.

Fernandes, T.V., Shrestha, R., Sui, Y.X., Papini, G., Zeeman, G., Vet, L.E.M., Wijffels, R.H. and Lamers, P. 2015. Closing Domestic Nutrient Cycles Using Microalgae. Environ Sci Technol 49(20), 12450-12456.

Gadkari, S., Gu, S. and Sadhukhan, J. 2018. Towards automated design of bioelectrochemical systems: A comprehensive review of mathematical models. Chem Eng J 343, 303-316.

Garg, A. and Lam, J.S.L. 2017. Design of explicit models for estimating efficiency characteristics of microbial fuel cells. Energy 134, 136-156.

Giddey, S., Badwal, S.P.S., Munnings, C. and Dolan, M. 2017. Ammonia as a Renewable Energy Transportation Media. Acs Sustain Chem Eng 5(11), 10231-10239.

Govindan, K., Im, S.J., Muthuraj, V. and Jang, A. 2021. Electrochemical recovery of H and nutrients (N, P) from synthetic source separate urine water. Chemosphere 269.

Goyal, K., Walton, L.J. and Tunnacliffe, A. 2005. LEA proteins prevent protein aggregation due to water stress. Biochem J 388, 151-157.

Guo, W.H., Zhang, K.X., Liang, Z.B., Zou, R.Q. and Xu, Q. 2019. Electrochemical nitrogen fixation and utilization: theories, advanced catalyst materials and system design. Chem Soc Rev 48(24), 5658-5716.

Guo, X.B., Chen, J.H., Wang, X.S., Li, Y.F., Liu, Y.J. and Jiang, B. 2023. Sustainable ammonia recovery from low strength wastewater by the integrated ion exchange and bipolar membrane electrodialysis with membrane contactor system. Sep Purif Technol 305.

Gurreri, L., Tamburini, A., Cipollina, A. and Micale, G. 2020. Electrodialysis Applications in Wastewater Treatment for Environmental Protection and Resources Recovery: A Systematic Review on Progress and Perspectives. Membranes-Basel 10(7).

Hamelers, H.V.M., ter Heijne, A., Stein, N., Rozendal, R.A. and Buisman, C.J.N. 2011. Butler-Volmer-Monod model for describing bio-anode polarization curves. Bioresource Technol 102(1), 381-387.

Hammoudi, M., Henao, C., Agbossou, K., Dubé, Y. and Doumbia, M.L. 2012. New multi-physics approach for modelling and design of alkaline electrolyzers. Int J Hydrogen Energ 37(19), 13895-13913.

Han, B., Butterly, C., Zhang, W., He, J.Z. and Chen, D.L. 2021. Adsorbent materials for ammonium and ammonia removal: A review. J Clean Prod 283.

Hasanoglu, A., Romero, J., Pérez, B. and Plaza, A. 2010. Ammonia removal from wastewater streams through membrane contactors: Experimental and theoretical analysis of operation parameters and configuration. Chem Eng J 160(2), 530-537.

He, L., Du, P., Chen, Y.Z., Lu, H.W., Cheng, X., Chang, B. and Wang, Z. 2017. Advances in microbial fuel cells for wastewater treatment. Renew Sust Energ Rev 71, 388-403.

He, W.H., Dong, Y., Li, C., Han, X.Y., Liu, G.H., Liu, J. and Feng, Y.J. 2019. Field tests of cubic-meter scale microbial electrochemical system in a municipal wastewater treatment plant. Water Res 155, 372-380.

Henstridge, M.C., Batchelor-McAuley, C., Gusmao, R. and Compton, R.G. 2011. Marcus-Hush-Chidsey theory of electron transfer to and from species bound at a non-uniform electrode surface: Theory and experiment. Chem Phys Lett 517(1-3), 108-112.

Henstridge, M.C., Laborda, E., Rees, N.V. and Compton, R.G. 2012. Marcus-Hush-Chidsey theory of electron transfer applied to voltammetry: A review. Electrochim Acta 84, 12-20.

Hou, D.X., Iddya, A., Chen, X., Wang, M.Y., Zhang, W.L., Ding, Y.F., Jassby, D. and Ren, Z.J. 2018. Nickel-Based Membrane Electrodes Enable High-Rate Electrochemical Ammonia Recovery. Environ Sci Technol 52(15), 8930-8938.

Hu, K.W., Fang, J.K., Ai, X.M., Huang, D.J., Zhong, Z.Y., Yang, X.B. and Wang, L. 2022. Comparative study of alkaline water electrolysis, proton exchange membrane water electrolysis and solid oxide electrolysis through multiphysics modeling. Appl Energ 312.

Hundertmark, M. and Hincha, D.K. 2008. LEA (Late Embryogenesis Abundant) proteins and their encoding genes in. Bmc Genomics 9.

Imran, M., Prakash, O., Pushkar, P., Mungray, A., Kailasa, S.K., Chongdar, S. and Mungray, A.K. 2019. Performance enhancement of benthic microbial fuel cell by cerium coated electrodes. Electrochim Acta 295, 58-66.

Ingram, J. 2020. Nutrition security is more than food security. Nat Food 1(1), 2-2.

Kannan, N. and Vakeesan, D. 2016. Solar energy for future world: - A review. Renew Sust Energ Rev 62, 1092-1105.

Kelly, P.T. and He, Z. 2014. Nutrients removal and recovery in bioelectrochemical systems: A review. Bioresource Technol 153, 351-360.

Kim, K.Y., Moreno-Jimenez, D.A. and Efstathiadis, H. 2021. Electrochemical Ammonia Recovery from Anaerobic Centrate Using a Nickel-Functionalized Activated Carbon Membrane Electrode. Environ Sci Technol 55(11), 7674-7680.

Kinidi, L., Tan, I.A.W., Wahab, N.B.A., Bin Tamrin, K.F., Hipolito, C.N. and Salleh, S.F. 2018. Recent Development in Ammonia Stripping Process for Industrial Wastewater Treatment. Int J Chem Eng 2018.

Kitano, M., Inoue, Y., Yamazaki, Y., Hayashi, F., Kanbara, S., Matsuishi, S., Yokoyama, T., Kim, S.W., Hara, M. and Hosono, H. 2012. Ammonia synthesis using a stable electride as an electron donor and reversible hydrogen store. Nat Chem 4(11), 934-940.

Koskue, V., Freguia, S., Ledezma, P. and Kokko, M. 2021. Efficient nitrogen removal and recovery from real digested sewage sludge reject water through electroconcentration. Journal of Environmental Chemical Engineering 9(5).

Kuntke, P., Arredondo, M.R., Widyakristi, L., ter Heijne, A., Sleutels, T.H.J.A., Hamelers, H.V.M. and Buisman, C.J.N. 2017. Hydrogen Gas Recycling for Energy Efficient Ammonia Recovery in Electrochemical Systems. Environ Sci Technol 51(5), 3110-3116.

Kuntke, P., Rodrigues, M., Sleutels, T., Saakes, M., Hamelers, H.V.M. and Buisman, C.J.N. 2018a. Energy-Efficient Ammonia Recovery in an Up-Scaled Hydrogen Gas Recycling Electrochemical System. Acs Sustainable Chemistry & Engineering 6(6), 7638-7644.

Kuntke, P., Sleutels, T.H.J.A., Arredondo, M.R., Georg, S., Barbosa, S.G., ter Heijne, A., Hamelers, H.V.M. and Buisman, C.J.N. 2018b. (Bio)electrochemical ammonia recovery: progress and perspectives. Appl Microbiol Biot 102(9), 3865-3878.

Kuntke, P., Sleutels, T.H.J.A., Saakes, M. and Buisman, C.J.N. 2014. Hydrogen production and ammonium recovery from urine by a Microbial Electrolysis Cell. Int J Hydrogen Energ 39(10), 4771-4778.

Kyriakou, V., Garagounis, I., Vourros, A., Vasileiou, E. and Stoukides, M. 2020. An Electrochemical Haber-Bosch Process. Joule 4(1), 142-158.

Largust T. Angenent, S.S. 2001. Development of anaerobic migrating blanket reactor (AMBR), a novlel anaerobic treatment system. Water Research 35(7), 1739-1747.

Lee, G., Kim, D. and Han, J.I. 2021a. Gas-diffusion-electrode based direct electro-stripping system for gaseous ammonia recovery from livestock wastewater. Water Res 196.

Lee, G., Kim, K., Chung, J. and Han, J.I. 2021b. Electrochemical ammonia accumulation and recovery from ammonia-rich livestock wastewater. Chemosphere 270.

Lee, H.S., Torres, C.I. and Rittmann, B.E. 2009. Effects of Substrate Diffusion and Anode Potential on Kinetic Parameters for Anode-Respiring Bacteria. Environ Sci Technol 43(19), 7571-7577.

Levy-Booth, D.J., Prescott, C.E. and Grayston, S.J. 2014. Microbial functional genes involved in nitrogen fixation, nitrification and denitrification in forest ecosystems. Soil Biol Biochem 75, 11-25.

Li, N., Wan, Y.X. and Wang, X. 2020. Nutrient conversion and recovery from wastewater using electroactive bacteria. Sci Total Environ 706.

Li, X.W., Zhou, X.W., Yang, B. and Wen, Z. 2021. Recovery phosphate and ammonium from aqueous solution by the process of electrochemically decomposing dolomite. Chemosphere 262.

Liao, Q., Zhang, J., Li, J., Ye, D.D., Zhu, X. and Zhang, B. 2015. Increased performance of a tubular microbial fuel cell with a rotating carbon-brush anode. Biosens Bioelectron 63, 558-561.

Lin, N., Feng, S.H. and Wang, J.G. 2022. Multiphysics modeling of proton exchange membrane water electrolysis: From steady to dynamic behavior. Aiche J 68(8).

Liu, F., Moustafa, H. and He, Z. 2024. Simultaneous recovery of nitrogen and phosphorus from actual digester centrate in an electrochemical membrane system. Resources, Conservation and Recycling 203.

Liu, F.B., Moustafa, H., Hassouna, M.S.E. and He, Z. 2022a. Effective nutrient recovery from digester centrate assisted by production of acid/base in a novel electrochemical membrane system. Chemosphere 307.

Liu, F.B., Worland, A., Tang, Y.J., Moustafa, H., Hassouna, M.S.E. and He, Z. 2022b. Microbial electrochemical ammonia recovery from anaerobic digester centrate and subsequent application to fertilize. Water Res 220.

Liu, M.J., Neo, B.S. and Tarpeh, W.A. 2020. Building an operational framework for selective nitrogen recovery via electrochemical stripping. Water Res 169.

Liu, R.D., Wang, Y.K., Wu, G., Luo, J.N. and Wang, S.G. 2017. Development of a selective electrodialysis for nutrient recovery and desalination during secondary effluent treatment. Chem Eng J 322, 224-233.

Liu, Y., Deng, Y.Y., Zhang, Q. and Liu, H. 2021. Overview of recent developments of resource recovery from wastewater via electrochemistry-based technologies. Sci Total Environ 757.

Logan, B.E., Hamelers, B., Rozendal, R.A., Schrorder, U., Keller, J., Freguia, S., Aelterman, P., Verstraete, W. and Rabaey, K. 2006. Microbial fuel cells: Methodology and technology. Environ Sci Technol 40(17), 5181-5192.

Lowy, D.A., Tender, L.M., Zeikus, J.G., Park, D.H. and Lovley, D.R. 2006. Harvesting energy from the marine sediment-water interface II - Kinetic activity of anode materials. Biosens Bioelectron 21(11), 2058-2063.

Lu, S.B., Zhang, X.L., Peng, H.R., Skitmore, M., Bai, X. and Zheng, Z.H. 2021a. The energy-food-water nexus: Water footprint of Henan-Hubei-Hunan in China. Renew Sust Energ Rev 135.

Lu, X.Y., Duan, H.R., Oehmen, A., Carvalho, G., Yuan, Z.G. and Ye, L. 2021b. Achieving combined biological short-cut nitrogen and phosphorus removal in a one sludge system with side-stream sludge treatment. Water Res 203.

Luo, S., Sun, H.Y., Ping, Q.Y., Jin, R. and He, Z. 2016. A Review of Modeling Bioelectrochemical Systems: Engineering and Statistical Aspects. Energies 9(2).

Luther, A.K., Desloover, J., Fennell, D.E. and Rabaey, K. 2015. Electrochemically driven extraction and recovery of ammonia from human urine. Water Res 87, 367-377.

MacFarlane, D.R., Cherepanov, P.V., Choi, J., Suryanto, B.H.R., Hodgetts, R.Y., Bakker, J.M., Vallana, F.M.F. and Simonov, A.N. 2020. A Roadmap to the Ammonia Economy. Joule 4(6), 1186-1205.

Manto, M.J., Xie, P.F., Keller, M.A., Liano, W.E., Pu, T.C. and Wang, C. 2018. Recovery of ammonium from aqueous solutions using ZSM-5. Chemosphere 198, 501-509.

Matsena, M.T. and Chirwa, E.M.N. 2022. Hexavalent chromium-reducing microbial fuel cell modeling using integrated Monod kinetics and Butler-Volmer equation. Fuel 312.

Mayer, B.K., Baker, L.A., Boyer, T.H., Drechsel, P., Gifford, M., Hanjra, M.A., Parameswaran, P., Stoltzfus, J., Westerhoff, P. and Rittmann, B.E. 2016. Total Value of Phosphorus Recovery. Environ Sci Technol 50(13), 6606-6620.

Mohammadi, R., Tang, W. and Sillanpää, M. 2021. A systematic review and statistical analysis of nutrient recovery from municipal wastewater by electrodialysis. Desalination 498.

Nawaz, A., Arora, A.S., Yun, D., Yun, C.M. and Lee, M.Y. 2021. Advanced predicting technique for optimal operation of wastewater treatment process: A ProActive scheduling approach. J Clean Prod 303.

Noodén, L.D. and Penney, J.P. 2001. Correlative controls of senescence and plant death in Arabidopsis thaliana (Brassicaceae). Journal of Experimental Botany 52(364), 2151-2159.

Nudehi, S., Larson, C., Prusinski, W., Kotfer, D., Otto, J., Beyers, E., Schoer, J. and Palumbo, R. 2018. Solar thermal decoupled water electrolysis process II: An extended investigation of the anodic electrochemical reaction. Chem Eng Sci 181, 159-172.

Ochs, P., Martin, B., Germain-Cripps, E., Stephenson, T., van Loosdrecht, M. and Soares, A. 2023. Techno-economic analysis of sidestream ammonia removal technologies: Biological options versus thermal stripping. Environ Sci Ecotech 13.

Osorio-Tejada, J., Tran, N.N. and Hessel, V. 2022. Techno-environmental assessment of small-scale Haber-Bosch and plasma-assisted ammonia supply chains. Sci Total Environ 826.

Palanisamy, G., Jung, H.Y., Sadhasivam, T., Kurkuri, M.D., Kim, S.C. and Roh, S.H. 2019. A comprehensive review on microbial fuel cell technologies: Processes, utilization, and advanced developments in electrodes and membranes. J Clean Prod 221, 598-621.

Pan, Y., Zhu, T. and He, Z. 2020. Minimizing effects of chloride and calcium towards enhanced nutrient recovery from sidestream centrate in a decoupled electrodialysis driven by solar energy. J Clean Prod 263.

Pandey, A.K., Kumar, R.R., Kalidasan, B., Laghari, I.A., Samykano, M., Kothari, R., Abusorrah, A.M., Sharma, K. and Tyagi, V.V. 2021. Utilization of solar energy for wastewater treatment: Challenges and progressive research trends. J Environ Manage 297.

Paredes, D., Kuschk, P., Mbwette, T.S.A., Stange, F., Müller, R.A. and Köser, H. 2007. New aspects of microbial nitrogen transformations in the context of wastewater treatment -: A review. Eng Life Sci 7(1), 13-25.

Park, S. and Kim, M. 2015. Innovative ammonia stripping with an electrolyzed water system as pretreatment of thermally hydrolyzed wasted sludge for anaerobic digestion. Water Res 68, 580-588.

Patel, R. and Deb, D. 2018. Parametrized control-oriented mathematical model and adaptive backstepping control of a single chamber single population microbial fuel cell. J Power Sources 396, 599-605.

Pawar, A.A., Karthic, A., Lee, S., Pandit, S. and Jung, S.P. 2022a. Microbial electrolysis cells for electromethanogenesis: Materials, configurations and operations. Environ Eng Res 27(1).

Pawar, R., Zhang, Z. and Vidic, R.D. 2022b. Laboratory and pilot-scale studies of membrane distillation for desalination of produced water from Permian Basin. Desalination 537.

Pikaar, I., Matassa, S., Rabaey, K., Bodirsky, B.L., Popp, A., Herrero, M. and Verstraete, W. 2017. Microbes and the Next Nitrogen Revolution. Environ Sci Technol 51(13), 7297-7303.

Qazi, A., Hussain, F., Abd Rahim, N., Hardaker, G., Alghazzawi, D., Shaban, K. and Haruna, K. 2019. Towards Sustainable Energy: A Systematic Review of Renewable Energy Sources, Technologies, and Public Opinions. Ieee Access 7, 63837-63851.

Qin, M.H., White, C., Zou, S.Q. and He, Z. 2018. Passive separation of recovered ammonia from catholyte for reduced energy consumption in microbial electrolysis cells. Chemical Engineering Journal 334, 2303-2307.

Qin, Y.J., Wang, K.C., Xia, Q., Yu, S.Q., Zhang, M.A., An, Y., Zhao, X.D. and Zhou, Z. 2023. Up-concentration of nitrogen from domestic wastewater: A sustainable strategy from removal to recovery. Chem Eng J 451.

Qing, G.L., Foster, S.L., Anari, Z., Matlock, M., Thoma, G. and Greenlee, L.F. 2021. Disinfection/ammonia removal from aquaculture wastewater and disinfection of irrigation water using electrochemical flow cells: A case study in Hawaii. Water Environ Res 93(10), 2149-2168.

Radeef, A.Y. and Ismail, Z.Z. 2021. Resource recovery in potato chips processing industry: green bioelectricity production using continuous mediatorless microbial fuel cell. Int J Green Energy 18(9), 910-919.

Raghavulu, S.V., Modestra, J.A., Amulya, K., Reddy, C.N. and Mohan, S.V. 2013. Relative effect of bioaugmentation with electrochemically active and non-active bacteria on bioelectrogenesis in microbial fuel cell. Bioresource Technol 146, 696-703.

Rajan, A.G. and Carter, E.A. 2020. Microkinetic model for pH- and potential-dependent oxygen evolution during water splitting on Fe-doped β-NiOOH. Energ Environ Sci 13(12), 4962-4976.

Raychaudhuri, A. and Behera, M. 2020. Review of the Process Optimization in Microbial Fuel Cell using Design of Experiment Methodology. J Hazard Toxic Radio 24(3).

Ren, Z.J., Jia, B., Zhang, G.M., Fu, X.L., Wang, Z.X., Wang, P.F. and Lv, L.Y. 2021. Study on adsorption of ammonia nitrogen by iron-loaded activated carbon from low temperature wastewater. Chemosphere 262.

Rocha, L.C., Teixeira, F.A., Pedreira, M.D., Fries, D.D., Dias, D.L.S., Costa, E.G.L., de Figueiredo, A.J., Seixas, A.A., Pacheco, C.C. and Santiago, B.M. 2020. Plant growth regulator and soil fertilizer improve production and growing stage of. Grassl Sci 66(2), 102-109.

Rodrigues, M., Lund, R.J., ter Heijne, A., Sleutels, T., Buisman, C.J.N. and Kuntke, P. 2022. Application of ammonium fertilizers recovered by an Electrochemical System. Resour Conserv Recy 181.

Rout, P.R., Shahid, M.K., Dash, R.R., Bhunia, P., Liu, D.Z., Varjani, S., Zhang, T.C. and Surampalli, R.Y. 2021. Nutrient removal from domestic wastewater: A comprehensive review on conventional and advanced technologies. J Environ Manage 296.

Santoro, C., Arbizzani, C., Erable, B. and Ieropoulos, I. 2017. Microbial fuel cells: From fundamentals to applications. A review. J Power Sources 356, 225-244.

Schaubroeck, T., De Clippeleir, H., Weissenbacher, N., Dewulf, J., Boeckx, P., Vlaeminck, S.E. and Wett, B. 2015. Environmental sustainability of an energy self-sufficient sewage treatment plant: Improvements through DEMON and co-digestion. Water Res 74, 166-179.

Shao, Q., Zhang, Y., Liu, Z., Long, L.Z., Liu, Z.Z., Chen, Y.Q., Hu, X.M., Lu, M.M. and Huang, L.Z. 2022. Phosphorus and nitrogen recovery from wastewater by ceramsite: Adsorption mechanism, plant cultivation and sustainability analysis. Sci Total Environ 805.

Shen, M.Z., Bennett, N., Ding, Y.L. and Scott, K. 2011. A concise model for evaluating water electrolysis. Int J Hydrogen Energ 36(22), 14335-14341.

Shi, L., Dong, H.L., Reguera, G., Beyenal, H., Lu, A.H., Liu, J., Yu, H.Q. and Fredrickson, J.K. 2016. Extracellular electron transfer mechanisms between microorganisms and minerals. Nat Rev Microbiol 14(10), 651-662.

Shin, C., Szczuka, A., Liu, M.J., Mendoza, L., Jiang, R.J., Tilmans, S.H., Tarpeh, W.A., Mitch, W.A. and Criddle, C.S. 2022. Recovery of Clean Water and Ammonia from Domestic Wastewater: Impacts on Embodied Energy and Greenhouse Gas Emissions. Environ Sci Technol 56(12), 8712-8721.

Song, J., Li, Y.W., Yin, F., Zhang, Z.T., Ke, D.K., Wang, D.B., Yuan, Q.P. and Zhang, X.E. 2020. Enhanced Electrochemical Impedance Spectroscopy Analysis of Microbial Biofilms on an Electrochemically Generated Graphene Interface. Acs Sensors 5(6), 1795-1803.

Subramani, A. and Jacangelo, J.G. 2015. Emerging desalination technologies for water treatment: A critical review. Water Res 75, 164-187.

Talekar, G.V. and Mutnuri, S. 2021. Electrochemical removal and recovery of ammonia and phosphates from blackwater and wetland passed blackwater. Sustain Energy Techn 47.

Tansel, B., Lunn, G. and Monje, O. 2018. Struvite formation and decomposition characteristics for ammonia and phosphorus recovery: A review of magnesium-ammonia-phosphate interactions. Chemosphere 194, 504-514.

Tarpeh, W.A., Barazesh, J.M., Cath, T.Y. and Nelson, K.L. 2018. Electrochemical Stripping to Recover Nitrogen from Source-Separated Urine. Environ Sci Technol 52(3), 1453-1460.

Torres, C.I., Marcus, A.K., Lee, H.S., Parameswaran, P., Krajmalnik-Brown, R. and Rittmann, B.E. 2010. A kinetic perspective on extracellular electron transfer by anode-respiring bacteria. Fems Microbiol Rev 34(1), 3-17.

Torres, C.I., Marcus, A.K., Parameswaran, P. and Rittmann, B.E. 2008. Kinetic experiments for evaluating the Nernst-Monod model for anode-respiring bacteria (ARB) in a biofilm anode. Environ Sci Technol 42(17), 6593-6597.

Ursúa, A., Gandía, L.M. and Sanchis, P. 2012. Hydrogen Production From Water Electrolysis: Current Status and Future Trends. P Ieee 100(2), 410-426.

Van Eekert, M., Weijma, J., Verdoes, N., De Buisonj´e, F., Reitsma, B., Van den Bulk, J., Van Gastel, J. 2012. Explorative research on innovative nitrogen recovery. Amersfoort: STOWA.

Vaneeckhaute, C., Lebuf, V., Michels, E., Belia, E., Vanrolleghem, P.A., Tack, F.M.G. and Meers, E. 2017. Nutrient Recovery from Digestate: Systematic Technology Review and Product Classification. Waste Biomass Valori 8(1), 21-40.

Veeramani, K., Janani, G., Kim, J., Surendran, S., Lim, J., Jesudass, S.C., Mahadik, S., Lee, H.Y.J., Kim, T.H., Kim, J.K. and Sim, U. 2023. Hydrogen and value-added products yield from hybrid water electrolysis: A critical review on recent developments. Renew Sust Energ Rev 177.

Wang, J.L. and Liu, X.J. 2021. Forward osmosis technology for water treatment: Recent advances and future perspectives. J Clean Prod 280.

Wang, J.X., Wang, Z.X., Liang, J.D. and He, Z. 2021. Electrolysis-assisted recovery of reverse-fluxed solutes in forward osmosis. Desalination 520.

Wang, M., Payne, K.A., Tong, S. and Ergas, S.J. 2018. Hybrid algal photosynthesis and ion exchange (HAPIX) process for high ammonium strength wastewater treatment. Water Res 142, 65-74.

Wang, Q.R., Guo, J.P. and Chen, P. 2019. Recent progress towards mild-condition ammonia synthesis. J Energy Chem 36, 25-36.

Wang, X.L., Zhang, X., Wang, Y.M., Du, Y.X., Feng, H.Y. and Xu, T.W. 2015. Simultaneous recovery of ammonium and phosphorus via the integration of electrodialysis with struvite reactor. J Membrane Sci 490, 65-71.

Wang, Z.X., Liu, F.B. and He, Z. 2023. Electrochemical phosphorus release and recovery from wastewater sludge: A review. Crit Rev Env Sci Tec 53(14), 1359-1377.

Ward, A.J., Arola, K., Brewster, E.T., Mehta, C.M. and Batstone, D.J. 2018. Nutrient recovery from wastewater through pilot scale electrodialysis. Water Res 135, 57-65.

Wu, H.T. and Vaneeckhaute, C. 2022. Nutrient recovery from wastewater: A review on the integrated Physicochemical technologies of ammonia stripping, adsorption and struvite precipitation. Chem Eng J 433.

Xia, C.S., Zhang, D.X., Pedrycz, W., Zhu, Y.M. and Guo, Y.X. 2018. Models for Microbial Fuel Cells: A critical review. J Power Sources 373, 119-131.

Xu, L.L., Liu, S., Zhao, S.Y., Li, K.L., Cao, A.X. and Wang, J. 2022. A novel electrocoagulation-membrane stripping hybrid system for simultaneous ammonia recovery and contaminant removal. Sep Purif Technol 296.

Xu, Y., Huang, M.H. and Luo, X.B. 2019. Enhanced phosphate adsorption performance by innovative anion imprinted polymers with dual interaction. Appl Surf Sci 467, 135-142.

Yan, T., Ye, Y.Y., Ma, H.M., Zhang, Y., Guo, W.S., Du, B., Wei, Q., Wei, D. and Ngo, H.H. 2018. A critical review on membrane hybrid system for nutrient recovery from wastewater. Chem Eng J 348, 143-156.

Yang, T.T. and Saidi, W.A. 2022. Reconciling the Volcano Trend with the Butler-Volmer Model for the Hydrogen Evolution Reaction. J Phys Chem Lett 13(23), 5310-5315.

Yaqub, M. and Lee, W. 2019. Zero-liquid discharge (ZLD) technology for resource recovery from wastewater: A review. Sci Total Environ 681, 551-563.

Ye, Y.Y., Ngo, H.H., Guo, W.S., Liu, Y.W., Chang, S.W., Nguyen, D.D., Liang, H. and Wang, J. 2018. A critical review on ammonium recovery from wastewater for sustainable wastewater management. Bioresource Technol 268, 749-758.

Ye, Z.L., Ghyselbrecht, K., Monballiu, A., Pinoy, L. and Meesschaert, B. 2019. Fractionating various nutrient ions for resource recovery from swine wastewater using simultaneous anionic and cationic selective-electrodialysis. Water Res 160, 424-434.

Yuan, J., Choong, A.M.F. and Pehkonen, S.O. 2007. The influence of the marine aerobic strain on the corrosion of 70/30 Cu-Ni alloy. Corros Sci 49(12), 4352-4385.

Zamora, P., Georgieva, T., Ter Heijne, A., Sleutels, T.H.J.A., Jeremiasse, A.W., Saakes, M., Buisman, C.J.N. and Kuntke, P. 2017. Ammonia recovery from urine in a scaled-up Microbial Electrolysis Cell. J Power Sources 356, 491-499.

Zhang, C.Y., Ma, J.X., He, D. and Waite, T.D. 2018a. Capacitive Membrane Stripping for Ammonia Recovery (CapAmm) from Dilute Wastewaters. Environ Sci Tech Let 5(1), 43-49.

Zhang, C.Y., Ma, J.X., Song, J.K., He, C. and Waite, T.D. 2018b. Continuous Ammonia Recovery from Wastewaters Using an Integrated Capacitive Flow Electrode Membrane Stripping System. Environ Sci Technol 52(24), 14275-14285.

Zhang, C.Y., Ma, J.X. and Waite, T.D. 2019. Ammonia-Rich Solution Production from Wastewaters Using Chemical-Free Flow-Electrode Capacitive Deionization. Acs Sustain Chem Eng 7(7), 6480-6485.

Zhang, Y., Desmidt, E., Van Looveren, A., Pinoy, L., Meesschaert, B. and Van der Bruggen, B. 2013. Phosphate Separation and Recovery from Wastewater by Novel Electrodialysis. Environ Sci Technol 47(11), 5888-5895.

Zhang, Y.F. and Angelidaki, I. 2015. Recovery of ammonia and sulfate from waste streams and bioenergy production via bipolar bioelectrodialysis. Water Res 85, 177-184.

Zhou, Y., Fu, W.B., Si, F.L., Yan, Z.T., Zhang, Y.J., He, Q.Y. and Chen, B. 2019. UDP-glycosyltransferase genes and their association and mutations associated with pyrethroid resistance in Anopheles sinensis (Diptera: Culicidae). Malaria J 18.

Zou, S.Q. and He, Z. 2018. Efficiently "pumping out" value-added resources from wastewater by bioelectrochemical systems: A review from energy perspectives. Water Res 131, 62-73.

Zou, S.Q., Qin, M., Moreau, Y. and He, Z. 2017. Nutrient-energy-water recovery from synthetic sidestream centrate using a microbial electrolysis cell - forward osmosis hybrid system. J Clean Prod 154, 16-25.

Appendix A1: Supporting information for Chapter 2

This supporting information contains 7 figures, 8 tables and 2 sections

A1.1 Energy consumption calculation

Electric energy consumed by the power supply was calculated using Eq. A1.1.

$$Q_{\mathrm{E}} = UI_{\mathrm{avg}}t \tag{A1.1}$$

where QE is the electric energy consumed by the power supply, U is the output voltage of power supply (0.8 V), I_{ave} (A) is the average current, t is the time of each cycle (24 h). Q_E at different volume ratio were 836, 1241, and 1035 J, respectively.

The energy consumd by pump is calculated using Eq. A1.2.

$$P_{pump} = \frac{Q_{pump} \times \left(H_{hydraulic} + H_{dynamic}\right)}{\eta} = \frac{v\pi d^2/4 \times (\rho gh + \rho v^2/2)}{\eta} \tag{A1.2}$$

where Q_{pump} is the recirculation flow rate (m3 s^{-1}, 2.5 mL min^{-1} was used for recirculation of each channel in this study, and the total flow rate was 5 mL min^{-1} since anode and cathode were circulated separately), $H_{hydraulic}$ (Pa) and $H_{dynamic}$ (Pa) the hydraulic and dynamic pressure provided by pump, η the efficiency of this pump (assumed 100%), ρ the density of electrolyte (1000 kg m^{-3}), d the diameter of the pump tubing (0.16 cm in this study), v (m s^{-1}) the velocity. h (~ 0.01 m in this study) is the difference of water head before and after the pump, which was measured by experiments at recirculation rate of 2.5 mL min^{-1}. Therefore, the energy consumed by the pump is 43.5 J during 24-hour cycle, which equal to 6.5%, 4.4%, and 5.2% of the electric energy consumed by power supply, respectively, when volume ratio was 1:1, 3:1, and 7:1. This pump energy was ignored when comparing the energy at different ratios of digester centrate and food wastewater

because the ratios would change the electric power of the power supply (possibly by changing the inner resistance) while have little influence on the pump.

A1.2 RNA extraction and gene expression (provided by Novogene)

A1.2.1 RNA extraction

After cell lysis, impurities removal, and inhibition of RNAse activity, total RNA was extracted by using phase separation method from cell debris. Then Agilent bioanalyzer 2100 were used to check RNA integrity and concentration.

A1.2.2 Library preparation and sequencing

Messenger RNA was purified from total RNA using poly-T oligo-attached magnetic beads. After fragmentation, the first strand cDNA was synthesized using random hexamer primers, followed by the second strand cDNA synthesis using either dUTP for directional library or dTTP for non-directional library. For the non-directional library, it was ready after end repair, A-tailing, adapter ligation, size selection, amplification, and purification. The library was checked with Qubit and real-time PCR for quantification and bioanalyzer for size distribution detection. Quantified libraries will be pooled and sequenced on Illumina platforms, according to effective library concentration and data amount. The clustering of the index-coded samples was performed according to the manufacturer's instructions. After cluster generation, the library preparations were sequenced on an Illumina platform and paired-end reads were generated.

A1.2.3 Read mapping

The raw paired end reads were trimmed and quality controlled by fastp. Raw reads filtering is as follows: (1) remove reads with adaptor contamination; (2) remove reads when uncertain nucleotides constitute more than 10 percent of either read (N > 10%); (3) remove reads when low

quality nucleotides (Base Quality less than 5) constitute more than 50 percent of the read. Then clean reads were separately aligned to reference genome downloaded from genome website browser (NCBI/UCSC/Ensembl) directly. HISAT2 algorithm is selected to map the filtered sequenced reads to the reference genome. The HISAT2 algorithm can be divided into three parts: (1) align reads entirely to a single exon of the genome; (2) reads are segmented and then mapped to the adjacent exons; (3) reads are segmented and then mapped to three or more exons. The quantity of total mapped reads and its percentage of clean reads is calculated, including the quantity of multiple mapped reads and its percentage of clean reads, and the quantity of uniquely mapped reads and its percentage of clean reads. The TMR (Total Mapped Reads or Fragments) should be larger than 70% and MMR (Multiple Mapped Reads or Fragments) should be no more than 10%.

A1.2.4 Gene expression level analysis

The abundance of transcript reflects gene expression level directly. In RNA-seq experiments, gene expression level is estimated by the abundance of transcripts (count of sequencing) that mapped to genome or exon. Read counts is proportional to gene expression level, gene length and sequencing depth. FPKM (short for the expected number of Fragments Per Kilobase of transcript sequence per Millions base pairs sequenced) is the most common method of estimating gene expression levels, which takes the effects into consideration of both sequencing depth and gene length on counting of fragments. The FPKM file got from this study is used for all the gene expression level analysis.

For samples with biological replicates, differential expression analysis of two conditions/groups was performed using the DESeq2 R package (Anders and Huber, 2010). It provides statistical routines for determining differential expression in digital gene expression data using a model based on the negative binomial distribution. Therefore, if the readcount of the i-th gene in j-th sample is

K_{ij}, there is: $K_{ij} \sim NB(\mu_{ij}, \sigma_{ij}^2)$ And the resulting P values were adjusted using the Benjamini and Hochberg's approach for controlling the false discovery rate.

A1.2.5 Functional analysis

Through the enrichment analysis of the differential expressed genes, we can find out which biological functions or pathways are significantly associated with differential expressed genes. In this study, the clusterProfiler software is used for enrichment analysis, including GO Enrichment, DO Enrichment, KEGG and Reactome database Enrichment.

GO is the abbreviation of Gene Ontology (http://www.geneontology.org/), which is a major bioinformatics classification system to unify the presentation of gene properties across all species. It includes three main branches: cellular component, molecular function and biological process. GO terms with padj < 0.05 are significant enrichment.

The interactions of multiple genes may be involved in certain biological functions. KEGG (Kyoto Encyclopedia of Genes and Genomes, http://www.kegg.jp/) is a collection of manually curated databases containing resources on genomic, biological-pathway and disease information. Pathway enrichment analysis identifies significantly enriched metabolic pathways or signal transduction pathways associated with differentially expressed genes, comparing the whole genome background. KEGG terms with padj < 0.05 are significant enrichment.

Table A1.3 Summary of the methods to prepare various fertilizers applied in each group.

Fertilizer group	Preparing methods
a	House fertilizer supplied by the facility directly
b	Diluted catholyte to match total nitrogen concentration with Group a
c	Same diluted catholyte with Group b added with P and K
d	Same diluted catholyte with Group b added with P, K, and trace elements

Table A1.4 The performance of the MES under three volume ratios of anaerobic digester centrate and food wastewater, 1:1, 3:1, and 7:1. EC: electrical conductivity, subscript i and f refer to initial and final results.

	Index	Units	1:1	3:1	7:1
anolyte	pH_i	-	7.37 ± 0.02	7.78 ± 0.02	8.86 ± 0.07
	pH_f	-	5.07 ± 0.14	6.03 ± 0.03	7.69 ± 0.04
	EC_i	mS cm^{-1}	3.80 ± 0.08	5.52 ± 0.04	5.91 ± 0.06
	EC_f	mS cm^{-1}	1.16 ± 0.05	1.81 ± 0.11	3.76 ± 0.09
	NH_4^+-N_i	mg L^{-1}	393 ± 12	627 ± 12	690 ± 8
	NH_4^+-N_f	mg L^{-1}	117 ± 5	197 ± 9	360 ± 8
	COD_i	mg L^{-1}	1620 ± 28	1156 ± 20	940 ± 25
	COD_f	mg L^{-1}	992 ± 23	771 ± 16	754 ± 20
catholyte	pH_i	-	8.52 ± 0.10	8.92 ± 0.06	8.86 ± 0.07
	pH_f	-	6.73 ± 0.62	7.65 ± 0.41	7.69 ± 0.04
	EC_i	mS cm^{-1}	0.50 ± 0.08	0.51 ± 0.01	0.53 ± 0.01
	EC_f	mS cm^{-1}	3.32 ± 0.08	4.05 ± 0.05	3.06 ± 0.06
	NH_4^+-N_i	mg L^{-1}	0 ± 0	0 ± 0	0 ± 0
	NH_4^+-N_f	mg L^{-1}	310 ± 8	407 ± 12	280 ± 1

Table A1.5 pH, conductivity, and concentrations of major anions and cations in house fertilizer.

Anions (mg L^{-1})		Cations (mg L^{-1})		Others
Cl^-	33.8 ± 2.3	Na^+	145.0 ± 8.7	pH
HCO_3^-	35.8 ± 3.1	NH_4^+-N	42.6 ± 2.1	6.59 ± 0.05
SO_4^{2-}	213.6 ± 8.1	K^+	180.4 ± 6.6	
NO_3^--N	92.4 ± 5.0	Mg^{2+}	18.2 ± 1.2	Conductivity
PO_4^{3-}-P	72.7 ± 4.8	Ca^{2+}	28.8 ± 2.0	1.56 ± 0.03 mS cm^{-1}

Table A1.6 Components of trace elements in house fertilizer.

Elements	Percent (%)	Concentration* (μg L^{-1})
B	0.0150	135
Mn	0.0375	338
Fe	0.0750	675
Cu	0.0075	68
Zn	0.0375	338
Mo	0.0075	68

* Concentrations are calculated based on the percent ratio between trace elements and nitrogen (15%) listed on labeling receipt and total nitrogen concentration (around 135 mg L^{-1}) from preliminarily experiments.

Table A1.7 The detailed information of sequenced data for samples applied with different fertilizers.

Sample	raw reads	clean reads	rate of clean reads %	Q20 %	Q30 %
a1	19897695	19440914	97.70	98.50	95.27
a2	21866191	21273130	97.29	98.61	95.58
b1	11663033	11014171	94.44	96.60	91.23
b2	13422155	12845745	95.71	97.47	93.11
d1	4187189	4179522	99.82	96.73	91.90
d2	18166316	17774832	97.85	96.48	90.86

Table A1.8 Differentially expressed genes with largest log2 fold changes between groups a, b and d. In d vs. a, for example, the log2 fold change represents the increase or decrease in gene expression of group d compared to group a. A positive log2 value represents upregulation in group d.

d vs. a	gene	log2	gene description
Top 20 upregulated genes (positive log2 fold change)	ATCG00920	8.5634	chloroplast-encoded 16S ribosomal RNA
	AT5G35510	8.2753	TIR-NBS-LRR class disease resistance protein
	ATCG01210	8.2387	chloroplast-encoded 16S ribosomal RNA
	AT2G43000	7.9383	Transcription factor JUNGBRUNNEN 1
	AT5G53740	7.7946	Putative uncharacterized protein
	ATMG00480	7.5916	ATPase subunit 8
	AT2G07787	7.5384	Uncharacterized protein
	ATMG01080	7.5246	ATP synthase subunit 9, mitochondrial
	AT4G11040	7.5069	Probable protein phosphatase 2C 54
	AT4G01925	7.4248	Cysteine/Histidine-rich C1 domain family protein
	AT1G02940	7.4194	glutathione S-transferase (class phi) 5
	AT3G42570	7.3952	Peroxidase family protein
	AT3G06970	7.3641	RNA recognition motif-containing protein
	AT2G01021	7.2987	Uncharacterized protein
	AT2G35070	7.2618	transmembrane protein
	AT3G28580	7.1314	AAA-ATPase At3g28580
	AT1G17065	7.0587	Uncharacterized protein
	AT1G12950	7.0576	Protein DETOXIFICATION
	AT1G49290	7.0081	Rho guanine nucleotide exchange factor
	AT1G73330	6.9788	Dr4 protein; drought-repressed 4
Top 20 downregulated genes (negative log2 fold change)	AT4G32280	-10.2945	Auxin-responsive protein
	AT4G16590	-8.8167	cellulose synthase-like A01
	AT4G06115	-8.7460	-
	AT4G20140	-8.0121	LRR receptor-like serine/threonine-protein kinase GSO1
	AT4G37770	-8.0030	1-aminocyclopropane-1-carboxylate synthase-like protein
	AT2G23170	-7.8030	Indole-3-acetic acid-amido synthetase GH3.3
	AT3G21330	-7.7647	Transcription factor bHLH87
	AT5G43155	-7.7463	QWRF motif protein
	AT4G30450	-7.7236	glycine-rich protein
	AT4G28720	-7.6904	Flavin-containing monooxygenase
	AT1G66400	-7.5220	Probable calcium-binding protein CML23
	AT2G11215	-7.5112	Uncharacterized protein
	AT3G44220	-7.4902	Late embryogenesis abundant (LEA) hydroxyproline-rich glycoprotein
	AT3G14460	-7.3902	Putative disease resistance protein At3g14460
	AT3G42670	-7.3798	Chromatin remodeling 38
	AT1G15050	-7.2245	Auxin-responsive protein IAA34
	AT1G69970	-7.2058	CLAVATA3/ESR (CLE)-related protein 26
	AT5G62165	-7.1586	MADS-box protein AGL42
	AT2G43870	-7.1304	Pectin lyase-like superfamily protein
	AT5G45960	-7.1248	GDSL esterase/lipase At5g45960

d vs. b	gene	log2	gene description
Top 20 upregulated genes (positive log2 fold change)	AT3G55710	8.8296	UDP-glycosyltransferase 76F2
	AT5G06250	8.7283	DPA4; AP2/B3-like transcriptional factor family protein
	AT1G73620	8.5891	Pathogenesis-related thaumatin superfamily protein
	AT4G17480	8.4450	Alpha/beta-Hydrolases superfamily protein
	AT1G04110	8.4350	SDD1; Subtilase family protein
	AT1G63710	8.3886	Cytochrome P450 86A7
	AT5G37950	8.3742	Glucosyltransferase-like protein
	AT1G65890	8.2914	Probable acyl-activating enzyme 12, peroxisomal
	AT3G49690	8.1782	RAX3; transcription factor MYB, plant
	AT1G04800	8.1541	glycine-rich protein
	AT1G30160	8.0469	Uncharacterized protein
	AT4G11911	7.9685	magnesium dechelatase; STAY-GREEN-like protein
	AT5G36920	7.7789	Transmembrane protein
	AT5G64810	7.7684	Probable WRKY transcription factor 51
	AT2G17525	7.7512	Pentatricopeptide repeat-containing protein At2g17525, mitochondrial
	AT2G06355	7.7048	-
	AT2G31900	7.6840	myosin-like protein XIF
	AT2G20550	7.6831	HSP40/DnaJ peptide-binding protein
	AT3G18217	7.5196	MIR157C; miRNA
	AT5G27000	7.4854	Kinesin-like protein KIN-14G
Top 20 downregulated genes (negative log2 fold change)	AT1G73010	-11.7146	Inorganic pyrophosphatase 1
	AT1G23110	-11.2637	Fold protein
	AT4G30290	-10.5572	Xyloglucan endotransglucosylase/hydrolase
	AT5G20790	-10.2701	unknown protein
	AT3G03260	-9.7268	Homeobox-leucine zipper protein HDG8
	AT3G12580	-9.6930	Probable mediator of RNA polymerase II transcription subunit 37c
	AT1G17710	-9.6223	Inorganic pyrophosphatase 2
	AT1G69260	-9.3399	Ninja-family protein AFP1
	AT3G09922	-9.3004	induced by phosphate starvation1
	AT3G43110	-9.1771	transmembrane protein
	AT5G09470	-8.9980	DIC3 (mitochondrial dicarboxylate transporter)
	AT3G51860	-8.9016	Vacuolar cation/proton exchanger
	AT5G15500	-8.7436	Ankyrin repeat family protein
	AT3G44510	-8.7140	Alpha/beta-Hydrolases superfamily protein
	AT4G37400	-8.7012	Cytochrome P450 81F3
	AT5G55010	-8.3412	Putative uncharacterized protein
	AT3G13404	-8.1859	Uncharacterized protein
	AT4G08570	-8.1671	Heavy metal-associated isoprenylated plant protein 24
	AT3G02480	-7.9159	Late embryogenesis abundant protein (LEA) family protein
	AT5G03545	-7.8984	expressed in response to phosphate starvation protein

b vs. a	gene	log2	gene description
Top 20 upregulated genes (positive log2 fold change)	AT1G23110	11.1965	Fold protein
	AT3G03260	11.1019	Homeobox-leucine zipper protein HDG8
	AT1G17710	10.9974	Inorganic pyrophosphatase 2
	AT3G09922	10.6756	induced by phosphate starvation1
	AT1G13609	10.5092	Defensin-like protein 287
	AT5G09470	10.3732	DIC3 (mitochondrial dicarboxylate transporter)
	AT3G44510	10.0896	Alpha/beta-Hydrolases superfamily protein
	AT5G03545	9.6601	expressed in response to phosphate starvation protein
	AT2G35070	9.5769	transmembrane protein
	AT5G20790	9.4805	unknown protein
	AT3G02480	9.2902	Late embryogenesis abundant protein (LEA) family protein
	AT3G25240	9.2292	Sulfate/thiosulfate import ATP-binding protein, putative (DUF506)
	AT5G35510	9.1406	TIR-NBS-LRR class disease resistance protein
	AT3G43110	9.1100	transmembrane protein
	AT2G08820	9.0404	-
	AT3G44460	9.0159	ABSCISIC ACID-INSENSITIVE 5-like protein 1
	AT5G59320	8.9170	Non-specific lipid-transfer protein 3
	AT1G02310	8.9059	MAN1; mannan endo-1,4-beta-mannosidase; Glycosyl hydrolase
	AT5G15500	8.6764	Ankyrin repeat family protein
	AT2G11810	8.5126	Monogalactosyldiacylglycerol synthase 3, chloroplastic
Top 20 downregulated genes (negative log2 fold change)	AT1G06080	-11.2304	Delta-9 acyl-lipid desaturase 1
	AT3G55710	-9.3216	UDP-glycosyltransferase 76F2
	AT2G17525	-8.9934	Pentatricopeptide repeat-containing protein At2g17525, mitochondrial
	AT3G18217	-8.7253	MIR157C; miRNA
	AT3G50800	-8.5961	Uncharacterized protein At3g50800
	AT1G62914	-8.4814	Pentatricopeptide repeat-containing protein At1g62914, mitochondrial
	AT1G02060	-8.2848	Pentatricopeptide repeat-containing protein At1g02060, chloroplastic
	AT2G39690	-8.2090	Protein of unknown function, DUF547
	AT1G18250	-7.9998	Pathogenesis-related thaumatin superfamily protein
	AT4G28720	-7.8890	Flavin-containing monooxygenase
	AT2G42840	-7.8831	Protodermal factor 1
	AT3G56220	-7.8482	transcription regulator
	AT1G04800	-7.8480	glycine-rich protein
	AT5G11510	-7.8257	Transcription factor MYB3R-4
	AT1G63100	-7.7088	Scarecrow-like protein 28
	AT2G11215	-7.7022	Uncharacterized protein
	AT5G51350	-7.6820	Leucine-rich repeat receptor-like protein kinase
	AT4G17970	-7.6547	Aluminum-activated malate transporter 12
	AT4G34770	-7.6356	SAUR-like auxin-responsive protein family
	AT5G57390	-7.6213	AP2-like ethylene-responsive transcription factor AIL5

Table A1.9 Average of the absolute value of log2 fold changes of genes in central metabolic processes, ± the standard deviation. The top line shows the average of the top differentially expressed genes between each group.

	d vs. a	b vs. a	d vs. b
Top 20 (+/-) DEGs	**7.652 ± 0.623**	**8.966 ± 0.989**	**8.676 ± 1.107**
Photosynthesis	0.316 ± 0.222	0.729 ± 0.335	0.640 ± 0.450
TCA cycle	0.457 ± 0.606	0.654 ± 0.985	0.631 ± 0.754
Glycolysis	0.553 ± 0.578	0.767 ± 0.901	0.875 ± 0.943
Pentose phosphate	0.521 ± 0.603	0.571 ± 0.406	0.620 ± 0.564
Oxidative phosphorylation	0.719 ± 1.019	0.455 ± 0.703	0.753 ± 1.068
Sulfur metabolism	0.733 ± 0.788	0.620 ± 0.812	0.667 ± 0.757
DNA replication	0.553 ± 0.377	0.622 ± 0.512	0.935 ± 0.733
Nitrogen metabolism	1.255 ± 1.535	1.256 ± 1.198	1.216 ± 1.138
Nucleotide metabolism	0.520 ± 0.416	0.535 ± 0.789	0.556 ± 0.637

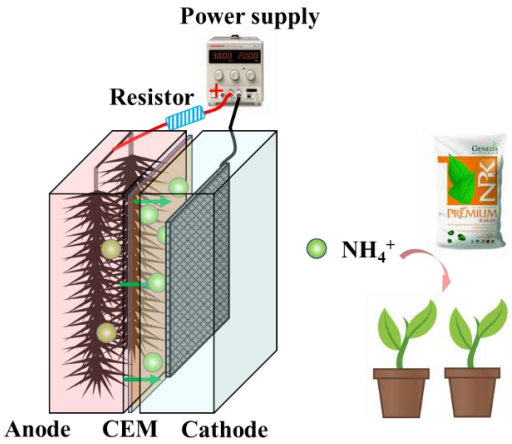

Figure A1.1 Schematic of microbial electrochemical cell. Carbon brush as anode and carbon cloth coated with activated carbon as cathode. CEM: cation exchange membrane. Ammonium transported from anode to cathode, and finally used by plants as nitrogen source in fertilizer.

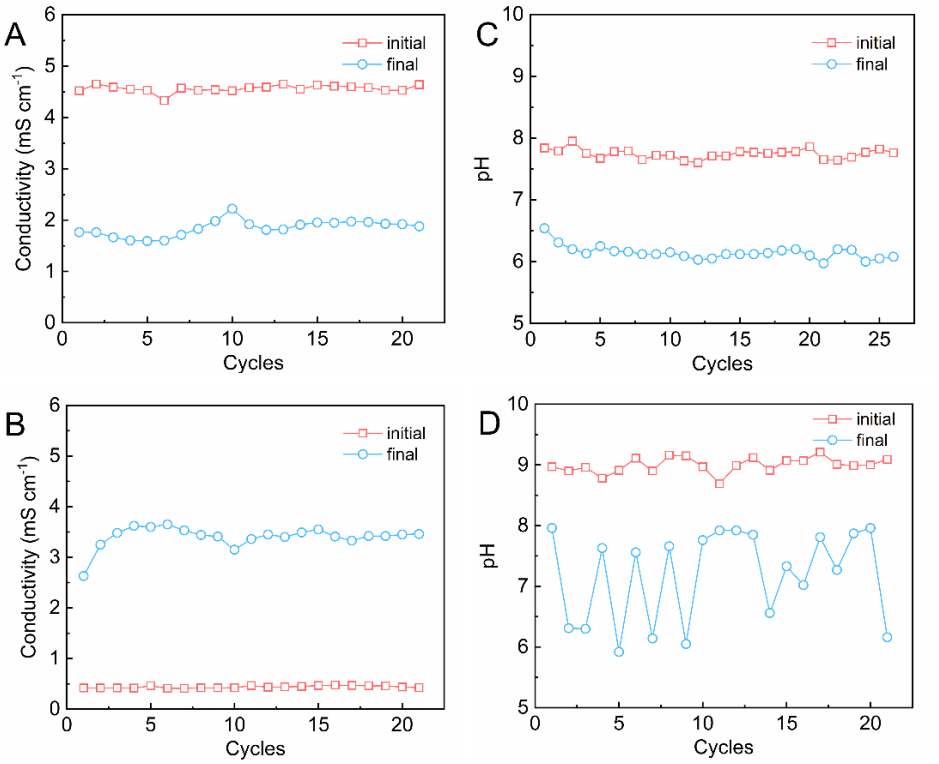

Figure A1.2 Performance of microbial electrochemical system during the three-week test fertilizer production period: (A) conductivity and (C) pH of initial and final anolyte; (B) conductivity and (D) pH of initial and final catholyte.

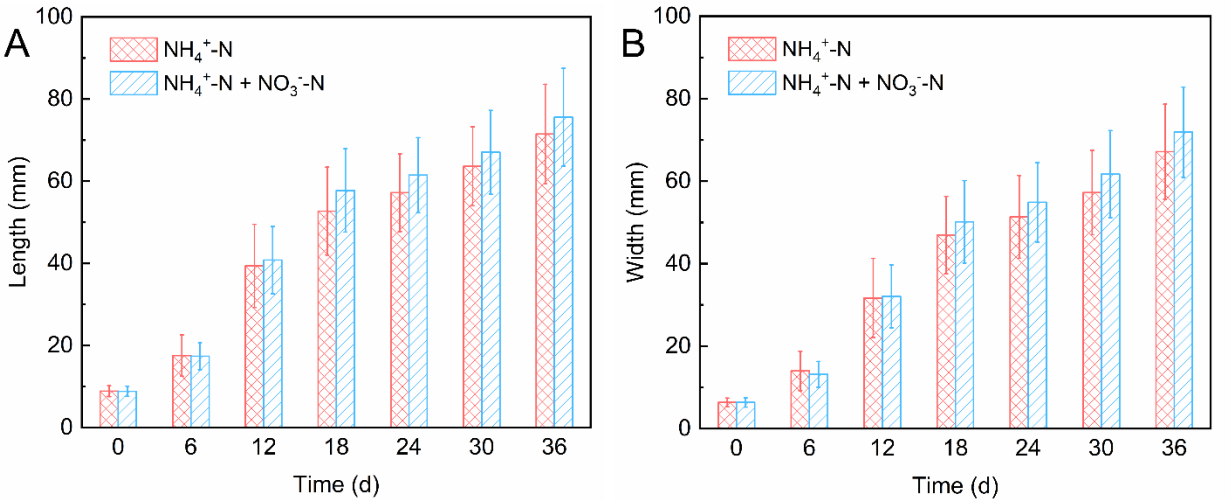

Figure A1.3 Change of the size of *A. thaliana* in terms of the (A) average length and (B) width over the pre-experiment fertilizing period. The first group (red) was fed with test fertilizer that was prepared from diluted catholyte added with phosphorus, potassium, and trace elements. The second group (blue) was fed with the same test fertilizer with extra ammonia oxidizing bacteria (commercial bacteria used in fish tank for oxidizing ammonia and nitrite to nitrate, Microbe-Lift Nite Out Ⅱ).

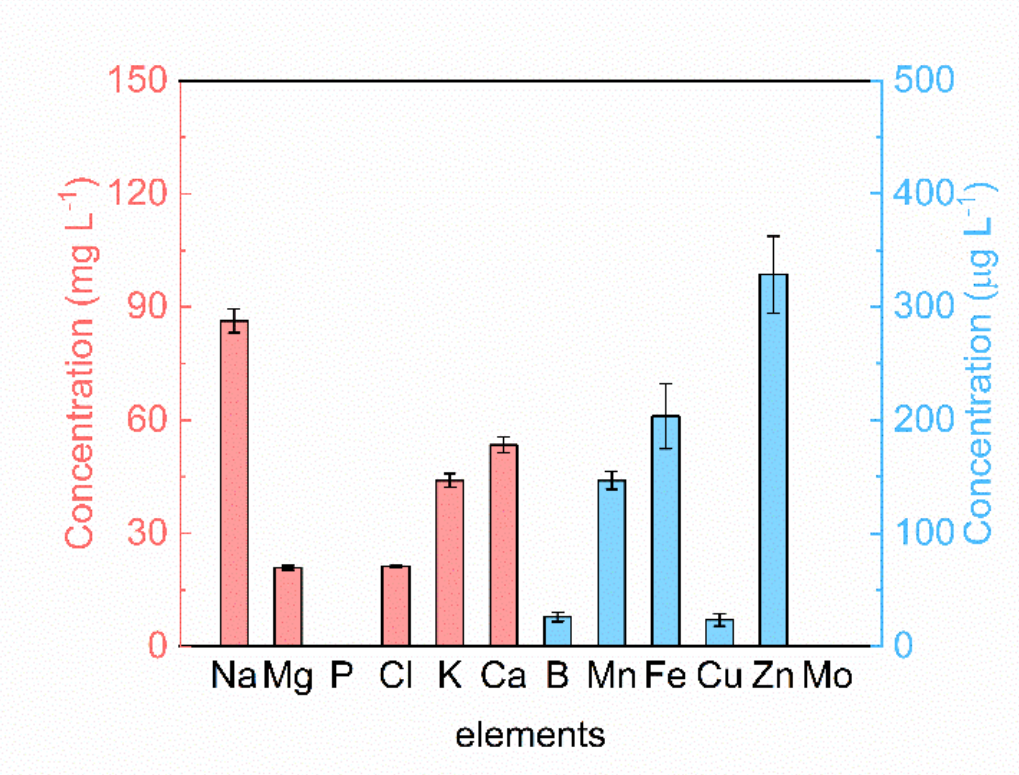

Figure A1.4 Average concentrations of selected major and trace elements in the final catholyte.

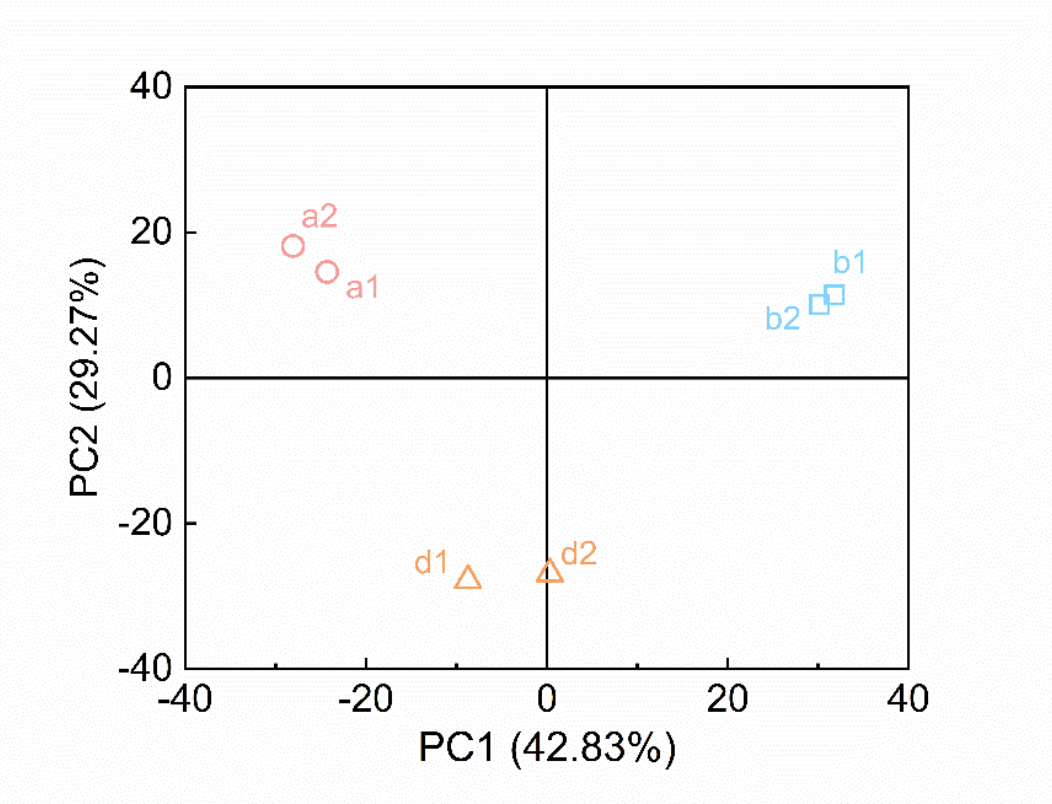

Figure A1.5 Principle component analysis of samples in Groups a, b, and d.

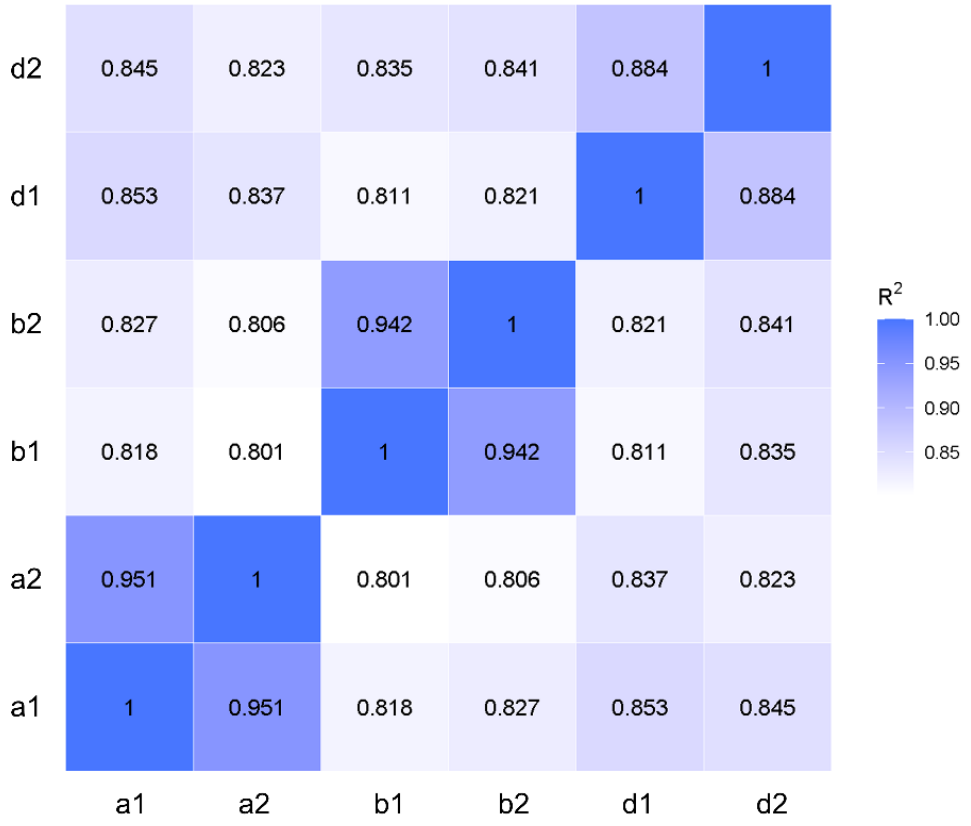

Figure A1.6 Pearson correlation coefficient matrix of samples in Groups a, b, and d.

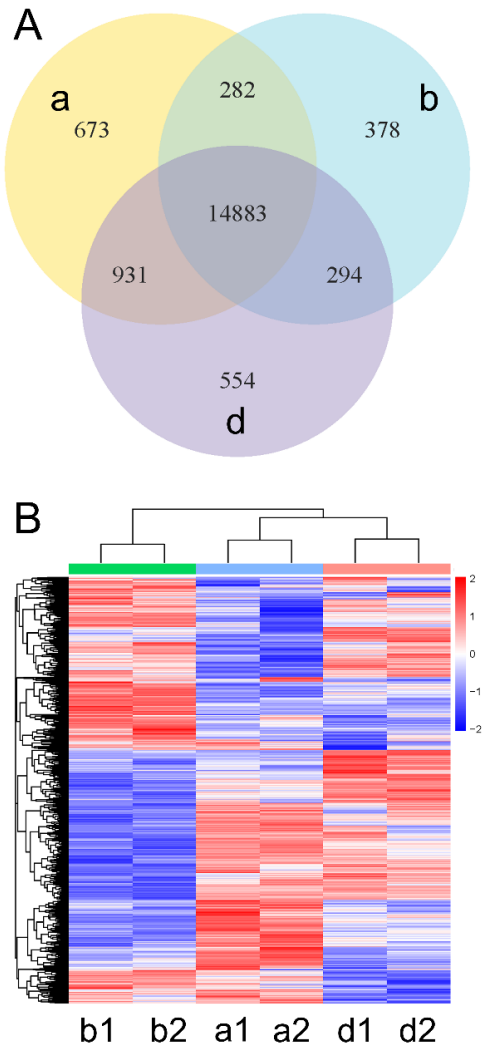

Figure A1.7 (A) co-expression Venn diagram (of the number of differentially expressed genes) within Groups a, b, and d. (B) Hierarchical clustering heatmap among samples in Group a, b, and d using the log2(FPKM+1) value. Red color indicates genes with high expression levels, and blue color indicates genes with low expression levels. The color ranging from red to blue indicates that log2(FPKM+1) values are from large to small.

Appendix A2: Supporting information for Chapter 3

This supporting information contains 1 figure and 4 tables.

Table A2.1 pH, conductivity, and concentration of major anions and cations in digester centrate.

Anions (mg L^{-1})		Cations (mg L^{-1})		Others
Cl^-	182.5 ± 7.0	Na^+	143.3 ± 5.7	pH
HCO_3^-	867.5 ± 3.9	NH_4^+-N	806.6 ± 10.8	8.01 ± 0.06
SO_4^{2-}-S	49.2 ± 2.3	K^+	95.8 ± 5.6	
NO_3^--N	6.0 ± 0.2	Mg^{2+}	8.6 ± 0.3	Conductivity
PO_4^{3-}-P	65.9 ± 3.0	Ca^{2+}	60.2 ± 0.4	6.33 ± 0.09 mS cm^{-1}

Table A2.2 Summary of N recovery performance in electrochemical ammonia stripping systems.

wastewater type	NH_4^+-N g L^{-1}	current density mA cm^{-2}	Cycle time h	recovery efficiency %	energy consumption kWh kg^{-1} N	reference
Source-separated urine	~5	1-5	2.7-12	70-80	16-41	(Luther et al., 2015)
synthetic wastewater	0.04	0.5-1.2	4	~60	9.1-21.1	(Zhang et al., 2018a)
synthetic centrate	1	NA	12	NA	1.6	(Hou et al., 2018)
Source-separated urine	3.8	10	24	93	8.5	(Tarpeh et al., 2018)
Source-separated urine	4.6	2	24	49	6.5	(Christiaens et al., 2019)
synthetic centrate	3	10	7	~70	~30	(Liu et al., 2020)
synthetic centrate	1	7.1-21.4	5	NA	16.0-38.0	(Kim et al., 2021)
digester centrate	1	7	4	82	50-100	(Koskue et al., 2021)
livestock wastewater	3.1	10	4	56-98	13.4	(Lee et al., 2021a)
livestock wastewater	2.5-3	93.8	6.7	NA	28.2	(Lee et al., 2021b)
synthetic wastewater	0.3	4	1	68.6	5.87–7.93	(Xu et al., 2022)
digester centrate	0.8	2.5-10	8	33-79	15.6-52.2	This study

Table A2.3 Mass balance coefficients of phosphorus and nitrogen in electrolysis-stripping system under different current density.

Current density mA cm^{-2}	Phosphorus -	Nitrogen -
0	-	0.98 ± 0.03
2.5	0.73 ± 0.06	0.83 ± 0.08
5	0.89 ± 0.06	1.00 ± 0.14
10	0.94 ± 0.04	0.98 ± 0.02
15	1.01 ± 0.07	1.09 ± 0.06
20	0.93 ± 0.02	1.01 ± 0.04

Table A2.4 Mass balance coefficients of phosphorus and nitrogen in electrochemical membrane system when different amount of extra acid (25% H_2SO_4) was added.

Amount mmol	Phosphorus -	Nitrogen -
0	1.11 ± 0.11	1.06 ± 0.06
5	1.02 ± 0.08	0.92 ± 0.11
7.5	1.03 ± 0.04	1.13 ± 0.04
10	1.15 ± 0.02	1.14 ± 0.02

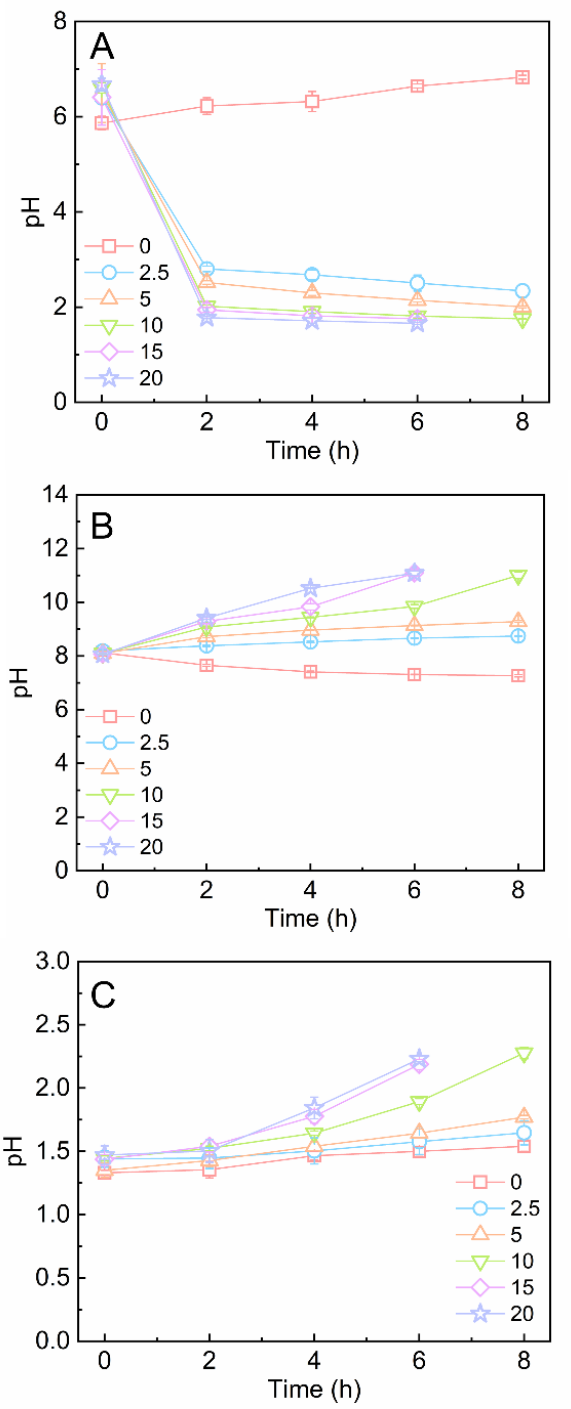

Figure A2.1 pH of (A) anolyte, (B) catholyte, and (C) acid absorption solution under different current densities

Appendix A3: Supporting information for Chapter 4

This supporting information contains 2 tables and 3 figures.

Table A3.1 pH, conductivity, and concentration of major anions and cations in digester centrate.

Anions (mg L^{-1})		Cations (mg L^{-1})		Others
Cl^-	182.5 ± 7.0	Na^+	143.3 ± 5.7	pH
HCO_3^-	867.5 ± 3.9	NH_4^+-N	806.6 ± 10.8	8.01 ± 0.06
SO_4^{2-}-S	49.2 ± 2.3	K^+	95.8 ± 5.6	
NO_3^--N	6.0 ± 0.2	Mg^{2+}	8.6 ± 0.3	Conductivity
PO_4^{3-}-P	65.9 ± 3.0	Ca^{2+}	60.2 ± 0.4	6.33 ± 0.09 mS cm^{-1}

Table A3.2 Prices used for cost calculation.

Items	Price	Units
Electricity	0.06	\$ kWh^{-1}
Sulfuric acid	0.03~0.5	\$ kg^{-1}
Sodium hydroxide	0.35	\$ kg^{-1}

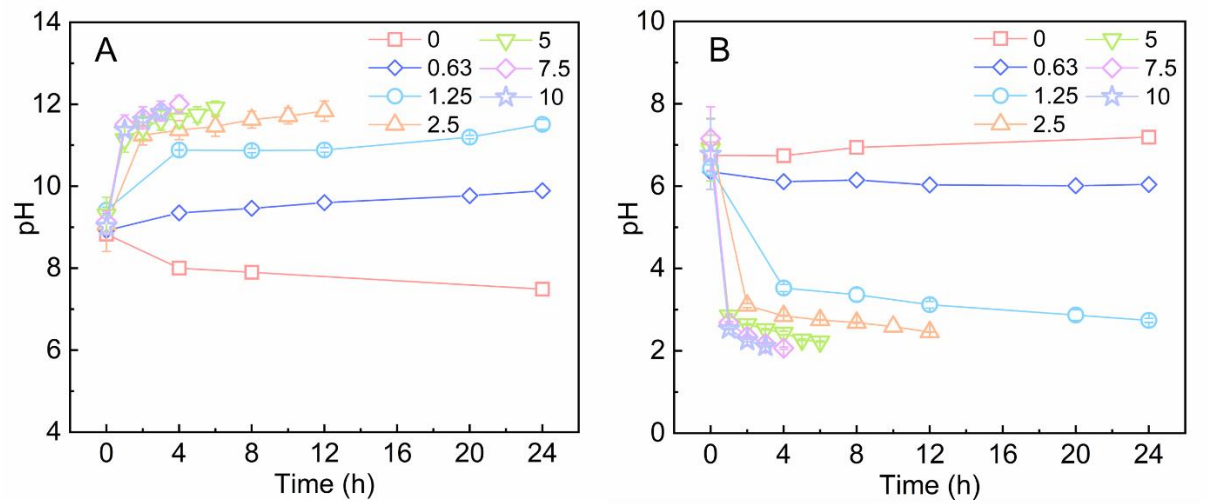

Figure A3.1 pH in the 4C-EMS under a current density varied from 0 to 10 mA cm^{-2}: (A) the pH in the catholyte; (B) pH in the anolyte.

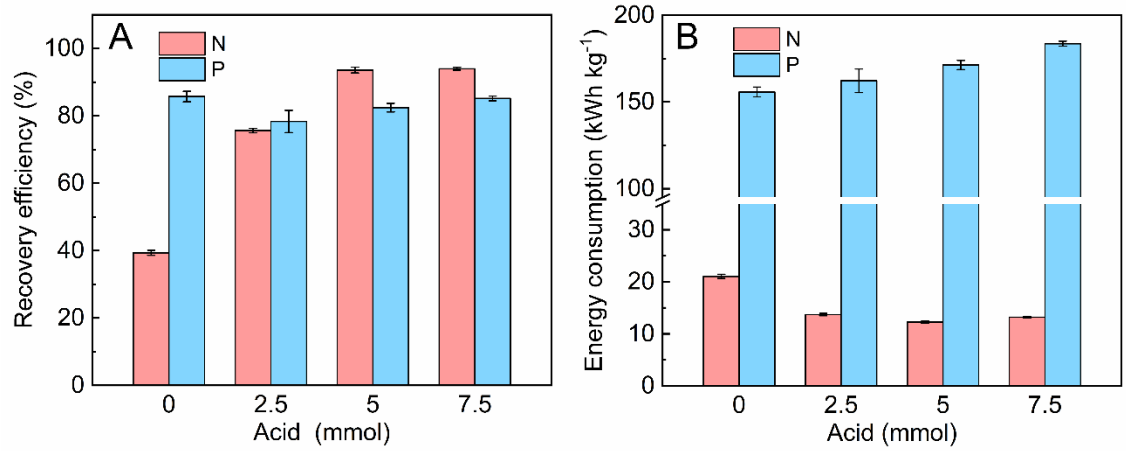

Figure A3.2 Recovery efficiency (A) and Specific energy consumption (B) of NH_4^+-N and PO_4^{3-}-P when different acid dosages were applied in the absorption solution when current density was 2.5 mA cm^{-2}.

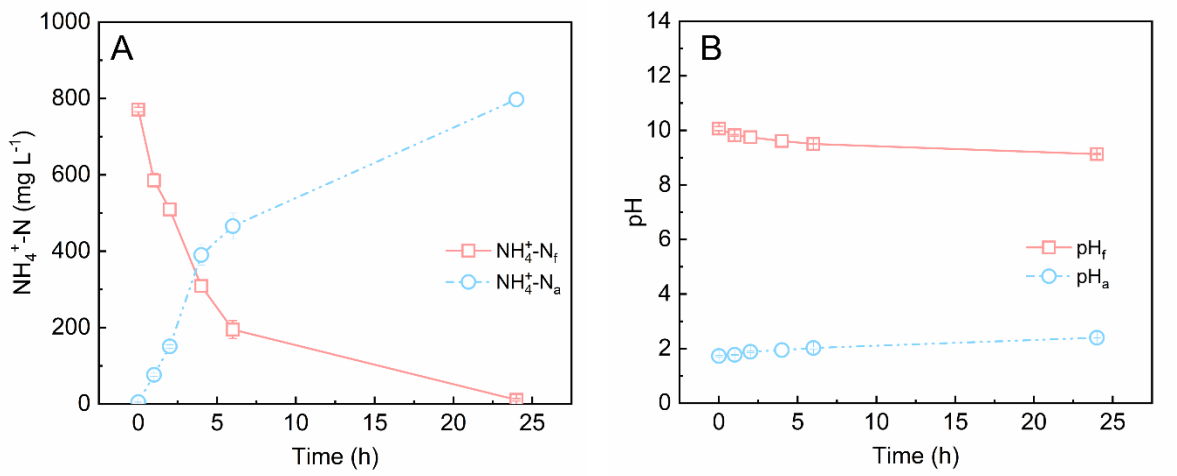

Figure A3.3 (A) NH_4^+-N concentration and (B) pH of the membrane contactor in the feed solution (subscript f) and acid absorption solution (subscript a) over 24 h when the initial pH of feed solution (digester centrate) was adjusted to 10.

Appendix A4: Supporting information for Chapter 5

This supporting information contains 3 tables and 5 figures.

Table A4.1 Fitting results of electrochemical impedance spectroscopy (EIS).

Time	R_x (Ω)	R_s (Ω)	f (Hz)
One week	1.73	137.00	0.01259
One month	0.76	36.37	0.03983
Three months	1.05	76.07	0.01259
Five months	1.36	69.06	0.01413

Note: R_x is the real resistance of the start point of the semicircle on Nyquist plot. R_s is the fitting diameter of the semicircle. f is the frequency during the EIS test of the peak point of the semicircle.

Table A4.2 Fitting parameters of Butler-Volmer-Monod model with various transferred electron number (n) based on data of 1 week, 1 month, 3 months, and 5 months.

Time	n	j_{max}	α	K_1	K_2	K_3
	-	A m^{-2}	-	-	-	-
1 week	1	5.72	0.92	-3.12	137.71	4.66
	2	0.34	0.49	-7.87	55.55	1.00
	4	0.63	0.91	1.69	523.03	1.00
	8	0.99	0.77	62.65	5697.27	1.88
1 month	1	8.06	0.50	-17.50	133.45	4.50
	2	6.72	0.01	-3.99	282.89	10.68
	4	1.23	0.90	4.91	273.42	1.00
	8	1.68	0.86	30.66	2184.29	1.00
3 months	1	31.94	0.92	35.22	134.79	1.00
	2	3.59	0.95	3.61	66.14	1.12
	4	1.19	0.84	3.58	73.37	1.00
	8	2.60	0.84	29.24	620.44	2.30
5 months	1	5.91	0.91	-3.03	57.98	7.44
	2	0.49	0.20	-5.51	20.89	1.00
	4	1.73	0.86	10.44	175.49	1.00
	8	1.23	0.81	26.19	496.47	1.98

Table A4.3 Fitting parameters of Marcus-Hush-Chidsey model with various transferred electron number based on data of 1 week, 1 month, and 5 months.

	1 week		1 month		5 months	
Electron number n	Pre-exponential factor A	Reorganization energy λ	Pre-exponential factor A	Reorganization energy λ	Pre-exponential factor A	Reorganization energy λ
-	A m^{-2}	-	A m^{-2}	-	A m^{-2}	-
1	0.18	5	0.25	5	0.25	5
2	0.10	6	0.20	8	0.17	7
4	0.07	10	0.09	9	0.09	9
8	0.03	14	0.05	12	0.05	11

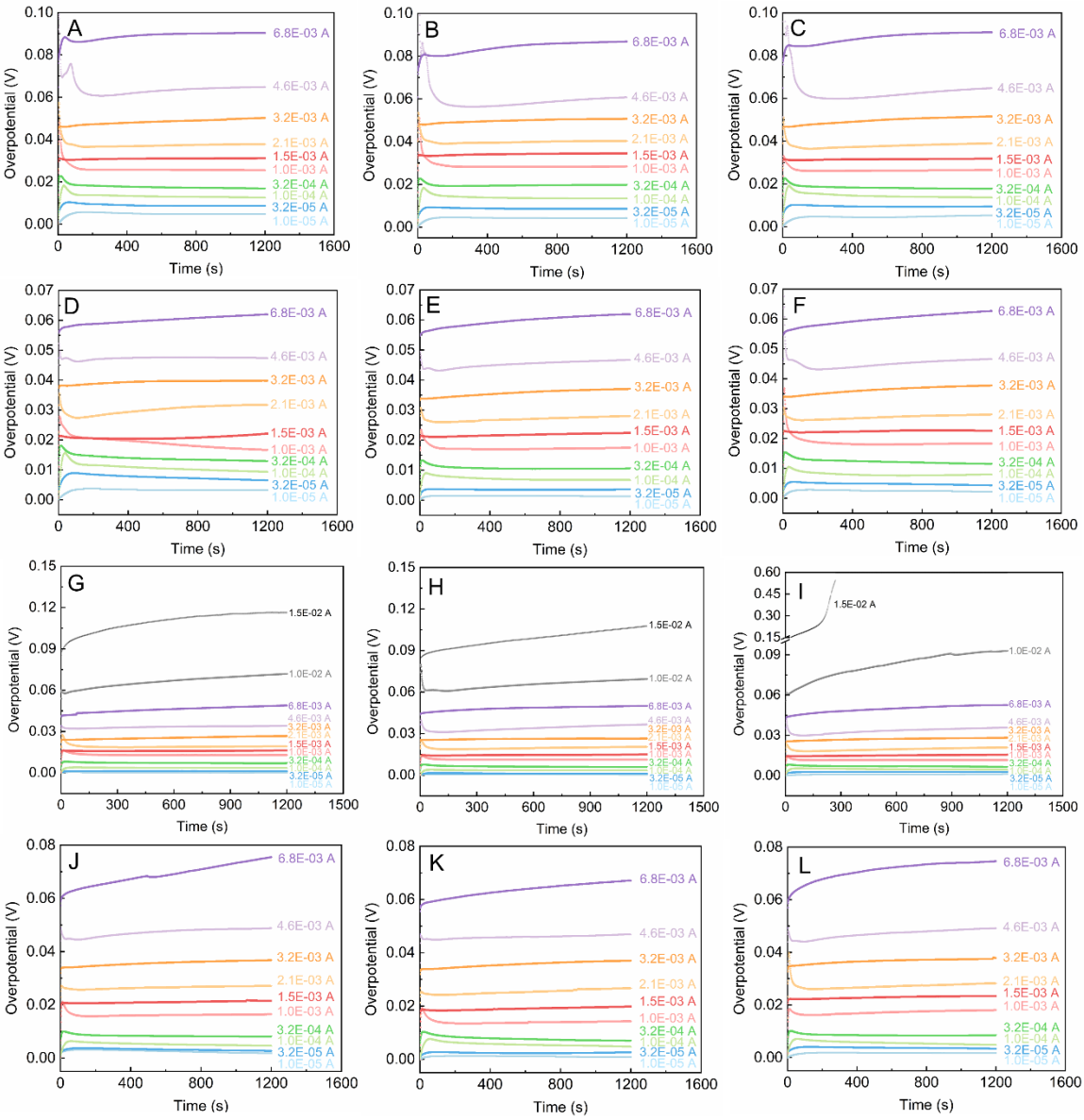

Figure A4.1 Chronopotentiometry curve of MES at (A-C) one week, (D-F) one month, (G-I) three months, and (J-L) five months. Triplicate tests were performed at each time. Data from Fig. A4.1I was not used to calulate the average overpotential at 0.015 A.

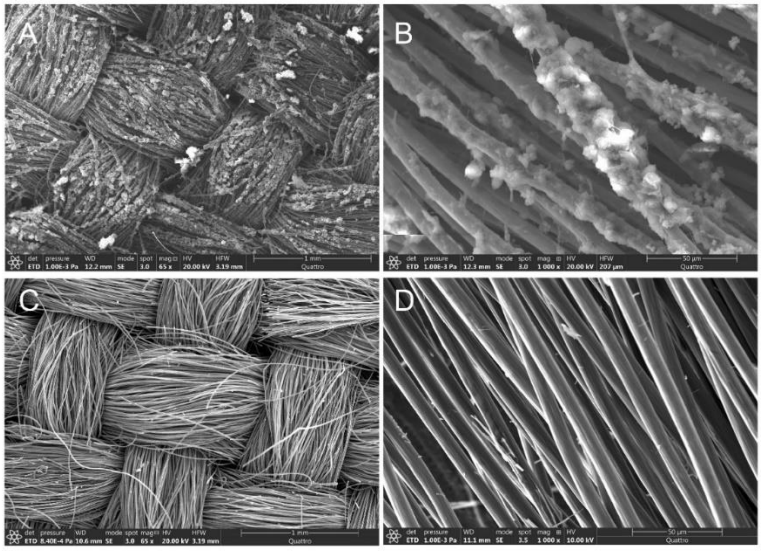

Figure A4.2 Scanning electron microscopy images of carbon cloth at the end of experiment with magnification of (A) 65, and (B) 1000. Clean carbon cloth with magnification of (C) 65, and (D) 1000.

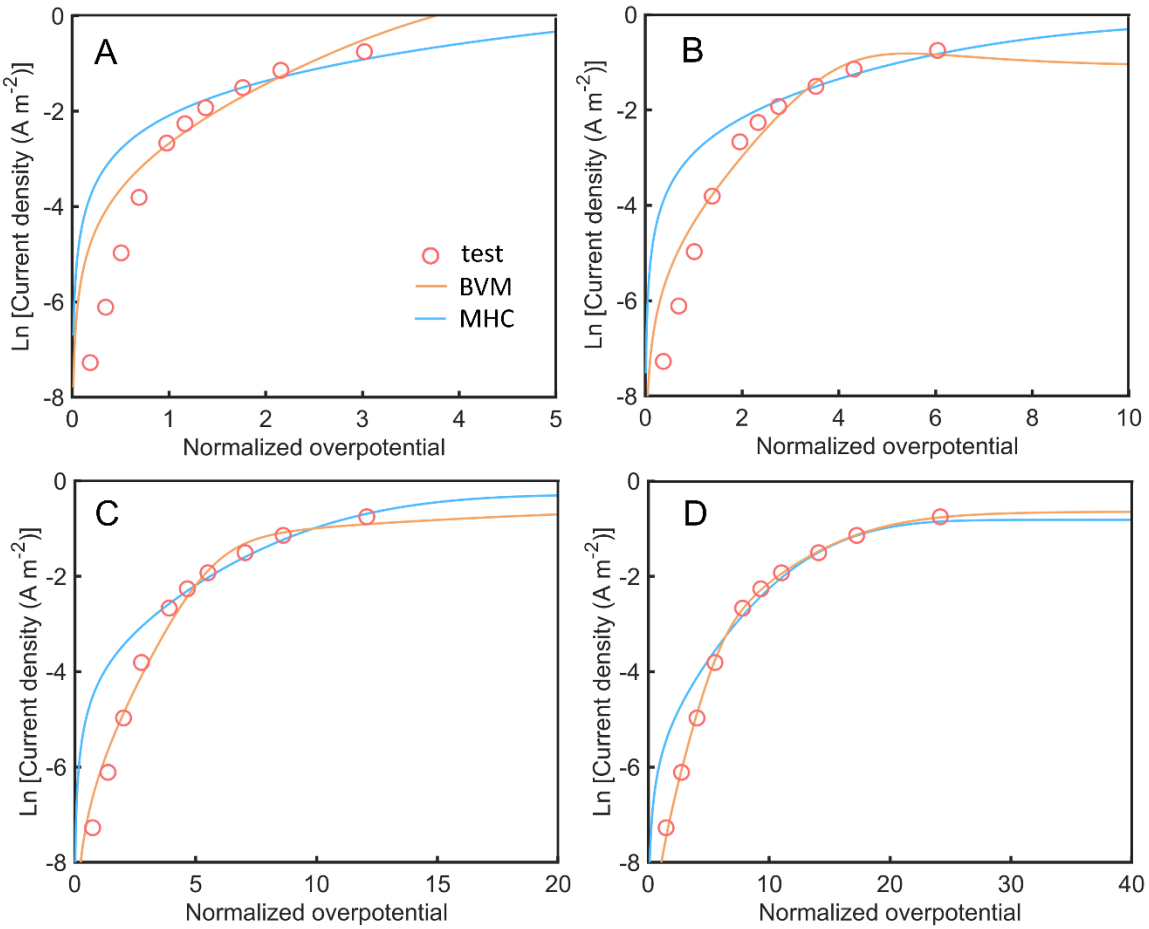

Figure A4.3 Comparison of the fitting curves based on Marcus-Hush-Chidsey model (blue line), Butler-Volmer-Monod model (orange line) and the test data (red circle) at 1 week when the stoichiometric number of the transferred electron equals to (A) 1, (B) 2, (C) 4, and (D) 8.

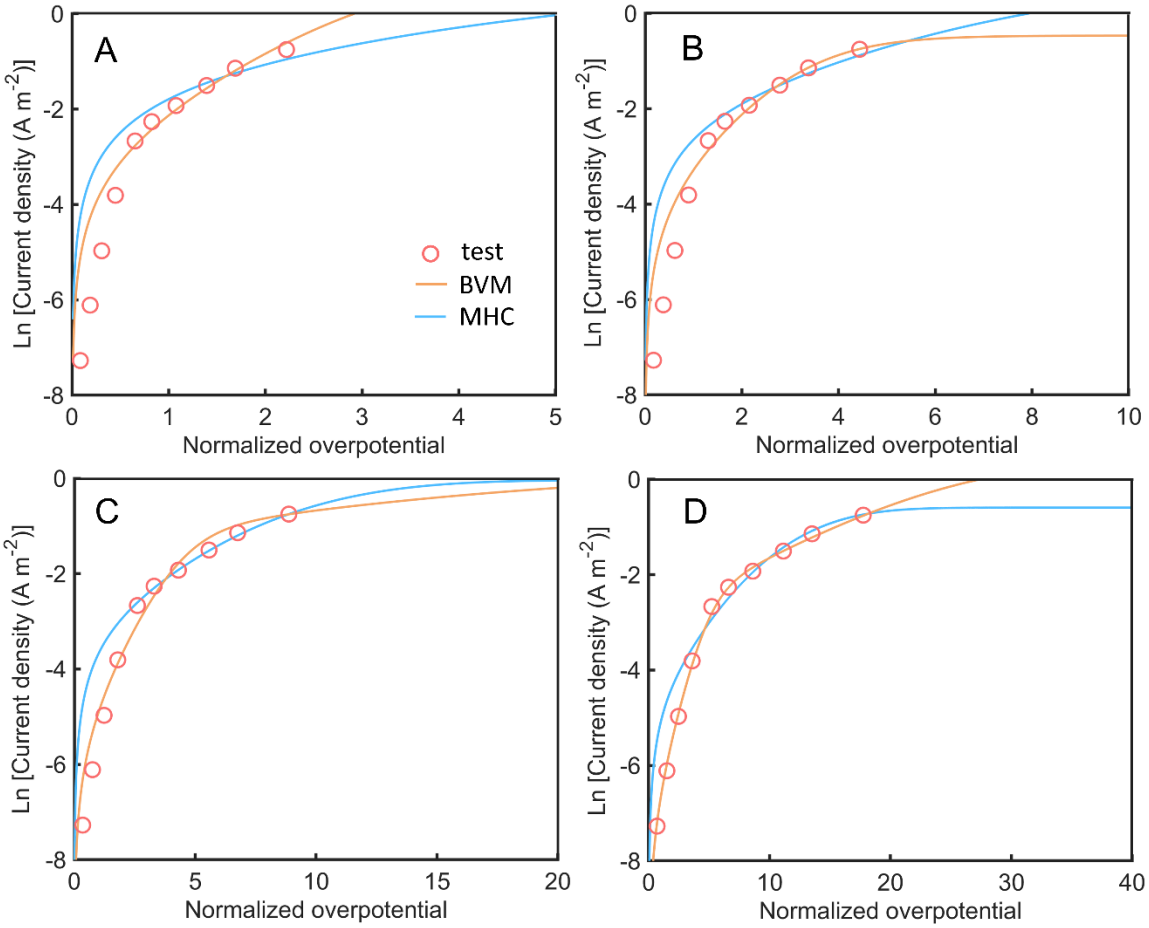

Figure A4.4 Comparison of the fitting curves based on Marcus-Hush-Chidsey model (blue line), Butler-Volmer-Monod model (orange line) and the test data (red circle) at 1 month when the stoichiometric number of the transferred electron equals to (A) 1, (B) 2, (C) 4, and (D) 8.

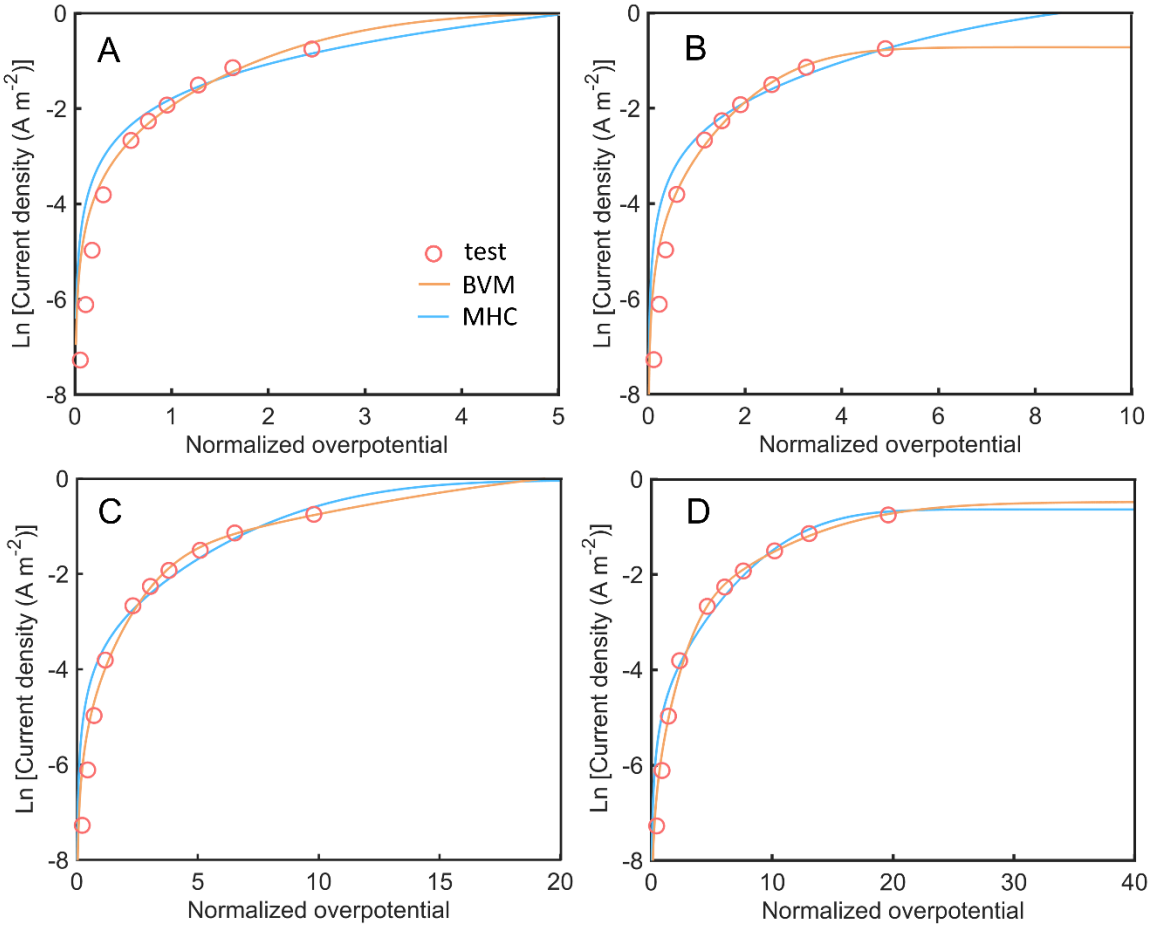

Figure A4.5 Comparison of the fitting curves based on Marcus-Hush-Chidsey model (blue line), Butler-Volmer-Monod model (orange line) and the test data (red circle) at 5 months when the stoichiometric number of the transferred electron equals to (A) 1, (B) 2, (C) 4, and (D) 8.